Improvement of a Molecular Docking Approach and

Its Applications Using QXP^{+}

Von der Fakultät für Naturwissenschaften
Department Chemie
der Universität Paderborn

zur Erlangung des Grades eines
Doktors der Naturwissenschaften

- Dr. rer. nat. –
genehmigte Dissertation

von

Laleh Alisaraie

aus Teheran, (IRAN)

Paderborn 2005

Eingereicht am: 22.02.05
Mündliche Prüffung am: 17.03.05

Referent: Prof. Dr. G. Fels
Koreferent: Prof. Dr. G. Henkel

The present work was carried out in the Department of Organic Chemistry at University of Paderborn-Germany, under the supervision of Prof. Dr. Fels from **November 2001** until **February 2005**.

First and foremost, I thank GOD, the light and the guidance in my life.

It is also a great pleasure to express my gratitude to people, who assisted me during these three years.
I am especially grateful to my supervisor, Prof. Dr. G. Fels for the useful comments, fruitful discussions and his continuous support.
I wish to thank Prof. Dr. G. Henkel, Prof. Dr. M. Grote and Prof. Dr. C. Schmidt for willing to read my thesis and attend in my examination committee.

I am thankful to Dr. D. Lamba, in International Center for Genetic Engineering and Biotechnology in Trieste-Italy, for generously providing us with the crystallographical data of BHG and PPG, prior to publication.

I wish to thank Dr. Edgar Luttmann, Jens Krüger and Oliver Stüker for patiently answering my questions and the technical supports.

I am thankful to Dr. Brigitta Elsässer for reading the correction of this work and being always ready to help.

My special warm thanks go to my former and present colleagues in research group of Prof. Dr. Fels for the very friendly workplace atmosphere.

All of my colleagues in Organic Chemistry Department are thanked for their helpfulness and the pleasant social environment.

Laleh Alisaraie

Contents

Summary

Finding the correct binding mode of highly flexible ligands is a demanding approach in molecular docking studies. With this respect, in some earlier efforts, the docking of these sorts of inhibitors of AChE was not successfully accomplished. For instance E2020, BHG and DECA using QXP^+, FlexX, Auto Dock and G.O.L.D, which is even true for their docking into the ligand-bounded protein. Furthermore, even finding the very final possible binding mode of the ligand that forms the most stable complex with the protein was not confidently obtainable. In this presented work, the difficulties of docking studies on very flexible ligands were addressed by improvement of a consensus method that is based on QXP^+ and local Monte Carlo search algorithm to reduce the conformational search space. The method has been developed using BHG and was successfully applied to other AChE ligands including E2020 and DECA. Although, the procedure has been particularly developed for study and prediction of the binding mode of AChE inhibitors, it was successfully employed for docking the very high flexible inhibitors of other proteins like human Rhinovirus 14, Win52084 (1RUH), and Win51711 (1PIV). The method was also employed for the prediction of binding mode of a few CDK2 inhibitors through docking them into the ligand unbounded proteins as well as into their ligand bounded proteins, while the latter was performed to improve the quality of complexation energy and better scoring of the ligand-protein binding mode to estimate the inhibitory constant of them as a result of molecular docking study.

The method was also used for detailed study on the various AChE inhibitors such as:

- The possible protonation state for the ligand in its complexed state with AChE.
- Definition of the amino acids that are dominantly involved in binding the ligand.
- Importance and influence of particular water molecules on the conformational pose of the ligand in the binding site.
- Selection of particular structural posture of the ligand in the case of PPG with two crystallographicaly possible poses of the ligand in its conformationaly convertible piperidine moiety.
- Prediction of the binding mode of a new derivative of galanthamine and elucidation of its structural details in complex state with docking into a non-complexed protein.
- Study on the possibility of leaving the binding site of AChE through an alternative path way based on “Back door” hypothesis that results finding only one pathway as the most possible one, among four suggested back and side doors.

1 Introduction

1.1 Alzheimer's disease

Alzheimer's disease (AD) is a slow progressive neurodegenerative disorder that clinically is characterized by cognitive decline and defined by losing memory and learning ability. It also decreases the ability of performing the basic daily activities. Other arrays of the disease are apathy, verbal and physical agitation, anxiety, depression, delusions and hallucinations. Currently, the loss of cholinergic function is an evidential finding responsible for cognitive decline, hence therapeutical development has focused on this theory. Aging is often regarded as the main factor in memory impairment and decline in other mental functions. Memory loss and other neuro psychologics symptoms such as impairments of judgment, language, learning and abstract thinking, which are descriptive of AD, may be attributed to normal aging. In this context, the relationship between normal aging and AD is a debatable concept [1]. The fact that AD increases with advancing the age, nowadays represents a major public health problem and it is probably becoming the most important pathology of the 21st century in the developed countries [2].

1.2 Cholinergic hypothesis

In cholinergic hypothesis is simply stated, that the cognitive loss associated with AD is related to decreasing the cortical cholinergic neurotransmission. Therefore, it is as that increasing cholinergic transmission may enhance cognitive function [3].

1.3 Approaches for treatment of AD's

The most AD treatment methods are studied towards two main aims: the ß-amyloid peptide (Aβ) and the cholinergic neurotransmission. There are thus two major approaches for treatment of AD. Since Aβ is known as a component of the senile plaques [4], thus the first approach of the treatment deals with preventing of formation of amyloid peptides or at least decreasing their generation or deposition. Aβ is produced from proteolytic processing of amyliod precursor protein (APP) through two pathways: one way is from cleavage of the protein with α-secretase and generates soluble APP fragments (APPs). The second way is cleavage of APP by β- or γ- secretases those are responsible of producing Aβ peptides (Figure 1.1).

The trace amount of Aβ has been detected as a normal cellular metabolism of APP, therefore it should be tried to prevent of more production and consequently deposition of the insoluble amyloid plaques to prohibition of the disease progress [5].

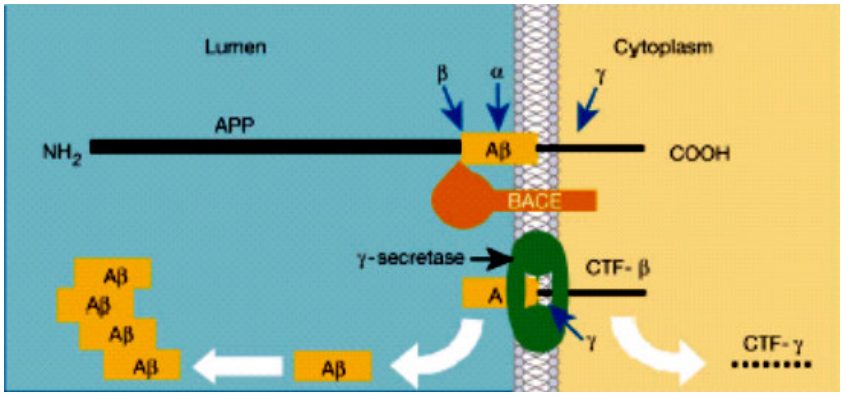

Figure 1.1 The cleavage of α- β- and γ-Secretase (A. Khalid)

1.4 Cholinergic enhancement therapy

The cholinergic theory has provided the rational basis for therapeutic developments in AD. Based on this theory and in accord with the mechanism of action in different parts of the cholinergic neurotransmission system (Figure 1.2), six classes of drugs have been developed to enhance cholinergic deficit in AD patient. These are [6]:

a. Cholinesterase inhibitors (ChEI), which block the AChE enzyme thereby stimulating cholinergic activity to enhance cognitive function.

b. Choline precursors, such as phosphatidylcholine, aimed at increasing the bioavailability of choline.

c. ACh releasers, which should facilitate the release of ACh from presynaptic end terminals.

d. Nicotinic agonists or substances having nicotinic-like effects, which should enhance ACh release.

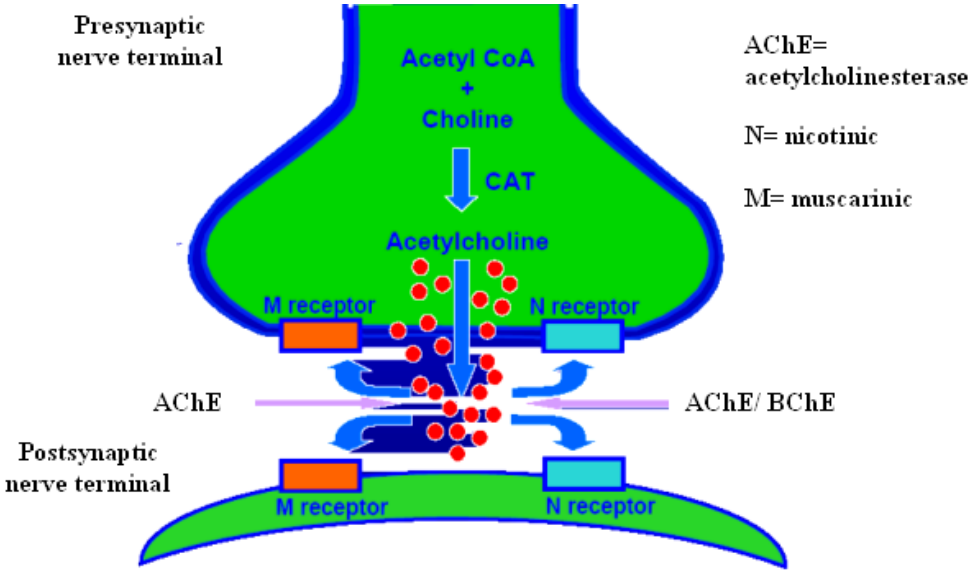

Figure 1.2: The mechanism of cholinergic neurotransmission (R. Bullock)

Among the above pharmacological agents, AChE inhibitors seem to be the most effective method to improve cholinergic deficit for reducing the symptoms of the disease [6].

1.5 Structure of AChE

The principal biological role of acetylcholinesterase (AChE, acetylcholine hydrolyser, EC 3.1.1.7) is the termination of impulse transmission at the cholinergic synapses by rapid hydrolysis of the neurotransmitter acetylcholine (ACh) [7]. AChE possesses a remarkably high specific activity, especially for a serine hydrolyses [8]. Knowledge of the three-dimensional structure of AChE is essential for understanding its remarkable catalytic efficacy.

1.6 Overview of the three-dimensional structure of AChE

The AChE monomer has an ellipsoidal shape, with dimensions of ca. 45 x 60 x 65 Å. The subunits contain 11-standard β-sheets surrounded by 15 α-helices and there are also 3 short standard β-sheets, which are not hydrogen-bonded to the central sheet [9] (Figure 1.3).

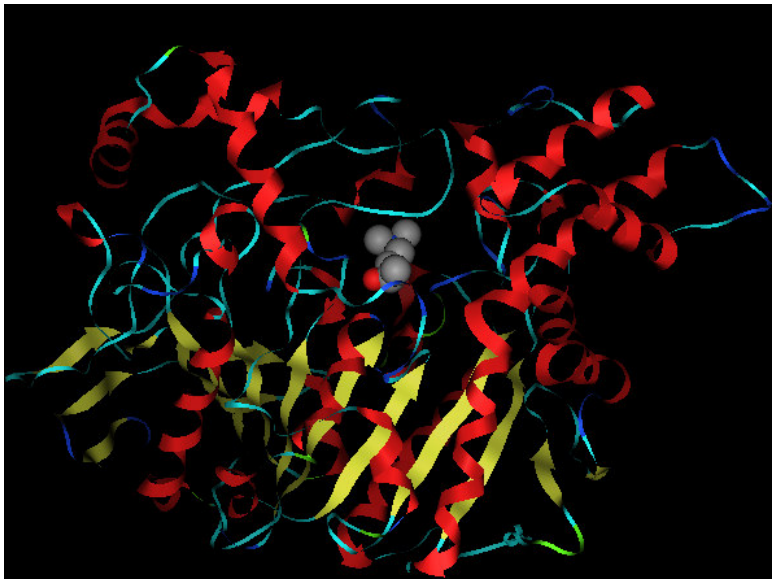

Figure 1.3: Schematic ribbon diagram of the 3-D structure of *T. californica* AChE monomer. 11-standard β-sheets (yellow) surrounded by 15 α-helices (red) and 3 β-sheets without any hydrogen bond to the central sheet. ACh in the binding site has been rendered in CPK.

1.6.1 The active center and the catalytic triad

Glu327, His440 and Ser200 are the components of the catalytic triad located at the base of a narrow gorge with 20 Å depth [10]. The gorge is lined with 14 aromatic residues, some are deep within the gorge while most others define a large aromatic area on the wall of the gorge. Two most important anionic amino acids are Asp72 and Glu199. Asp72 is located below the rim of the gorge, while Glu199 located at the base of the gorge. Also several other anionic residues are farther from the mouth of the binding site. Glu199 is the closest anionic side to trimethylamonium group of ACh in its bonded state. Aromatic residues clearly play an important role in stabilization of the complex. The choline moiety appears to be stabilized by Trp84 and Phe330 in quaternary ammonium binding site, whose orbital are close to the trimethylammonium surface as defined by its van der Waals' radii [11] (Figure 1.4).
The carbonyl oxygen of ACh is stabilized through hydrogen bonding to amide back bone at position of Gly118, Gly119 and Ala201 in oxyanion hole [10] (Figure1.5).

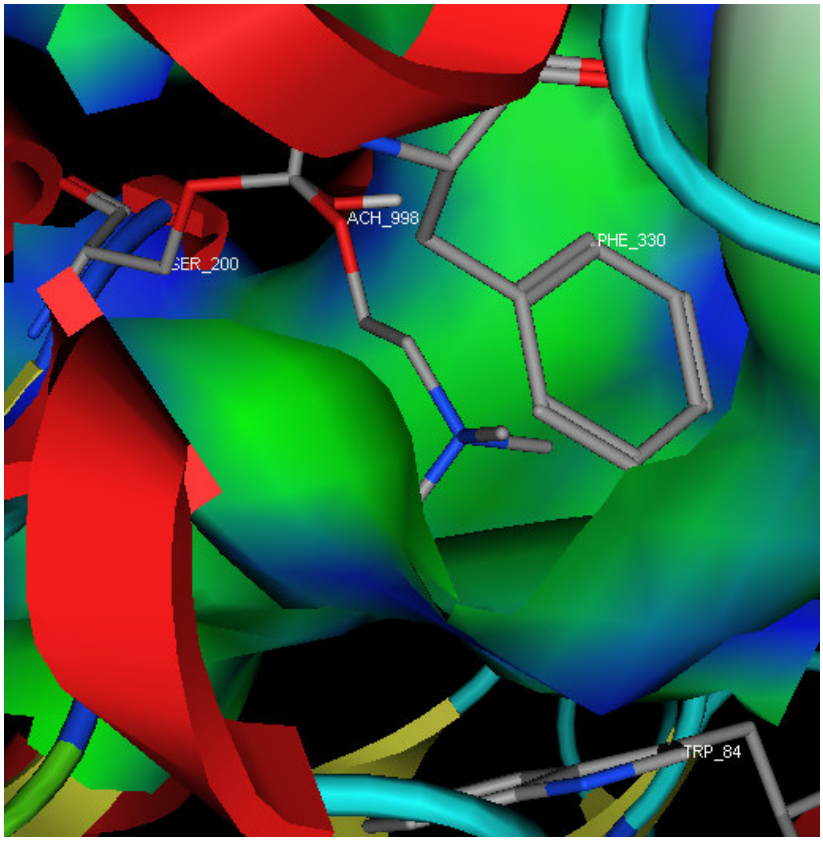

Figure 1.4: Trp84 and Phe330 are the residues in quaternary ammonium site of the gorge, which interacts with trimethyamonium moiety of ACh in its bonded state.

1.6.2 Peripheral anionic site

Trp279 and Tyr70 were introduced as the residues of peripheral anionic site (PAS). Furthermore, two sets of residues (270-278 and 251-266 in *Tc*AChE) contribute to the peripheral anionic subsite, which are located near the rim of the gorge. Hence, ligand association with the peripheral site may prevent access of substrate to the gorge by physical hindrance to restrict entry to the gorge by an allosteric mechanism, in which the active center conformation is altered [11] [12]. Recently, evidence was presented that AChE accelerates assembly of amyloid-β-peptides into the amyloid fibrils with involvement of PAS [13].
Figure 1.5 indicates the location of the peripheral site, quaternary ammonium binding site as well as oxyanion hole and catalytic triad within the gorge of AChE.

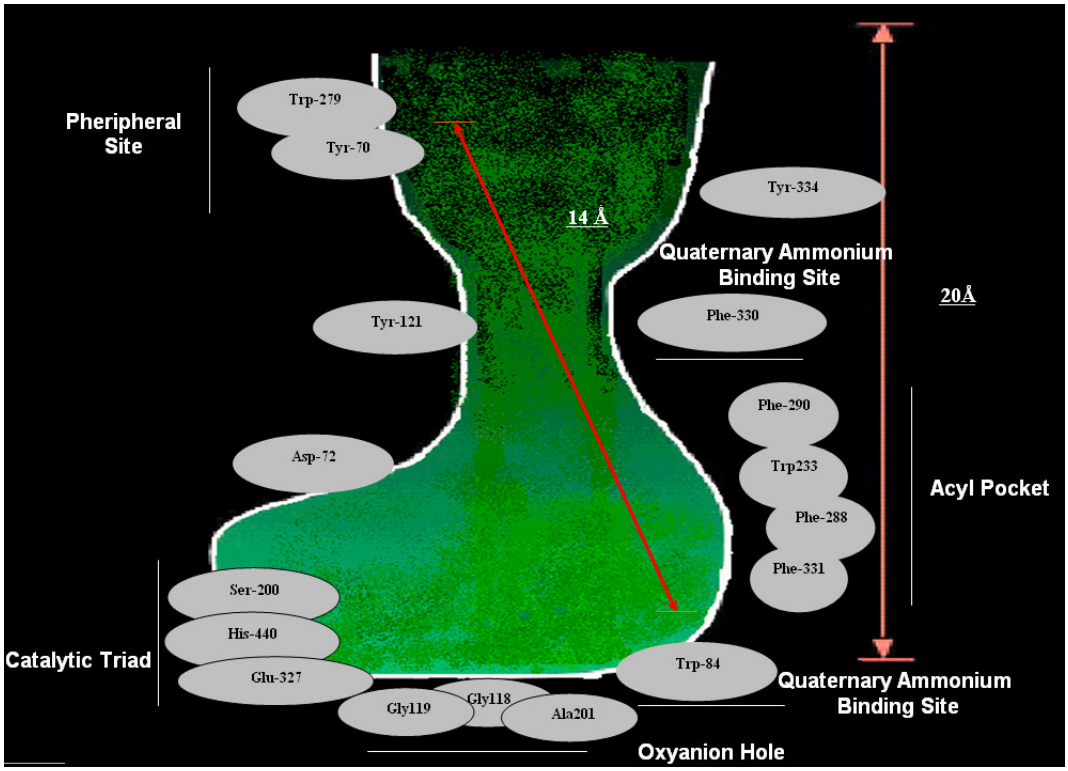

Figure 1.5: Shows the binding site gorge of AChE and its most important amino acids (A. Khalid)

1.6.3 Acylation of ACh within the binding pocket

AChE's physiological task is hydrolization of the cationic neurotransmitter. It acts through an acylation and deacylation process [14]. As it is shown in Figure 1.6 and 1.7, Ser200 and His440 in the active site are involved in the reaction with ACh. The acyl-enzyme is produced after proton transformation from Ser200 to imidazole moiety of His440 and then oxygen of Ser200 attacks to substrate (ACh), this part is acylation and then the acyl-enzyme is hydrolyzed with waters of binding pocket. This deacylation process alters the enzyme to its original form.

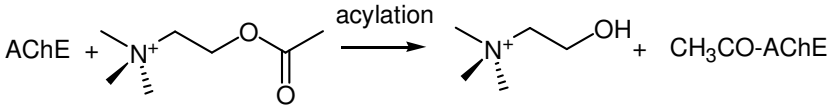

Figure 1.6: Indicates the involvement of ACh in acylation and deacylation reaction

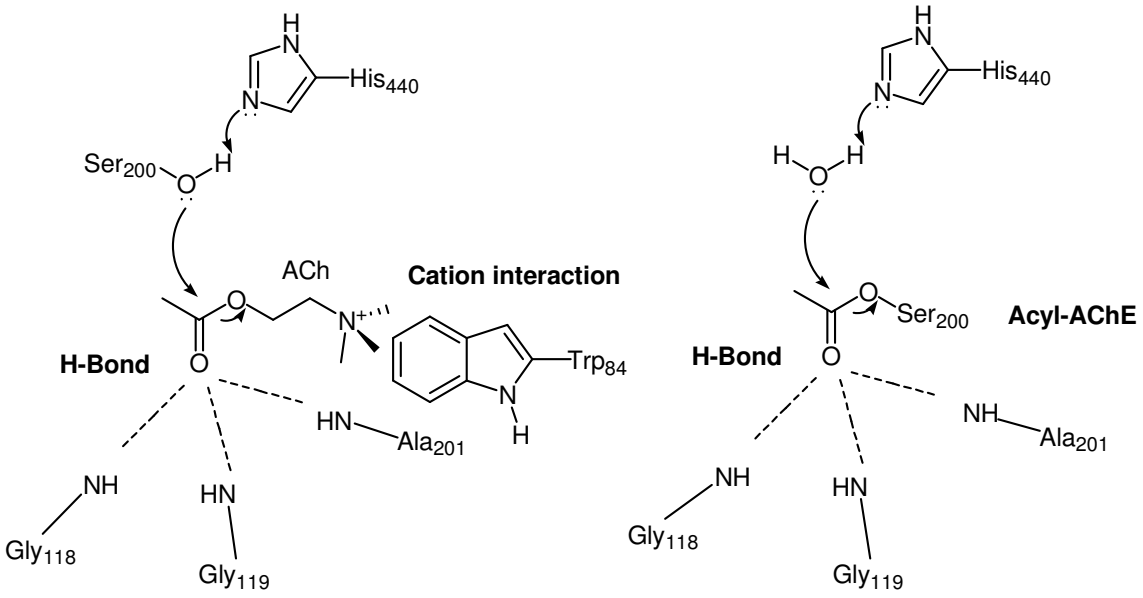

Figure 1.7: Hydrogen-bonding and cation-π-interactions

In the acylation process the cation-π-interaction takes place between the positively charged nitrogen in ACh and Trp84. Furthermore, the component of oxyanion holes (Gly118, Gly119 and Ala201) hydrogen bond to carbonyl group of ACh [14] (Figure 1.7).
In the acylation process, both the cation interaction and the H bonds exist during the reaction. However, these two kinds of interactions indirectly affect the proton transfer from Ser200 to His440 and the nucleophilic attack of the oxygen atom of Ser200 to the carbonyl of ACh (Figure 1.7).

1.7 Acetylcholinesterase inhibitors (AChEI)

1.7.1 Synaptic cholinergic drugs

In tissues the most abundant of cholinesterase types are acetylcholinesterase (AChE) and butyrylcholinesterase (BChE). As it was described earlier, AChE is the predominant one in brain that is responsible for hydrolyzing ACh to acetate and choline, by which it terminates the neurotransmitter effect at cholinergic synapses. Therefore inhibition of AChE causes more bioavailability of ACh at synaptic area and consequently improving neurotransmission process. Principally this method is more useful for treatment of patients with undamaged presynaptic neurons those are still active for synthesizing and releasing ACh, thus it works in early stages of AD and loses effectiveness after usage in a period of time. The activation of M2 muscarinic receptors that leads to inhibition of presynaptic release of ACh might decrease

the efficacy of acetylcholine inhibitors (AChEIs), through the counteracting effect. Despite of this AChEIs have shown suitable therapeutic effect. The only drugs currently accepted to treat the AD are AChEIs (i.e. tacrine, donepezil, rivastigmine and galanthamine) [15].
Based on the mechanism of action in AChE (described in section 1.2.4), different sort of AChEIs have been designed and classified as pseudo-irreversible, irreversible, transition state analogue inhibitors and reversible inhibitors.

1.7.2 Pseudo-irreversible AChEIs

This class of AChEIs includes the compounds having carbamates functional group. They are carbamylated by catalytic triad of AChE binding site. The rate of hydrolization of their carbamoylated complex with Ser200 is slower than the rate of hydrolization of ACh-AChE complex. The first AChEI of this class that was studied for treatment of AD was physostigmine, but because of the lack of efficacy resulting from its short half-life and variable bioavailability it was rejected. To improve its potency, several analogues of that with more lipophilic side chains have been designed. The miotine derivative (rivastigmine) is another AChEIs in carabamate group (Figure 1.8) that is less potent than physostigmine and inhibits also BChE. However it shows a good combination in brain selectivity, long duration *in vivo* activity and its good neuro protective property, which caused it to be accepted as a drug for AD treatment [19].

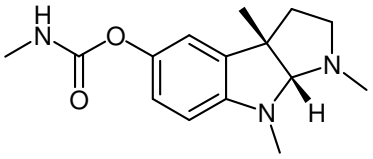

physostigmine

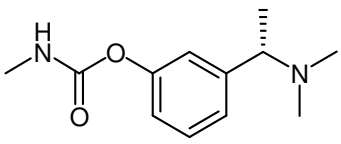

miotine

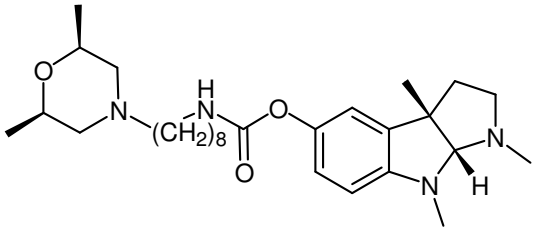

MF268

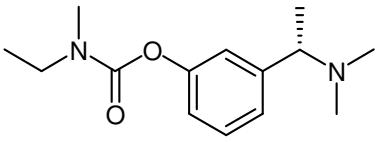

rivastigmine (SDZ-ENA-713, Exelon)

Figure 1.8: Chemical structure of pseudo-irreversible inhibitors of AchE

1.7.3 Irreversible AChEIs

Organophosphates are included in this group. One of the representatives of this group is metrifonate. Although its efficacy was acceptable, its application as a drug was withdrawn due to causing problems such as muscle weakness and respiratory problem in small proportion of patients.

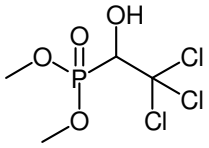

Figure 1.9: Chemical structure of metrifonate

1.7.4 Transition state analogue inhibitors

Trifluoromethylketones are effective inhibitors of this group having a reversible covalent interaction with Ser200 of the active site forming a tetrahedral-hemiketal transition state [24]. In fact, among AChEIs, m-(*N,N,N*-trimethylamino)trifluoroacetophenone is a highly potent reversible inhibitor (Figure 1.10), however its ionic nature prevents its capability to cross blood brain barrier (BBB), therefore a more lipophilic and non-ionic derivative of that can function better. One of the representations of this sort of inhibitor is zifrosilone (MDL-73745) in Figure 1.10 that works as a transition state analogue form, as well.

Figure 1.10: Chemical structure of m-(*N,N,N*-trimethylamino)trifluoroacetophenone (left) and zifrosilone (MDL-73745) (right) as transition state analogue AChEIs

1.7.5 Reversible AChEIs

In contrast to the three above described classes of AChEIs, reversible AChEIs binds to the binding site of the enzyme and inhibit of the activity of substrate. Of this group aminoacridines, *N*-benzylpiperidines and alkaloids are known.

1.7.5.1 Aminoacridines

One of the members of this group is tacrine (Cognex), which was the first AChE inhibitor approved by FDA in 1993. Interestingly, it is more potent to BChE than AChE, however it has other features including blocking sodium and potassium channels and has a direct effect on muscarinic receptors [19]. Some disadvantage of that are short half-life and induction of hepatotoxicity. However it was the lead compound for synthesizing new derivatives, such as velnacrine and suronacrine (Figure 1.11), those have shown reduced toxicity [20].

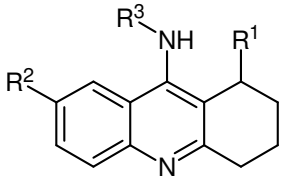

R^1=R^2=R^3=H, tacrine

R^1=OH, R^2=R^3=H, velnacrine (HP-029)

R^1=OH, R^2=H, R^3=benzyl, suronacrine (HP-128)

Figure 1.11: Chemical structure of tacrine, velnacrine and suronacrine

1.7.5.2 *N*-Benzylpiperidines

Donepezil (E2020) is the prototype of this structural class that was the second drug approved by FDA to treat the mild to moderate type of AD. It is a potent, long-acting and selective AChEI and shows this selectivity for AChE 1250 times more than for BChE. TAK-147 (Figure 1.12) is another *N*-benzylpiperidine derivative, which has less potency than donepezil but its effect on animals showed fewer side effects and is undergoing clinical testing. Other *N*-benzylpiperidine derivatives have been introduced, in which indanone moiety of donepezil has been replaced by different heterocyclic systems [21], such as N-benzylpiperidine benzisoxazoles (Figure 1.12). One of benzisoxazole derivatives is morpholino substituted one that showed higher potency and selectivity than donepezil and was effective in animal models [22].

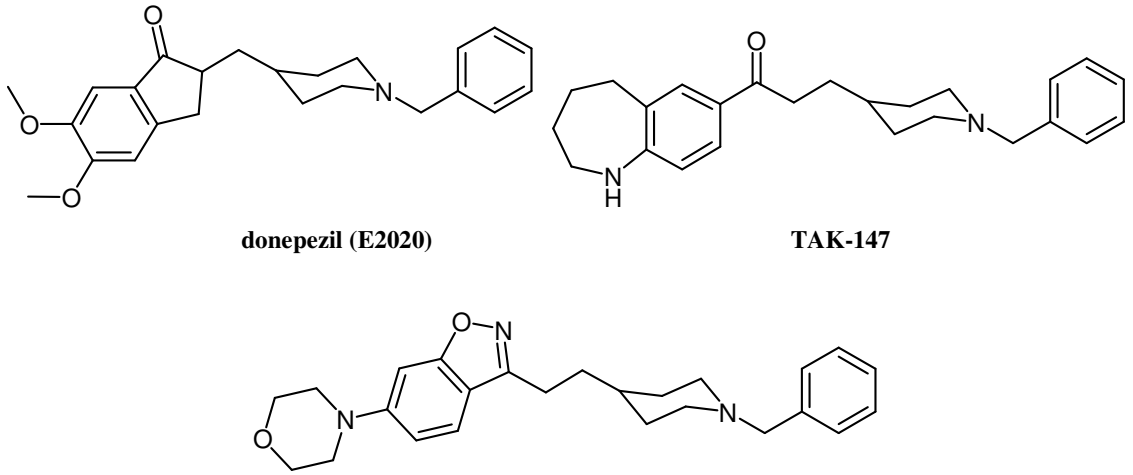

donepezil (E2020) **TAK-147**

***N*-benzylpiperidinemorpholinobenzisoxazole**

Figure 1.12: Chemical structures of donepezil (E2020), TAK-147 and *N*-benzylpiperidinemorpholino-benzisoxazole

1.7.5.3 Alkaloids

Galanthamine (Reminyl) is a tertiary amine alkaloid, isolated from Amaryllidaceae (Galanthus woronowi, the Caucasian snowdrop), has been approved in several countries for treatment of AD [23]. It is a reversible and competitive inhibitor of AChE and enhances the response of nicotinic receptors to ACh, which causes increasing ACh release and other neurotransmitters plus increasing bioavailability of ACh to inhibit AChE. To develop the potency of galanthamine derivatives of it have been suggested, which are P11012 and P-11149 (Figure 1.13) that are 10-fold more potent and 6-fold more selective than galanthamine [24].

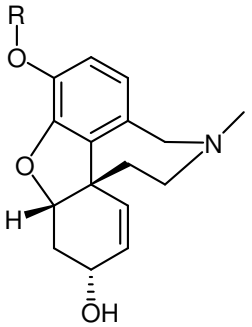

R= CH_3, galanthamine

R= $COCH_3$, P11012

R= CO (1-adamantly), P11149

Figure 1.13: Chemical structures of galanthamine, P11012 and P11149

(-)-Huperzine A is another alkaloid, isolated from the Chinese medicinal herb *Huperzia serrata*, is a very potent, selective and long-acting AChEI with low toxicity. It has been a lead compound to design derivative such as the 10-methyl substituted that has 8-fold more potency than (-)-huperzine (Figure 1.14)**.**

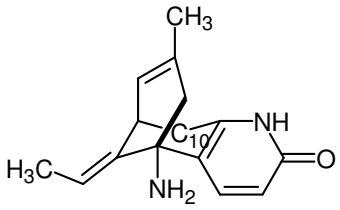

Figure 1.14: Chemical structure of (-)-huperzine A

1.8 Protein-Ligand docking

Molecular docking can be defined as the prediction of the structure of receptor-ligand complexes, where the receptor is usually a protein or a protein oligomer and the ligand is either a small molecule or another protein. Different simplifications are used to make molecular docking useful in different applications. Initially, molecular docking was used to predict and reproduce protein-ligand complexes [25].

Docking is defined by placing the putative ligand(s) in appropriate configurations for interaction with a protein. Therefore in molecular docking, it is attempted to predict the structure (or structures) of intermolecular complex, which is formed between two or more molecules to suggest binding modes of protein inhibitors. Most docking algorithms are able to generate a large number of possible structures and they also require a mean to score each structure to identify, which are of the most interest. Recent efforts in structural biology have led and will lead to growth numbers of compounds, which could be potential drug targets. Because of the recent advances in docking algorithms, *in silico* screening provides an attractive alternative to find suitable drug leads *in vitro.*

1.8.1 General procedure of docking

For a docking program, search algorithm and scoring function are the fundamental parts of the docking programs. The docking process can be broken down into five phases, which are modeling of the target, generating the possible conformations of the ligand, docking each conformation, scoring each docked ligand and selecting candidate ligands for further investigations [26]. High-resolution X-ray crystallographic structures are routinely used for ligand docking. In addition, structures derived from NMR experiments or those predicted by homology modeling may also be used. If the target protein is extracted from a structure, in which a ligand is bound to the protein, then docking experiments using that structure is termed "*bound docking.*" Otherwise, those experiments are termed "*unbound docking*" [27]. Because of the conformational changes that occur between the liganded and unliganded forms of many proteins, performing bound docking is preferable to unbound docking that typically yields better results than of the unliganded state in most of docking algorithms.

Not surprisingly, the most important part of the model is the protein's binding site. By homology-modeled protein, if the binding site is modeled poorly, virtual ligand screening will not yield useful results [27].

In docking of each conformation into the target, the goal is to quickly and correctly predict the binding geometry of the ligand complexed with the protein. For this purpose, there are several programs available, which differ in complexity, theoretical orientation, and implementation. Performance of a docking algorithm is the most time-consuming step in docking process. All modern docking algorithms used in structure-aided drug design, model the ligand as flexible, though the receptor does not need to be set flexible.
Flexible docking algorithms can be easily categorized [28]. In this respect, the search algorithms used in this project are shortly described

1.8.2 Docking Algorithms implemented in this collection

Program	Search Algorithm	Scoring Function
QXP (FLO+ 0802)	Monte Carlo	Amber Force Field
FlexX (1.9.0)	Incremental Construction	Empirical Score
G.O.L.D (2.1.2)	Genetic	Empirical Score

Table 1.1: The programs used as the docking tools in this presented work

1.8.2.1 Incremental construction algorithm in FlexX

This search algorithm is performed in three steps, which are selecting a base fragment, placing the base fragment in the binding site and building up the ligand inside the active site. The base fragment (the ligand core) is selected and is placed into the binding site, using an algorithmic approach based on a pattern recognition technique called pose clustering. In the next step, the remainder of the ligand is built up incrementally from the fragments. The construction method is so that the new fragment is added in all possible conformations to all placements found in the previous iteration, but only the ‘n’ best placements are taken on to the next construction step, generating multiple conformations for each fragment and including all in the ligand building steps. It means that after finding a good set of placements, the remaining portion of the ligand are divided into small fragments and incrementally grown on to the base alternatives [29].

1.8.2.2 Genetic algorithm in G.O.L.D

A genetic algorithm (GA) involves a population of possible solutions through genetic operations, such as mutation, crossover and migration. This is to reach to the final population

of low energy conformations employing the energy function or the fitness function. For the purpose of conformational sampling, the translational, rotational and the internal degrees of freedom are encoded into 'genes', which are represented by the real number values (codes) of those degrees of freedom [30]. Each conformation is named a chromosome, which consists of a collection of genes and is represented by the suitable string of the real numbers. A fitness value (energy) is assigned to each chromosome. The two most fundamental operators are schematically shown in Figure 1.15. The mutation operator (a) changes the value of a randomly selected gene by random value and the crossover operator (b) exchanges a set of genes between two parent chromosomes, creating new gene. Additional operator is migration operator, which moves individual chromosomes from one subpopulation to another in different islands.

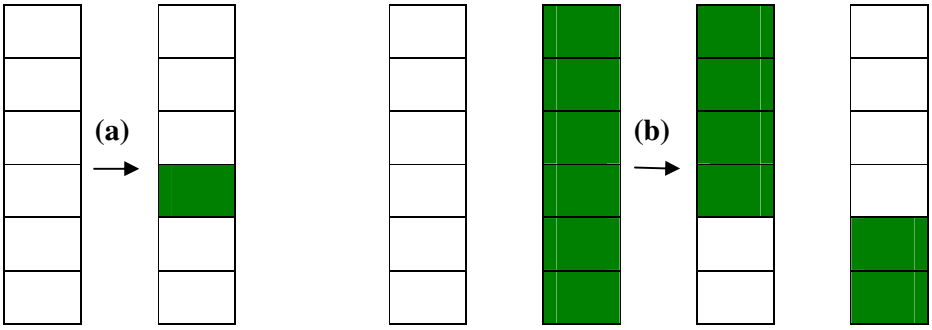

Figure 1.15: Genetic operators used to create a population of children chromosome from a population of parent. (a): mutation operator; (b): cross over operator
The crossover point is selected randomly, and the genes are exchanged between the two parents. Two children are created, each having genes from both parents.

The advantage of GA is that it requires less iteration than Monte Carlo to generate a large population of low energy conformation [31].

1.8.2.3 Monte Carlo Algorithm in QXP$^+$

In a Monte Carlo searching method, starting from any given conformation the program chooses a random number to decide what will be the next trial. In the case of a molecule, it randomly selects a bond among several possible rotatable bonds (or torsion angle), by which the molecular structure could be modified. It then randomly selects a new value for this torsion angle from a predefined set of values. Multiple-torsion moves as well as Cartesian-coordinates moves are among the many possible variations on this procedure. Once a new trial conformation is created, it is necessary to determine whether this conformation will be

accepted or rejected. If rejected, the above procedure will be repeated by randomly creating string of conformations until one of them is accepted. If accepted, the new conformation becomes the 'current' conformation, and the search process continues from it. The trial conformation is usually accepted or rejected according to the '*P'*, probability of existence of a conformation.

$$\boldsymbol{P} = \min[1, \exp^{-\beta\Delta U}] \qquad \textbf{Eq. 1.1}$$

β is $(\beta = 1/kT)$ and ΔU is the change in the potential energy. This means that if the energy of the new trial conformation is lower than of that in the current conformation, $\Delta U < 0$, the new conformation could be accepted. But even if the energy of the trail conformation is higher than the current energy, $\Delta U > 0$, there should be an especial probability, proportional to the Boltzmann factor, to be accepted. To find whether a higher energy trial conformation is accepted, a random number r in the range $[0,1]$ is selected and is compared to the '*P'* in equation 1.1. If $r < P$, the conformation is accepted, otherwise it is rejected. According to this principle of acceptance, the process continues for a long enough time, till a stationary solution will be achieved (Equation 1.1).

1.8.2.4 Definition of the energy terms

All the non-bonded interaction energies represent the pair-wise sum of the energies of the possible interaction between non-bonded atoms i and j of the ligand and protein, respectively (Figure 1.16).

$$E = \sum_{1}^{i}\sum_{1}^{j} -\frac{A_{ij}}{r_{ij}^{6}} + \frac{B_{ij}}{r_{ij}^{12}} + \sum_{1}^{i}\sum_{1}^{j} \frac{q_i q_j}{r_{ij}} \qquad \textbf{Eq. 1.2}$$

van der Walls (attraction)

van der Walls (repulsion)

Electrostatic term

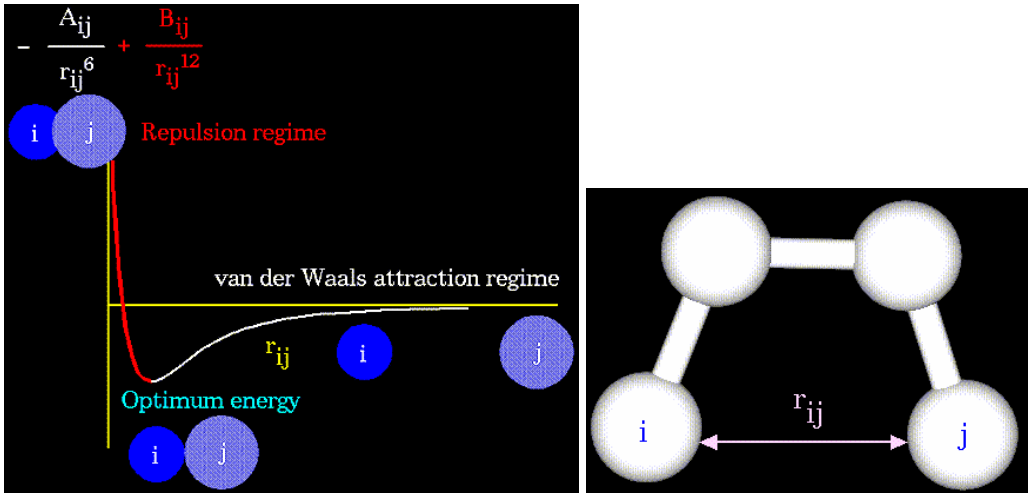

Figure 1.16: The graph indicates the variation of van der Walls interaction and repulsion (left) versus changes in inter-atomic distances (right)

The non-bonded energy accounts for repulsion, van der Waals attraction and electrostatic interactions (Equation 1.2). Van der Waals attraction occurs at short range, and rapidly dies as the interacting atoms move apart by a few Angstroms. Repulsion occurs, when the distance between interacting atoms becomes slightly less than the sum of their contact radii (Figure 1.16). Repulsion is modeled by an equation that is designed to rapidly blow up at close distances (with r^{-12} dependency). These effects as a 6-12 equation are used in QXP^{+}. The plot in Figure 1.16 displays the circumstances, which cause the attraction and repulsion situation between a pair of atoms. The "A" and "B" parameters control the depth and position (inter-atomic distance) of the potential energy well for a given pair of non-bonded interacting atoms. In fact, "A" determines the degree of "stickiness" of the van der Waals attraction and "B" determines the degree of "hardness" of the atoms. The "A" parameter can be obtained from atomic polarizability measurements, or it can be calculated quantum mechanically. The "B" parameter is typically derived from crystallographic data to reproduce observed average contact distances between different kinds of atoms in crystals of various molecules. The electrostatic contribution is modeled using a Columbic potential. The electrostatic energy is a function of the charge on the non-bonded atoms, their inter-atomic distance and a molecular dielectric expression, which the later is counted to weaken the electrostatic interaction coming from the environment (e.g. solvent or the molecule itself). Often, the molecular dielectric is set to a constant value between 1.0 and 5.0. A linearly changeability and distance-dependency of the molecular dielectric feature (i.e. 1/r) is sometimes used to account for the increase in environmental bulk as the separator distance between interacting atoms.

2 Description of the consensus molecular docking approach

2.1 The initial requirements

Quick eXPlore (QXP^+) [32] was employed as a docking program that for the force field parameters takes advantage of AMBER force field [33]. For docking experiments, proteins retrieved from Protein Data Bank (PDB) were utilized, which are *Torpedo Californica* acetylcholinesterase (*Tc*AChE), kinase and rhinovirus type proteins. Due to the limitation in QXP^+ for using the number of atoms, which must be less than 2000, in the case of AChE a spherical region of 20.0 Å radius around hydroxyl oxygen of Tyr121 of each protein crystal structure was cut and using QXP^+ the position of the hydrogens on the polar atoms were optimized. Then the new subsets were utilized as the protein for docking experiments. In addition, the structure of the ligand was built up and the hydrogens on the polar atoms were added. Then it was minimized and utilized as the ligand for docking experiments.

2.2 Characteristic features of the consensus method

a. The target is represented by an experimental three-dimensional structure, which is not necessarily the binding site of the ligand-bounded protein.
b. An additional scoring procedure (consensus method, described later) is combined with scoring method of the program (QXP^+) to filter the output data after each step of the docking experiment.
c. The data filtration systematically considers all of the possible conformations (output solutions after docking) with regard to various energy terms, such as total non-bonding interaction, van der Waals, electrostatic, contact and positive van der Waals energy as well as the number of hydrophobic interactions.
d. To decrease the calculation time, the protein is kept rigid through out the entire docking experiment (except for simulated annealing), although there is no general limitation for flexibility of the receptor active site in MSD.
e. It is particularly applicable to docking experiments involving highly flexible ligands with large degrees of freedom.

2.2.1 Aim of the consensus method

For docking a user-defined structure, firstly one step of full Monte Carlo (MC) search with 10,000 search-cycles was carried out. The docking result of this first step includes 25 conformations of the ligand, which are ranked according to the corresponding total estimated binding energy of their complex with protein. Since among the 25 output answers of each docking run, there are conformations with better values in different energy terms than of those in the first rank answer, they thus must be also taken into account. This is to find out, if the best docking solution, among the 25 generated answers of QXP^+ can move to the first rank. This is because the best solution is often in any rank but the first hit solution. To recognize the best solution, it is necessary to give more searching time via enough additional runs to access an energetically better binding mode. This is carried out, through a multi-step docking (MSD) experiment. Therefore a particular scoring method is required for identification and ending the last step of docking experiment to achieve:

a. The best binding mode of the ligand with regard to the various factors, such as different energy terms and the number of hydrophobic interactions.
b. The best conformation at the first rank with the best total energy, by which the ranking procedure of the main program is also taken into consideration.

And

a. To study whether the first hit conformation of the very final docking step can also reach to global minima (as a sign of being native-like structure) [34] or it is trapped into local minima on the energy hyper surface [35]. This is important to be assured that the ligand in the very last obtained-binding mode is able to reach to better internal energy (ligand energy).
b. In the case that X-ray structure of the native complex of the ligand is available, it should be found out that how well the predicted conformation resembles the native structure, which is done in accordance with calculating the root mean square deviation of the docking solution (RMSD) with respect to the coordination of the ligand in X-ray structure

2.2.2 Multi-Step Docking (MSD) procedure

2.2.2.1 Data filtration

In data filtration the output numerical data of QXP^+ are analyzed in a way that each of the 25 answers of a docking run gains one score if it has either the best value (B_v) in a term or has a value within an optimal range of that ($B_v \pm 2$). The total score of each hit is calculated according to equation 2.1.

$$S_{Total} = S_{E_{ass}} + S_{LE} + S_{E_{nbd}} + S_{vdW} + S_{E_{est}} + S_{E_{cnt}} + S_{vdW^+} + S_{Nhph} \qquad \textbf{Eq. 2.1}$$

$$0 \le S_{Total} \le 8$$

Where S_{Total} is the final score of the hit, S_{Eass}, score of the total estimated binding energy, S_{LE}, score of the ligand energy relative to the global minimum, S_{Enbd}, score of total non bonding energy, S_{vdW}, score of the van der Waals energy, S_{Eest}, score of the electrostatic energy, S_{Ecnt}, score of the contact energy, S_{vdW+}, score of the positive van der Waals energy; and S_{Nhph}, score of the number of hydrophobic contacts. Finally the criterion for selection of a hit is the S_{Total}. Then the docking answer with the highest S_{Total} is selected as the starting point of the next iteration (see Table 2.1 and Table 2.2).

2.2.2.2 Search algorithm

Full Monte Carlo (MC) algorithm is always used in the first docking run of a Multi-Step procedure (MSD). The resulting 25 answers of the first docking run then are analyzed as described in data filtration and used as the starting point of the next iteration. In all the following docking runs, local Monte Carlo searching method (LMCS) is applied [36] [37] in which the rotational angle varies between 20°-30° degrees. This limits the conformational search space and increases the probability of success in the random search and quickly removes atomic clashes between the ligand atoms and the receptor. MSD with LMCS algorithm is repeated until the first rank answer gains the highest S_{Total}. Figure 2.1 summarizes MSD procedure. In the case that X-ray structure of the ligand is available the accuracy of the obtained solution can be tested by RMSD of the atom coordination's in docking solution, while R_i is the coordination of the atom in docking solution and $R_i^{'}$ is the coordination of the identical atom in the X-ray structure (Equation 2.2).

$$RMSD = \sum_{i}^{n} \sqrt{\frac{(R_i - R_i^{'})^2}{N}} \qquad \textbf{Eq. 2.2}$$

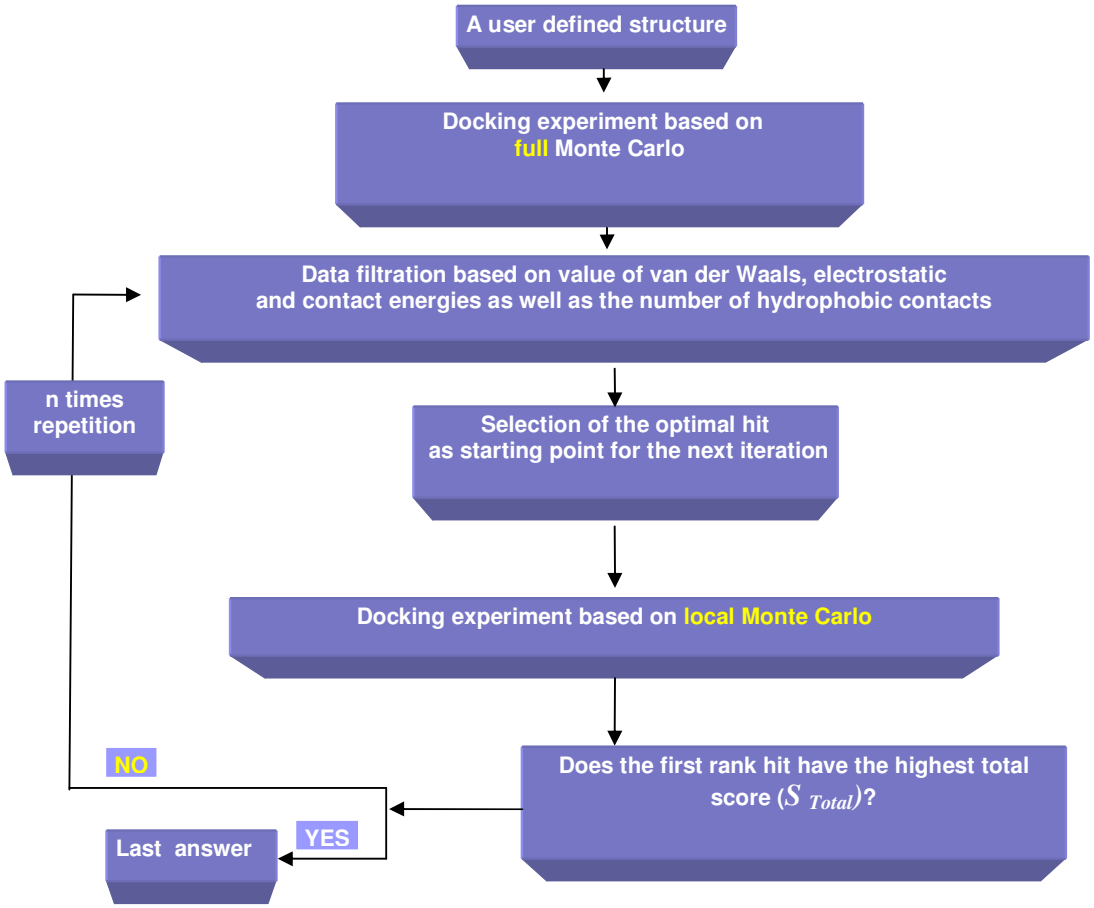

Figure 2.1: Flow chart of Multi-Step Docking approach

2.3 Application of MSD method for bound docking BHG

As an example of the application of MSD method, the procedure is described here for reproduction of benzosulfimidohexylgalanthamine (BHG) complexed with AChE [38]. BHG consists of three main moieties, a galanthamin, which is connected to the benzosulfimide moiety via a hexyl side chain (Figure 2.2).

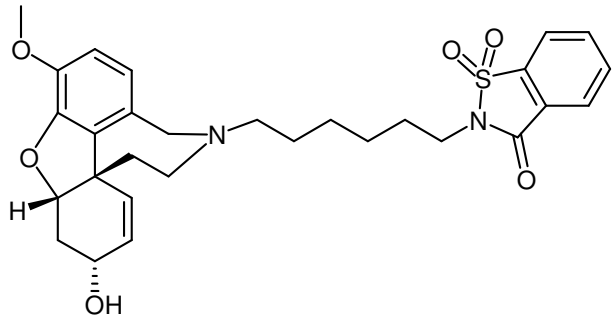

Figure 2.2: Chemical structure of BHG

At the first step of the multi-step bound docking of BHG, one step of full Monte Carlo (MC) search was carried out. In view of the fact that among 25 answers of the first docking run, there are still conformations with higher S_{Total} than the first rank, these docking solutions should all thus be taken into consideration. This is to find out whether they are capable to show up in the first rank with more time given (search-cycle). According to the Monte Carlo search algorithm the first rank solution has the highest probability with the best potential energy, ΔU (Equation 1.1). Using this method for data filtration, the selected binding mode is not necessarily the first rank, but rather the one with the highest possible value of S_{Total} among all the resulting solutions in the first step of docking (Equation 2.1and Table 2.1, 2nd rank).

From this step on, the local Monte Carlo search (LMCS) with restricted rotational angle (between 20°-30° degrees) was used until the first rank answer also shows the highest S_{Total} Table 2.2, 1st rank).

The first step docking using the Full Monte Carlo search algorithm generates a docking solution with a large magnitude of RMSD with value of 1.62Å, as the difference in the location of X-ray structure and docking solution is observable in Figure 2.3 (left). Application of MSD for docking BHG successfully refined the X-ray structure with RMSD of 0.64Å. This result was obtained after performance of three steps of local Monte Carlo runs. The overlaid structure of docking solution on the X-ray structure is shown Figure 2.3 (right).

Rank	RMSD	Eass*	LE*	Enbd*	vdW*	Eest*	Ecnt*	vdW+*	Nhph*	Nhyd*	Score*
1	1.62	-39.0	8.6	-47.6	-6.3	-8.4	-32.9	8.4	12	2	2
2	0.60	-38.3	11.9	-50.1	-12.6	0.1	-37.7	8.6	13	1	4
3	1.82	-37.1	10.2	-47.2	-9.9	-2.5	-34.7	6.1	13	3	2
4	1.39	-36.8	13.7	-50.6	-9.4	-6.2	-34.9	7.3	11	3	1
5	2.34	-36.3	8.7	-44.9	-7.9	-3.9	-33.1	7.7	11	2	0
6	0.69	-36.1	8.5	-44.5	-9.3	-1.4	-33.7	6.7	12	2	2
7	1.31	-35.8	12.5	-48.2	-8.0	-6.2	-32.0	6.6	13	2	3
8	1.67	-34.7	14.7	-49.3	-9.8	-3.8	-35.8	7.2	12	2	4
9	1.52	-34.7	9.8	-44.4	-4.4	-7.4	-32.6	11.0	12	3	1
10	1.81	-34.5	9.2	-43.8	-3.7	-5.1	-35.0	13.3	9	2	0
11	1.16	-34.4	9.5	-43.9	-7.8	-6.1	-30.1	6.2	13	2	2
12	1.53	-34.2	13.3	-47.6	-3.2	-9.5	-34.8	13.5	11	3	1
13	0.81	-34.2	9.2	-43.3	-8.8	-1.7	-32.9	8.9	11	2	1
14	2.39	-34.0	7.9	-41.8	-4.6	-4.4	-32.8	10.3	13	2	1
15	1.59	-33.8	11.1	-45.0	-6.5	-5.8	-32.7	8.6	12	2	1
16	0.93	-33.7	7.0	-40.6	-9.2	0.9	-32.3	6.0	12	2	2
17	0.79	-33.6	12.5	-46.1	-12.0	0.7	-34.8	5.2	14	1	3
18	0.94	-33.4	12.1	-45.5	-9.7	-3.1	-32.7	8.3	14	2	2
19	0.84	-33.4	11.3	-44.9	-10.0	0.5	-35.4	7.4	11	1	0
20	1.75	-33.4	12.8	-46.1	-7.0	-5.4	-33.7	8.4	13	2	1
21	0.98	-33.3	8.3	-41.4	-9.3	0.0	-32.1	6.8	2	1	1
22	1.97	-33.3	16.1	-49.3	-11.3	-2.3	-36.7	6.3	11	2	4
23	0.74	-33.3	13.0	-46.2	-8.2	-0.3	-37.7	9.5	13	1	2
24	1.85	-33.2	8.7	-41.9	-5.4	-6.2	-30.3	7.8	8	2	0
25	1.34	-33.2	11.4	-44.6	-9.4	-2.6	-32.6	6.8	12	1	2

Table 2.1: Output numbers of the first step of bound docking of BHG using Full Monte Carlo search algorithm. Rank number 2 is the optimal hit with the highest score of 4. The best value (B_V) has been shown with red color; numbers at interval value of (Bv±2) have been shown in yellow

*: E_{ass}: Total estimated binding energy kJ/mol; LE: Conformation energy of the ligand kJ/mol; vdW: van der Waals energy kJ/mol; vdW+: Positive van der Waals energy kJ/mol; E_{est}: Electrostatic energy kJ/mol; E_{cnt}: contact energy of interactions kJ/mol; E_{nbd}: Total energy of non-bonded interactions kJ/mol; Nhph: Number of hydrophobic contacts; Nhyd: Number of hydrogen bonds; Score: Total score of each hit (S_{Total})

3 LMCS steps

Rank	RMSD	Eass*	LE*	Enbd*	vdW*	Eest*	Ecnt*	vdW+*	Nhph*	Nhyd*	Score*
1	0.64	-57.7	6.6	-64.3	-10.4	-15.8	-38.1	7.7	14	3	5
2	1.64	-56.0	5.9	-61.9	-5.6	-23.0	-33.3	9.8	15	3	2
3	1.82	-54.5	7.5	-62.0	-8.8	-18.6	-34.9	7.8	15	4	3
4	0.57	-54.5	9.3	-63.8	-10.2	-15.4	-38.2	8.4	14	2	5
5	0.79	-54.0	6.4	-60.4	-10.2	-13.7	-36.8	7.3	15	2	4
6	1.39	-53.8	10.3	-64.2	-9.2	-19.7	-35.3	7.7	13	4	4
7	1.31	-53.6	9.5	-63.1	-5.7	-24.9	-32.5	9.1	14	3	4
8	1.47	-53.6	7.6	-61.2	-4.3	-28.0	-31.8	9.7	15	3	2
9	1.55	-53.5	10.0	-63.6	-4.5	-25.8	-33.3	11.1	15	3	3
10	0.71	-53.3	5.5	-58.8	-7.5	-17.2	-34.1	8.5	12	3	2
11	1.58	-52.9	7.6	-60.4	-4.3	-23.5	-32.7	10.8	13	3	1
12	1.59	-52.8	9.4	-62.2	-2.4	-23.9	-35.9	14.9	12	3	1
13	1.25	-52.7	10.0	-62.8	-7.1	-22.7	-32.8	7.9	15	3	3
14	1.31	-52.5	6.2	-58.7	-6.3	-20.3	-32.0	8.8	13	3	2
15	1.77	-51.9	10.2	-62.1	-4.2	-23.8	-34.1	11.6	15	4	2
16	0.72	-51.9	5.2	-57.1	-6.7	-16.6	-33.8	8.3	13	2	2
17	1.45	-51.9	6.7	-58.6	-4.0	-22.4	-32.2	10.9	14	4	1
18	1.20	-51.7	9.4	-61.1	-5.9	-22.6	-32.6	9.5	14	3	1
19	0.86	-51.6	6.2	-57.8	-5.7	-18.5	-33.6	9.2	12	3	1
20	2.41	-51.5	4.7	-56.3	-1.2	-21.3	-33.7	13.7	14	3	1
21	1.69	-51.3	12.4	-63.8	-8.8	-18.9	-36.3	8.8	14	3	5
22	0.86	-51.3	5.9	-57.2	-9.9	-10.7	-36.8	7.8	13	2	4
23	2.04	-51.2	11.2	-62.4	-3.4	-25.8	-33.2	11.7	12	4	2
24	1.86	-51.0	11.5	-62.5	-5.3	-21.1	-36.1	12.0	15	3	2
25	1.43	-50.9	7.3	-58.2	-3.4	-23.0	-31.8	11.1	13	3	1

Table 2.2: Output numbers after three steps of bound docking of BHG using local Monte Carlo search algorithm. Rank number 1 is the optimal hit with the highest score (5). The best value (B_V) has been shown with red color; numbers at interval value of (Bv±2) have been shown in yellow

Bound docking of BHG using MSD by employing LMCS generates the solution with RMSD of 0.76 Å (right in Figure 2.3) that is better than using one step MC with RMSD of 1.72 Å (left in Figure 2.3).

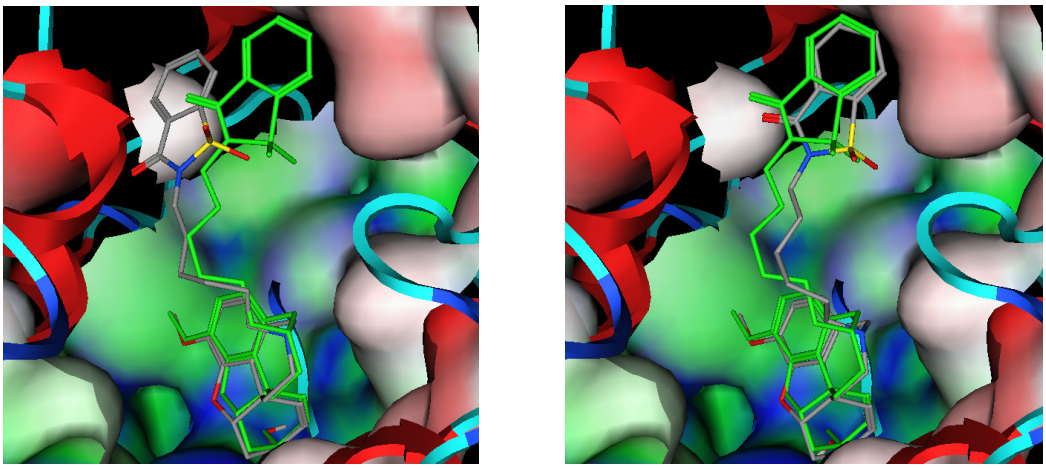

Figure 2.3: The overlaid structures of docking solution of the first step run (left) and the docking solution of the last step docking experiment using MSD (right) on the X-ray structure (green).

2.4 Study on the importance of data filtration by bound docking of BHG

For studying the effect of the selected starting point on the last result of MSD, two further MSD experiments were performed by docking the ligand (BHG) into its complexed protein. In experiment A, with Multi-Step Docking of First rank (MSDF), the first rank hit was always the starting point. In experiment B, with Multi-Step Docking of Selected hit (MSD), the solution with the highest S_{Total} was always the starting point of the next iteration.
Experiments A and B were performed as MSD run. The value at the final LMCS result as given in Table 2.3, which proves experiment B not only yields the better RMSD but also has the higher S_{Total} (red numbers in Table 2.3).

Docking solution	experiment	RMSD(Å)	E_{ass}	LE	vdW	E_{cnt}	E_{est}	vdW^{+}	Nhph	Nhbd
1	A (MSDF)	1.63	-57.1	4.8	-5.5	-23.2	-33.1	9.2	15	2
2	B (MSD)	0.64	-57.7	6.6	-10.4	-15.8	-38.1	7.7	14	3

Table 2.3: Numerical output data of experiment A, with Multi-Step Docking of First rank (MSDF) and experiment B, with Multi-Step Docking of Selected hit (MSD)

As illustrated in Figure 2.4 (upper), the third step of the experiment B produces the best answer with the lowest total estimated binding energy. By running additional steps, after third one, the absolute magnitudes of the energies as well as the rank of the highest scored hit (S_{Total}) are increased. From the third step on, if the experiment, by purpose additionally be continued, in the sixth step, it reaches almost to the same value as the third step of the experiment B (MSD). Figure 2.4 (upper) demonstrates that in experiment B the values of energies (MSD, blue bars) are decreasing until experiment 3 with very low RMSD 0.64 Å (lower diagram in Figure 2.4), whereas experiment A (MSDF) reaches to the lowest value of the energy in the experiment 2 of multi-step docking with a high value of RMSD 1.63 Å (lower diagram in Figure 2.4).

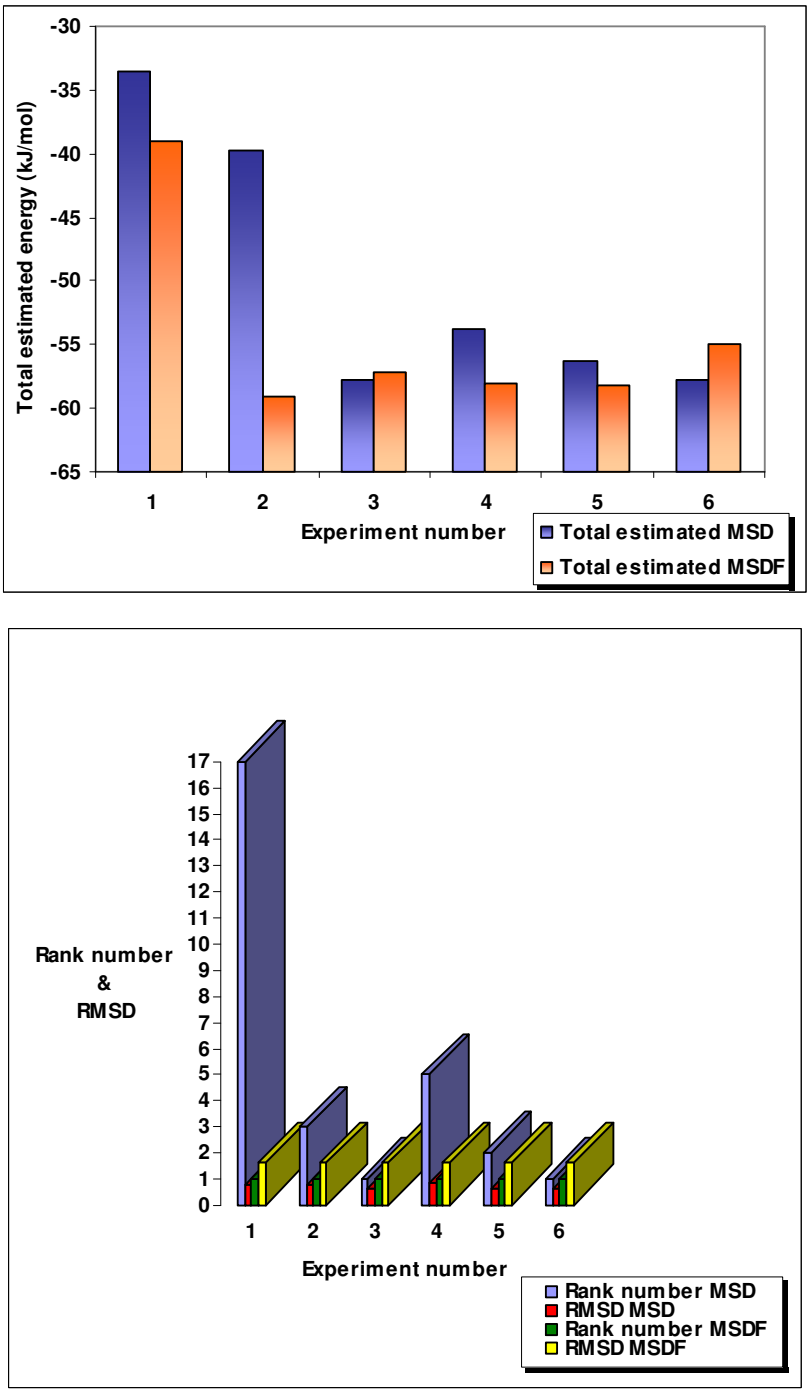

Figure 2.4: The variation of the total estimated binding energy (the upper plot), rank number and RMSD (the lower plot) when applying multi-step docking of BHG into its corresponding protein, using first rank answer (Experiment A or MSDF) and selected hit (Experiment B or MSD) for starting point

The differences among the RMSDs in experiment A (MSDF) and B (MSD) at the lower diagram in Figure 2.4 (red and yellow squares), demonstrate the priority of using MSD with selected conformation (see height-difference among red and yellow squares in the lower diagram, Figure 2.4). This means using the first rank answer for MSDF predicts the wrong

answer. Since in MSDF always the first rank hit is taken for the next iteration, therefore there is no particular way to recognize the step, which provides the best possible docking solution. In other word, for MSDF there is no limitation for the number of docking steps

2.5 Unbound docking study on BHG

To study if the Multi-Step Docking procedure is applicable as a predictive method, the unbound docking experiment of BHG was carried out into 1EVE [39].

1EVE is the X-ray structure of *Tc*AChE complexed with E2020 that was selected as the target protein. This was because E2020 is a long ligand that occupies a large space in binding site of AChE, which seems to be suitable enough for accommodation of BHG, as well.

In the case of docking BHG in the binding pocket of 1EVE, a total of 12 steps were necessary, 1 full and 11 local Monte Carlo runs, to generate the final answer (Figure 2.5). The detailed energy values and the calculated S_{Total} of all the hits from the first and the twelfth step are shown in Table 2.4 and Table 2.5, respectively. The docking experiment was stopped, when the first rank docking solution has the highest S_{Total} and no improvement in the ligand energy was observed (experiment Nr. 12 in Figure 2.6), such that the hit with the highest S_{Total} (Table 2.4, 5^{th} rank) moves to the first rank (Table 2.5, 1^{st} rank). In accord with the definition of the *Boltzman* factor, the final answer should have the highest population among all binding-modes. The total estimated binding energy and the ligand energies of the 13 runs are shown in Figure 2.6 along with the corresponding rank number.

Rank	RMSD	Eass*	LE*	Enbd*	vdW*	Eest*	Ecnt*	vdW+*	Nhph*	Nhyd*	Score*
1	1.72	-48.8	5.2	-53.9	4.3	-21.1	-37.1	20.3	14	2	2
2	1.51	-47.7	9.0	-56.3	-1.9	-16.4	-38.0	15.3	13	3	4
3	0.88	-46.2	3.3	-49.6	-1.0	-13.6	-35.0	13.8	11	2	1
4	1.62	-46.0	6.2	-52.2	4.5	-18.8	-36.9	20.9	14	2	2
5	0.77	-46.0	9.3	-55.3	-3.8	-12.0	-39.5	14.8	15	2	5
6	1.35	-45.9	10.6	-56.5	-1.1	-18.3	-37.1	15.8	13	3	2
7	1.72	-45.9	6.3	-52.2	0.7	-15.7	-37.2	17.6	13	3	1
8	1.87	-45.8	7.2	-53.0	-3.0	-15.1	-34.9	13.1	11	2	2
9	1.64	-45.3	5.5	-50.8	5.2	-19.8	-36.1	21.3	13	3	2
10	0.93	-45.2	5.5	-50.7	-1.5	-11.2	-37.0	16.1	12	1	1
11	0.73	-45.1	5.4	-50.4	-2.3	-12.5	-35.6	14.4	11	2	2
12	0.71	-45.0	8.5	-53.5	-0.2	-14.5	-38.8	17.1	15	1	2
13	1.33	-44.5	8.2	-52.7	2.8	-19.7	-35.8	19.0	13	3	2
14	1.38	-44.4	4.3	-48.7	1.3	-14.3	-35.7	17.1	12	3	0
15	1.49	-44.4	7.3	-51.7	5.1	-21.1	-35.7	20.6	13	2	2
16	1.09	-44.2	7.9	-52.1	-3.7	-9.5	-39.0	14.0	13	3	4
17	1.54	-44.0	7.2	-51.2	4.4	-18.6	-37.0	21.0	13	2	1
18	1.46	-43.5	9.0	-52.6	-3.2	-15.9	-33.5	13.0	12	3	2
19	1.56	-43.0	6.6	-49.6	1.3	-14.3	-36.5	17.6	14	3	1
20	1.25	-42.9	4.5	-47.5	-0.2	-11.6	-35.6	15.7	11	3	0
21	0.96	-42.6	4.1	-46.7	-1.6	-12.5	-32.6	12.9	11	2	1
22	1.74	-42.5	6.4	-48.9	2.9	-15.5	-36.3	20.1	12	2	0
23	1.32	-42.4	5.4	-47.8	0.1	-12.4	-35.6	15.5	12	3	0
24	1.03	-42.3	4.3	-46.6	0.5	-10.9	-36.2	16.6	13	3	1
25	1.01	-42.3	5.7	-48.1	-0.1	-13.5	-34.5	15.1	9	3	0

Table 2.4: Outputs of the first 25 hits, after first step full Monte Carlo. Rank number 5 is the selected hit with the highest score (5). ; Best value (B_V) has been shown with red color; numbers at interval value of (Bv±2) have been shown in yellow

*: E_{ass}: Total estimated binding energy kJ/mol; LE: Conformation energy of the ligand kJ/mol; vdW: van der Waals energy kJ/mol; vdW+: Positive van der Waals energy kJ/mol; E_{est}: Electrostatic energy kJ/mol; E_{cnt}: contact energy of interactions kJ/mol; E_{nbd}: Total energy of non-bonded interactions kJ/mol; Nhph: Number of hydrophobic contacts; Nhyd: Number of hydrogen bonds; Score: Total score of each hit (S_{Total})

11 LMCS steps

Rank	RMSD	Eass*	LE*	Enbd*	vdW*	Eest*	Ecnt*	vdW+*	Nhph*	Nhyd*	Score*
1	0.76	-55.1	0.0	-58.1	-3.4	-12.1	-30.6	14.7	14	2	4
2	0.73	-50.4	0.0	-50.4	-2.5	-12.5	-35.4	14.0	11	2	1
3	1.73	-48.9	5.0	-53.9	4.3	-21.1	-37.1	20.3	14	3	2
4	1.5	-47.8	8.8	-56.6	-2.3	-16.8	-37.5	14.8	13	4	3
5	1.8	-46.2	6.3	-52.5	1.4	-16.0	-37.9	18.5	13	3	1
6	1.32	-45.9	10.3	-56.3	-1.0	-18.1	-37.1	15.9	13	3	2
7	0.87	-45.9	3.4	-49.3	-0.4	-14.1	-34.8	14.2	11	2	0
8	1.86	-45.9	7.0	-52.9	-3.2	-15.1	-34.6	12.6	11	2	2
9	1.24	-45	8.7	-53.8	0.4	-17.5	-36.6	17.1	14	3	1
10	0.74	-44.8	4.3	-49.1	-1.9	-12.9	-34.3	13.6	11	2	1
11	0.88	-44.5	5.8	-50.3	-1.2	-10.7	-38.8	16.5	14	2	2
12	1.4	-44.4	4.5	-48.9	1.8	-15.0	-35.7	17.7	12	3	0
13	1.6	-44.4	7.1	-51.5	1.1	-15.4	-37.1	17.9	13	4	1
14	1.44	-44.2	8.0	-52.2	-4.3	-14.8	-33.2	11.6	12	3	2
15	1.51	-44.0	7.2	-51.2	4.0	-18.3	-36.9	20.6	13	2	1
16	1.91	-43.9	8.5	-52.4	-3.0	-14.7	-34.8	12.9	11	3	2
17	1.33	-43.9	8.1	-51.9	4.2	-21.0	-35.2	19.9	14	3	2
18	1.05	-43.4	8.0	-51.4	-0.7	-13.7	-37.0	16.2	13	3	1
19	1.3	-42.7	9.2	-51.8	3.3	-18.6	-35.6	19.3	15	3	2
20	1.43	-42.5	7.0	-49.6	5.8	-18.8	-35.5	21.4	14	3	2
21	1.32	-42.5	7.0	-49.5	-3.2	-13.6	-32.7	12.2	12	2	2
22	0.92	-42.5	7.3	-49.8	-0.4	-11.5	-37.9	16.2	14	1	1
23	1.03	-42.4	4.3	-46.8	-0.1	-10.2	-36.4	16.5	13	3	1
24	1.67	-42.4	6.8	-49.1	-1.1	-11.4	-36.7	14.8	13	2	1
25	0.94	-42.3	11.1	-53.4	-1.4	-11.9	-40.1	16.9	14	2	2

Table 2.5: Output numbers after eleven runs with local Monte Carlo. Rank number 1 is the optimal hit with the highest score (4) and the ligand energy (LE) of 0.0 kJ/mol; Best value (B_V) has been shown with red color; numbers at interval value of (Bv±2) have been shown in yellow

*: E_{ass}: Total estimated binding energy kJ/mol; LE: Conformation energy of the ligand kJ/mol; vdW: van der Waals energy kJ/mol; vdW+: Positive van der Waals energy kJ/mol; E_{est}: Electrostatic energy kJ/mol; E_{cnt}: contact energy of interactions kJ/mol; E_{nbd}: Total energy of non-bonded interactions kJ/mol; Nhph: Number of hydrophobic contacts; Nhyd: Number of hydrogen bonds; Score: Total score of each hit (S_{Total})

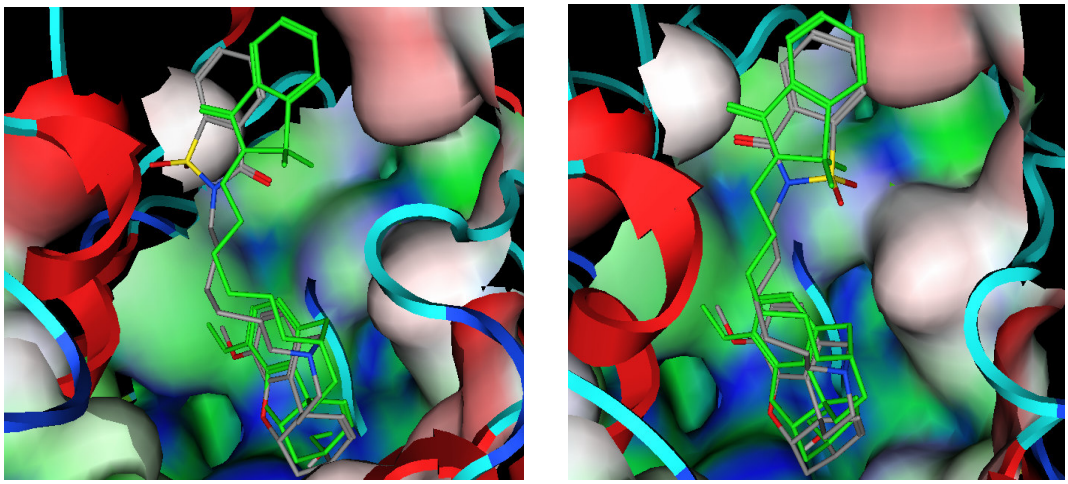

Figure 2.5: The structure of the first rank answer of one step MC from docking BHG into 1EVE with S_{Total} of 5, colored in gray (left), the structure of the first hit with the highest score (4) obtained after 12 steps LMC colored in gray (right) each overlaid on X-ray structure (colored in green)

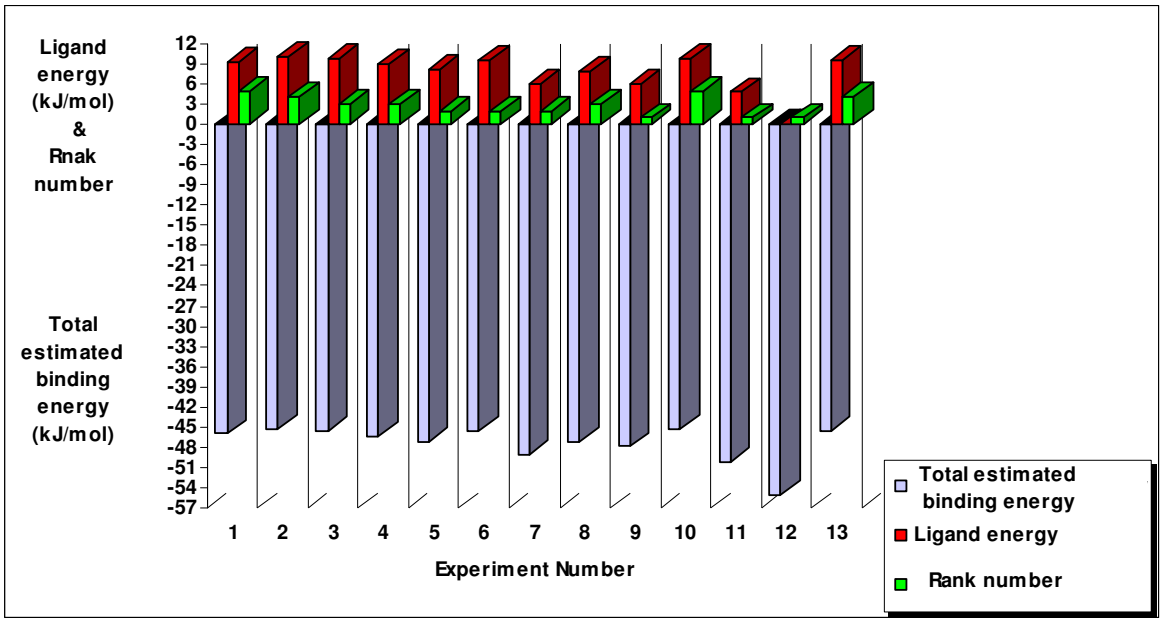

Figure 2.6: Displays the variation of total estimated binding energy and ligand energy with the corresponding rank number, resulting from multi-step docking of BHG into the binding site of 1EVE. The minimum value was obtained in the 12th step, where the answer with the highest S_{Total} appeared in the first rank

2.6 Importance of selection a suitable protein for unbound docking

To study the effect of selection a suitable X-ray structure of protein for unbound docking the next set of experiments were performed, for which, firstly three different *Tc*AChE crystal structures (1DX6 [40], 1QTI [41], 1EVE [39] were chosen as our target proteins. Among these three X-ray structures only 1EVE is the one with a long ligand that covers almost the entire space of the AChE-gorge, while 1QTI and 1DX6 are acetylcholinesterase complexed with galanthamine, which are located in the bottom of the deep gorge.

Secondly, BHG was built up in two states at galanthamine nitrogen with axial and equatorial conformations. Then the two prepared ligand structures were individually docked into the binding site of three different *Tc*AChE crystal structures.

This was to identify the favorable conformation of the galanthamine nitrogen as well as the conformational pose of the entire ligand, independent of availability of crystal structure of the ligand-bounded protein. After running six individual MSD, the best solution of each one was taken as the final answer for the purpose of evaluation. Firstly, comparing the result of the experiments show that docking result of the ligand with axial conformation has higher S_{Total} than the ligand with equatorial conformation at galanthamine nitrogen (red numbers in Table 2.6 & 2.7). It means the binding mode, associated with ligand having axial conformation is more preferable than equatorial one. Therefore three entries, correspond to axial ligand,

(Docking solutions 3, 5 and 7, Table 2.6, Figure 2.7) should be taken into particular consideration.

Docking solution	protein	E_{ass}	LE	E_{nhb}	vdW	E_{est}	E_{cnt}	vdW^{+}	Nhph	Nhb
(3) a	1QTI	-60.2	1.2	-61.4	-14.1	-10.7	-36.6	3.9	15	1
(4) e	1QTI	-55.6	4.3	-59.8	-8.7	-15.4	-35.8	8.9	9	3
(5) a	1DX6	-64.3	3.9	-68.2	-6.7	-23.8	-37.8	11.5	12	3
(6) e	1DX6	-60.7	4.0	-64.7	-8.1	-18.6	-38.1	10.0	13	3
(7) a	1EVE	-55.1	0.0	-55.1	-3.4	-12.1	-39.6	14.7	14	2
(8) e	1EVE	-50.1	0.9	-51.0	-4.1	-16.5	-30.4	10.5	9	2

Table 2.6: Numerical data obtained from docking BHG with axial and equatorial conformation

Docking Solution	RMSD (Å)	Conformation	Orienation of saccahrin ring
(3) a	0.85	a	Inverted
(4) e	1.94	e	Off
(5) a	1.79	a	Off
(6) e	2.15	e	Off
(7) a	0.76	a	Correct
(8) e	3.07	e	Off

Table 2.7: Illustrates the connection of the conformational state at galanthamine nitrogen to the ring orientation in saccharin moiety of BHG

For this class of the unprotonated BHG (all axial), the conformational pose of the ligand from docking the BHG into 1EVE is suggested as the best docking answer. This solution is the only one with the minimum value of intra molecular energy of the ligand (0.0 kJ/mol, Table 2.6), having high possibility of being the native-like pose of the ligand in complex form [34] (red structure in Figure 2.7). RMSD calculation of the final solution with respect to X-ray structure of the ligand gives a value of 0.76 Å that confirms the accuracy of the unbound docking result. It is also the only answer with correct orientation of saccharin ring among the other docking solutions (Docking solution 7, Table 2.7).

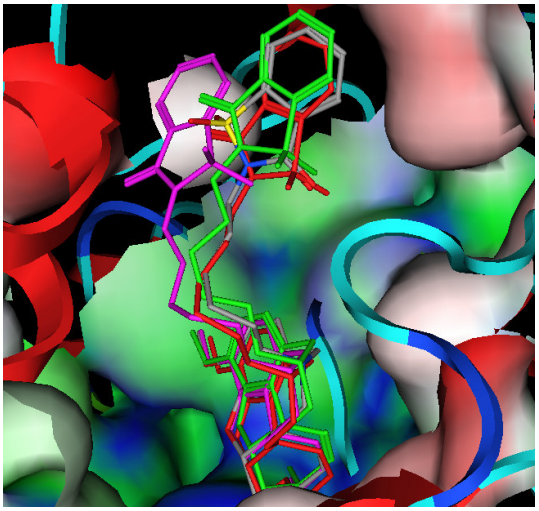

Figure 2.7: Obtained solutions of docking the axial BHG into 1DX6 (magenta), red (1EVE) and gray (1QTI), X-ray structure is green

The result of this experiment proves the significant role of the selected X-ray structure of the target protein, which should have a bounded ligand, whose occupied space in binding site be large enough for the desired ligand for the purpose of unbound docking.

2.7 A comparison between the result of unbound docking using simulated annealing (SA) and using MSD

In this step the selected conformation from the first step of the Monte Carlo Search (MCS), which was the 5th rank answer in Table 2.4 was utilized for the purpose of docking into a flexible binding site, through which the temperature allowed to be changed. In this experiment, temperature and flat-well radius (allowed radius for movement of binding site) must be carefully defined. Since this method mimics physical annealing, the key feature is reduction of temperature very slowly to achieve optimal solution with global minimum energy or to be trapped in good minima [35]. For the purpose of having a successful annealing, the optimal highest temperature should be found. Therefore, four individual docking runs with different starting temperatures were performed at 600, 500, 400 and 300 K. Then with a flat well radius of 0.1 Å, the system cooled down to 30 degrees. The results of the experiments show that the highest S_{Total} was obtained when the annealing temperature was defined to 600 K (Docking solution 12, Table 2.8). This means the optimal temperature for further annealing experiments is 600 K.

Docking solution	Temp (K)	RMSD (Å)	E_{ass}	LE	E_{nbd}	vdW	E_{est}	E_{cnt}	vdW^{+}	Nhph	Nhbd
9	300	1.90	-59.2	8.5	-67.8	-9.9	-20.6	-37.4	9.5	14	3
10	400	1.85	-59.8	9.2	-68.6	-7.0	-24.7	-36.9	10.6	13	3
11	500	0.88	-60.3	9.2	-69.7	-12.4	-18.3	-39.0	6.1	16	2
12	600	0.85	-60.6	9.1	-70.0	-12.5	-18.4	-39.0	6.4	16	2

Table 2.8: The numerical result of simulated annealing started from four different temperatures

To reveal the effect of a bigger flat-well radius, next experiment was performed with a 0.2 Å radius. The result again shows the higher S_{Total} for docking solution of 0.1 Å (Docking solution 12, Table 2.9) than the one with 0.2 Å radius (Docking solution 13, Table 2.9).

Docking solution	Flat-well (Å)	Temp (K)	RMSD (Å)	E_{ass}	LE	E_{nbd}	vdW	E_{est}	E_{cnt}	vdW^{+}	Nhph	Nhbd
12	0.1	600	0.85	-60.6	9.1	-70.0	-12.5	-18.4	-39.0	6.4	16	2
13	0.2	600	1.89	-65.2	9.0	-70.9	-7.8	-24.7	-38.4	10.5	13	3

Table 2.9: The numerical result of simulated annealing in 600 K with two different flat-well radiuses

According to the result of this experiment, the best solution was obtained at 600 K with 0.1 Å flat-well radius. Comparison of this solution with the result of the docking solution using MSD method reveals that the docking solution 12 in Table 2.9 does not correctly mimic the X-ray structure of the ligand in the benzosulfimide substructure of the BHG, although its RMSD obtained from QXP^{+} has a value of 0.85 Å (left in Figure 2.8), which has a wrong orientation in the benzosulfimido moiety of the ligand, while the result of MSD is correctly superimposed on the X-ray structure with RMSD of 0.76 Å (right in Figure 2.8).

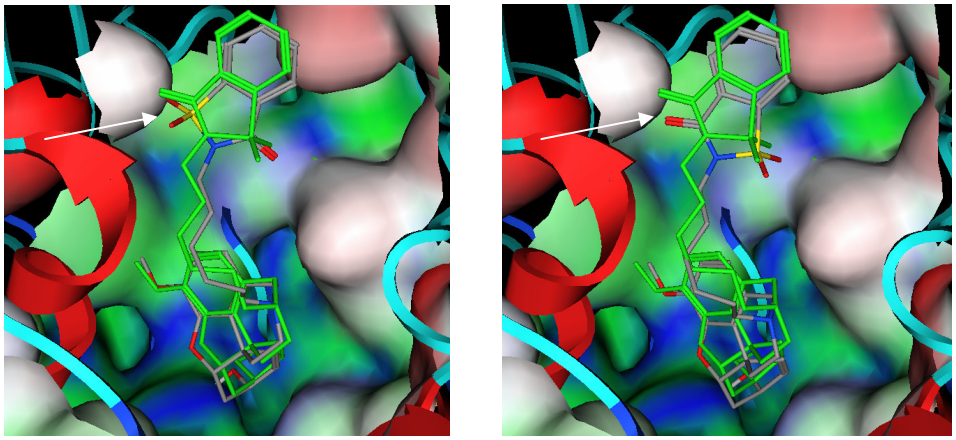

Figure 2.8: The answer of SA and MSD, each overlaid on X-ray structure (green). As can be seen the result of SA (left) has the wrong orientation in benzosulfimide moiety in the upper part of the ligand, whereas MSD results a correct pose of the ligand (right).

2.8 Comparison of the MSD result with various other docking methods

As is indicated in Table 2.10 and Figure 2.9, among five different docking method using three programs, FlexX, G.O.L.D, QXP^+ (one step, simulated annealing and multi-step docking), the best answer is obtained when MSD method was employed (Table 2.10).

Program	**Search Algorithm**	**Scoring Function**	***RMSD (Å)**	**Binding Site Flexibility**
QXP^+ (OSD)	Monte Carlo One Step	Amber Force Field	2.35	No
FlexX	Incremental Construction	Empirical Score	2.82	No
G.O.L.D	Genetic	Empirical Score	10.13	No
QXP^+ (SA)	Monte Carlo Simulated Annealing	Amber Force Field	1.71	Yes
QXP^+ (MSD)	Full and Local Monte Carlo Multi-Step Docking	Amber Force Field	0.79	No

Table 2.10: A comparison of docking results from FlexX, G.O.L.D and QXP+

*: RMSDs calculated by "DAG. v. 2" as a reference program

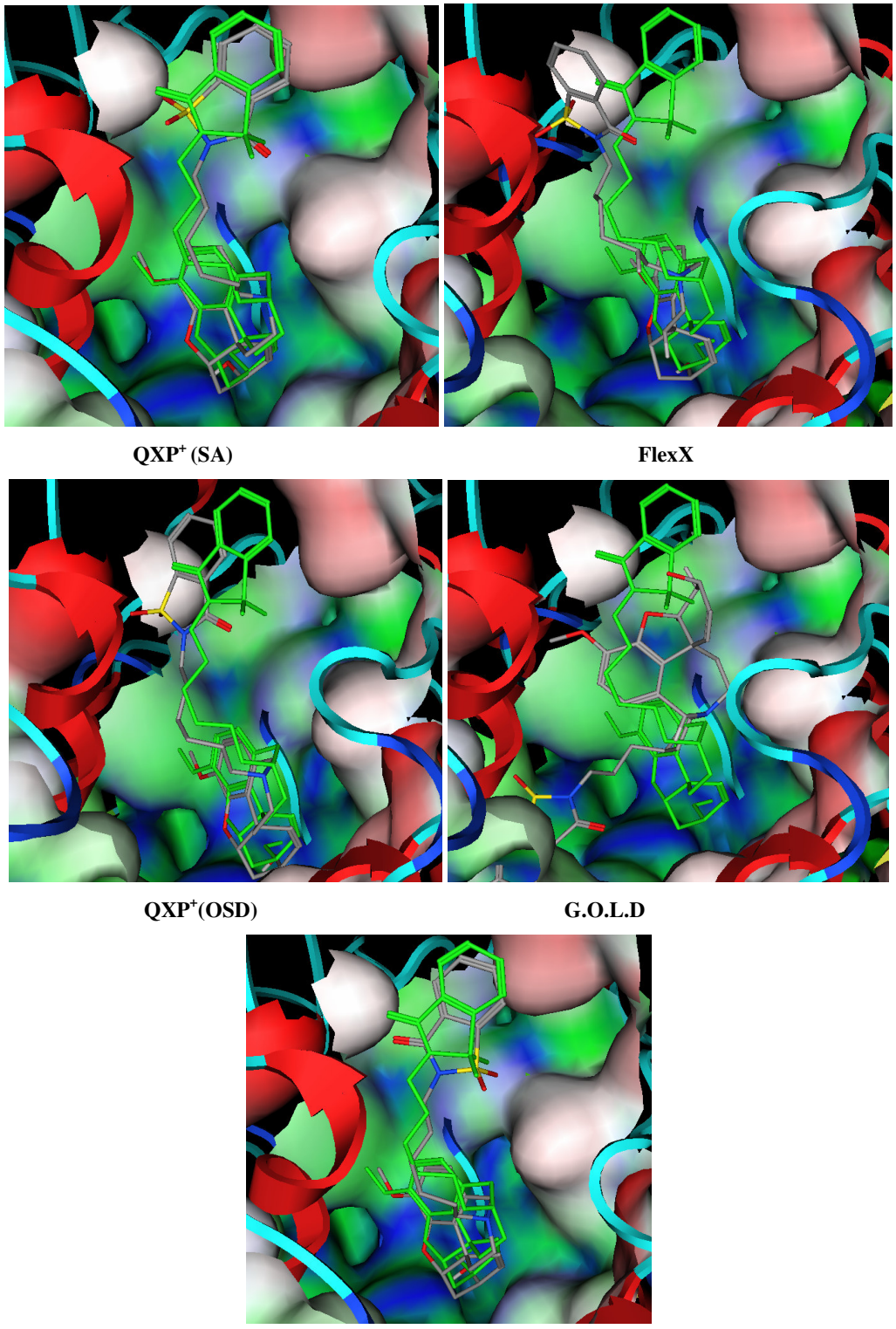

Figure 2.9: Docking solutions obtained from different docking programs (gray) overlaid on the X-ray structure of the BHG (green)

3 Evaluation of MSD Consensuses Approach

3.1 Application of MSD for elucidation of structural properties of (BHG)

As it was described in chapter 2, BHG is one of the galanthamine derivatives. Glanthamine was first isolated from snowdrops [42] and has long been known to exhibit esterase-blocking activity [43]. Jordis and Froehlich [44] have developed a sterospecific synthesis for a large-scale production of galanthamine that opened the door for therapeutic use of this compound, so that galanthamine is now commercially available as the fourth anti-Alzheimer drug.

Galanthamine is known not only to block the esterase activity, but also to display an allosteric potentiating effect on the nicotinic acetylcholine receptor (nAChR) [45]. This finding makes galanthamine a most valuable drug for Alzheimer treatment as this dual interaction enhances signal transmission of acetylcholine by twofold.

Inestrosa and coworkers [46] [47] have demonstrated that AChE, besides its established esterase cleavage activity, is also involved in the formation of β-amyloid plaques, which are known to play an essential role in the development of Alzheimer's dementia [48] [49].

Aggregation of this peptide seems to occur specifically at the peripheral anionic site (PAS) [50] [51] of AChE. More specifically, a 35 amino acids *Torpedo* derived peptide fragment corresponding to AChE-sequence position 274-308 is capable of amayloid complex formation [52]. However, Trp279 and Tyr70 play the most important roles in PAS located at the mouth of the gorge [53].

As it is shown in Figure 3.1, galanthamine binds to a region of the active site that is not connected to PAS, therefore there is no inhibition of β-amyloid plaque formation through application of galanthamine. In this respect, to improve capability of galanthamine to interact simultaneously with amino acids in the upper and the lower part of the gorge, new derivatives of galanthamine with long side chain are necessary to cover the entire gorge of AChE. With these aims molecular docking study have been reported on galanthamine derivatives, such as bis-galanthamines with varying lengths of a methylen spacer between two galanthamine moieties [54] as well as benzosulfimidohexylgalanthamine (BHG) [38].

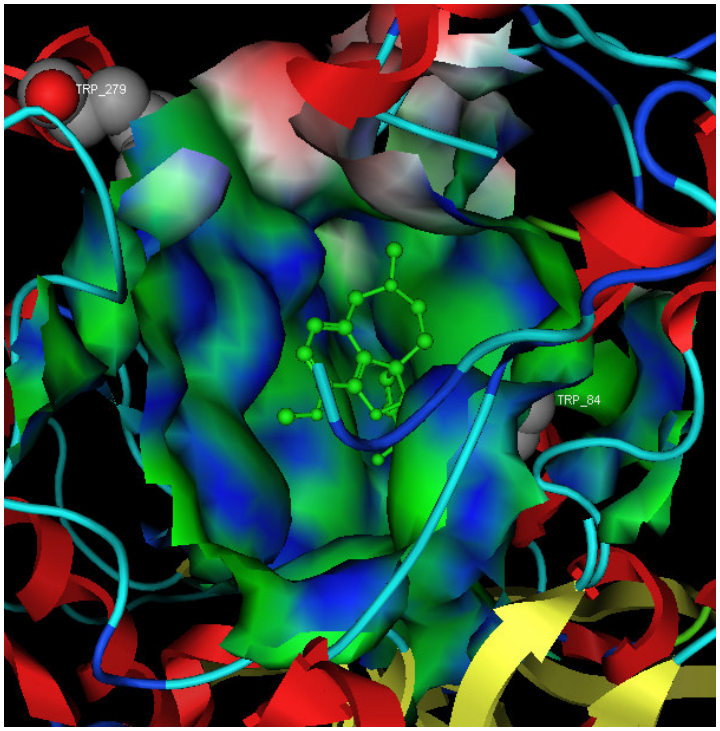

Figure 3.1: Galanthamine (green) is located in deep of the gorge without any interaction in rim of the gorge. Trp279 and Trp84, rendered in CPK, are located in PAS and quaternary ammonium subsite of the AChE binding site.

In this section the result of multi step docking of BHG will be presented, which was carried out to study on the possibility of the protonation in galanthamine moiety of the ligand. In this experiment the ligand is docked into the AChE-BHG complex [38] (bound docking). The obtained complex energy of the BHG-AChE will be compared to galanthamine and the other inhibitors of AChE. Furthermore, the most important water molecules will be identified and their contribution into the docking process will be investigated.

3.2 Bound docking experiment on BHG

Investigation on the BHG's binding mode was firstly carried out into the empty binding site of the AChE-BHG complex.

Docking* solution	Waters	RMSD (Å)	E_{ass}	LE	E_{she}	E_{nhb}	vdW	E_{est}	E_{cnt}	vdW^{+}	Nhph	Nhb	OSR**
1 (p)	empty	1.65	-56.2	7.0	0.0	-63.2	-6.6	-20.8	-35.8	10.2	13	3	off
2 (up)	empty	0.64	-57.7	6.6	0.0	-64.3	-10.4	-15.8	-38.1	7.7	14	3	Correct

Table 3.1: Numerical results of docking protonated and unprotonated ligand into empty binding site

*: 'p' stands for protonated and 'up' for unprotonated ligand

**: 'OSR'; stands for orientation of saccharin ring

The result of bound docking of BHG with protonated and unprotonated galanthamine into empty binding site is more in favor of unprotonated state as it shows that the unprotonated BHG has a lower RMSD 0.64Å (Docking solution 2, Table 3.1), when the protonated ligand has much higher RMSD of 1.65Å (Docking solution 1, Table 3.1).

3.3 Bound docking of BHG into binding site with waters

Furthermore, using QXP^+ six water molecules around BHG molecule was identified in the AChE gorge as the most important ones that are Wat17, Wat66, Wat121, Wat149, Wat289, and Wat230. These water molecules mediate interactions between amino acids in binding site and BHG atoms. In Figure 3.2, these waters are shown as red balls, while small blue balls represent all other water molecules in the protein. There are a total of 15 water molecules buried in the binding site of BHG (Figure 3.2, red and yellow balls). For comparison, Figure 3.2 (right) show six water molecules from the AChE complexed with ACh (2ACE) that correspond to the six most important waters in AChE-BHG complex, Wat603, Wat628, Wat643, Wat682, Wat719, Wat749 colored in cyan. The average displacement of them has a value of 1.21Å. Moreover, in the binding site of the native enzyme, 2ACE, there are 36 buried waters (middle in Figure 3.2) [55]. In Figure 3.2 (left and middle) the waters close to the wall of the active-site gorge (yellow balls) and their neighboring amino acids in 2ACE have been shown.

Comparing the position of these buried waters in two crystal structures shows that waters in 2ACE, close to Tyr70, Asp72, Gly118 and Glu199 are approximately in the same region as are in BHG (left and middle in Figure 3.2).

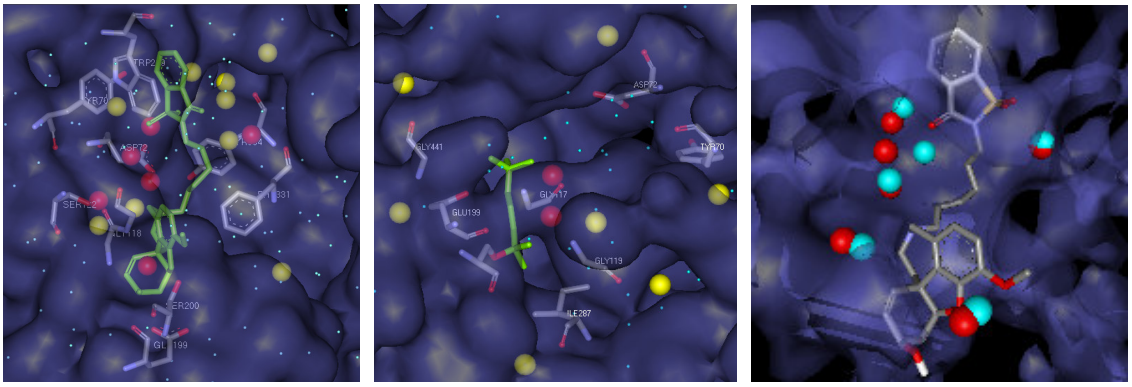

Figure 3.2: BHG with buried waters (yellow) and the six important waters included in docking (red), while the rest of the crystallographic waters are shown in blue (left); ACh, complexed with AChE (2ACE) with buried waters (yellow), two important waters interacting with ACh are in red, the rest of waters in X-ray structure have been colored in blue (the middle); Overlaid six important water molecules of the binding site of BHG (red) on their comparable waters in 2ACE coloured in cyan (right)

By contribution of the six important water molecules in bound docking of BHG, further steps of docking study were performed to analyze the effect of them on the possibility of protonation of galanthamine moiety in BHG. In this context, BHG in two different protonated and unprotonated states were individually docked into the binding site of the complexed protein. This means that two independent multi-step docking experiments were performed, in which either water hydrogens were defined flexible. The numerical results of the docking experiments are shown in Table 3.2.

From the result of docking the protonated BHG appears that for protonated ligand, in the case of docking into empty binding site, the docking solution is far from X-ray structure of the ligand (RMSD= 1.67 Å), while docking solution of the binding site with flexible water hydrogens has an upside down pose in binding site (RMSD= 12.26 Å) (Docking solution 3, Table 3.2).

In contrast, docking experiments on the unprotonated ligand generates answers with RMSDs less than 1.0 Å, in which one answer has only an inverted saccharine ring (Docking solution 4, Table3.2). In addition docking of both unprotonated and protonated ligands into the binding site with flexible waters generate correct answer with a RMSD lower than 1.0 Å for unprotonated ligand, while docking solution of the protonated BHG has upside down pose in binding site (data are not shown). Therefore the results are more in favor of the unprotonated state of the BHG rather than protonated one (Table 3.2).

Docking* solution	Waters	RMSD (Å)	E_{ass}	LE	E_{she}	E_{nhb}	vdW	E_{est}	E_{cnt}	vdW^{+}	Nhph	Nhb	OSR**
3 (p)	Flexible hydrogen	12.26	-40.1	4.1	-0.1	-44.1	-4.9	-21.8	-17.3	3.8	4	2	off
4 (up)	Flexible hydrogen	0.90	-63.3	3.7	7.1	-74.0	-5.5	-26.6	-41.9	15.0	12	5	Inverted

Table 3.2: Numerical results of docking protonated and unprotonated ligand in presence of waters in binding site

*: 'p' stands for protonated and 'up' for unprotonated ligand

**: 'OSR'; stands for orientation of saccharin ring

Possibility of protonation of an atom strongly depends on its position in the ligand structure and on its particular position with respect to the neighboring amino acids in the binding site. Depending on the residues surrounding the ligand, the p*Ka* value could vary (Figure 3.3) [56] [57] [58].

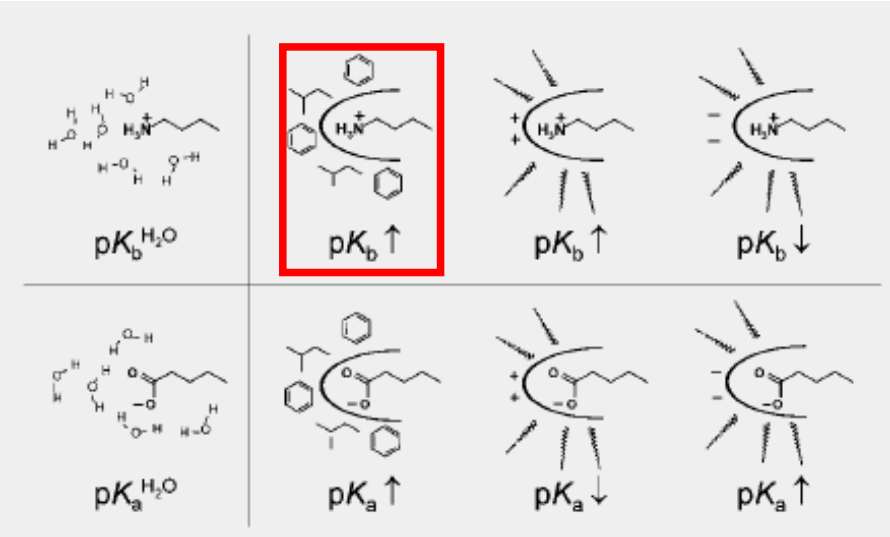

Figure 3.3: Impact of the protein environment on the pK_a values of a basic ligand group (upper row) and pK_a values of an acidic ligand group (lower row) compared to aqueous solution [58]

Generally, weaken in the basicity of the ligand in its complexed state can occur, because of the influence of surrounding aromatic amino acids (Figure 3.3). It can be also observed in Figure 3.4 that galanthamine moiety is surrounded by aromatic amino acids of binding site, which is very similar condition to the Figure 3.3 (in red square). The pK_a value of galanthamine in aqueous solution is 8.2 [59]. However, according to its position as a substructure in BHG and location of that in neighborhood of aromatic residues of the gorge, it loses some basic strength. This confirms the finding in previous step, as a result of docking study on BHG, the unprotonated BHG is the reliable state.

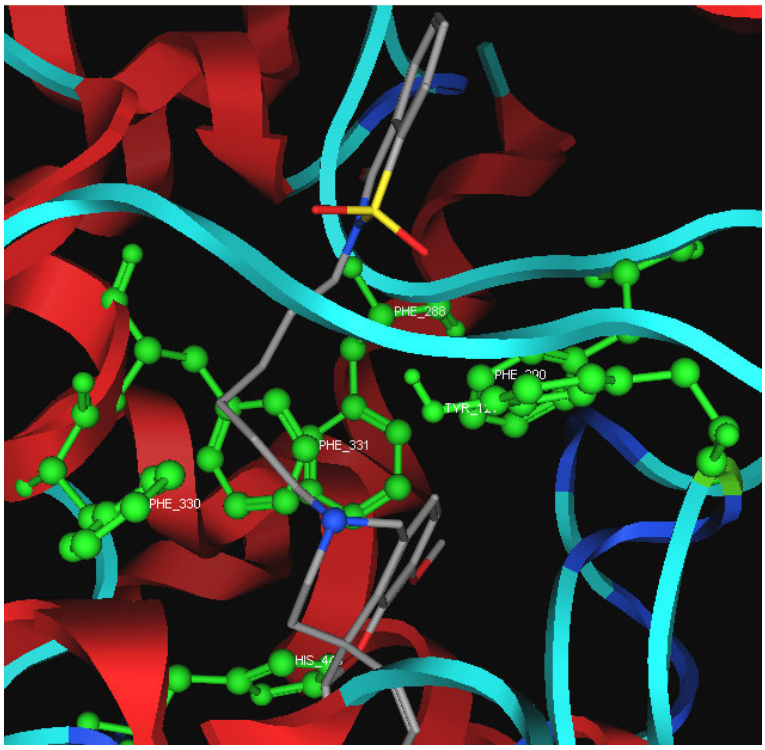

Figure 3.4: Shows the belt-like location of aromatic amino acids surrounding BHG, which affect on the pK_b value of galanthamine and its protonation state

Result of docking the galanthamine into 1QTI also confirms our finding in previous step, because it shows that unprotonated galanthamine is also the dominated state of the ligand (Table 3.3).

In docking protonated and unprotonated galanthamine into 1QTI, four most important crystallographic water molecules, Wat712, Wat756, Wat764, Wat803, were also included, in which waters were flexible, to consider whether the presence of the waters around the galanthamine allow that galanthamine becomes protonated at all.

Docking* solution	Waters	RMSD (Å)	E_{ass}	LE	BE	E_{nhb}	vdW	E_{est}	E_{cnt}	vdW^{+}	Nhph	Nhb
5 (up)*	Flexible	0.25	-45.9	0.6	0.1	-46.6	-6.3	-18.1	-22.2	5.2	4	2
6 (p)	Flexible	17.63	-40.4	0.2	0.0	-40.6	1.4	-36.1	-5.9	4.5	0	3

Table 3.3: Result of docking galanthamine into 1QTI

*: 'up' stands for unprotonated and 'p' for protonated

In docking experiment on galanthamine with protonated nitrogen, when the waters are flexible, the docking solution of the ligand is placed completely out of the binding site

(Docking solution 6, Table 3.4, whereas unprotonated galanthamine has a docking solution with a very low RMSD (0.25Å) in docking solution 5 in Table 3.3.

The results of docking galanthamine clear that in presence of the effective water molecules of binding site, there is no chance for protonated galanthamine to complex with protein within the active site gorge.

To study the efficacy of different inhibitors of AChE to interact with the binding site, the total non bonding interaction energies of them can be compared. Since the ligands are different therefore the ligand energy is subtracted from total estimated binding energy, which results total nonbonding interaction energy **(E_{nbd})**. These data are shown in the following plot. The five different inhibitors of AChE were chosen for the purpose of comparison, which are E2020, decamethonium, galanthamine, piperidinopropylgalanthamine (PPG) [38] and BHG, among which the most stable complex corresponds to BHG (Figure3.5).

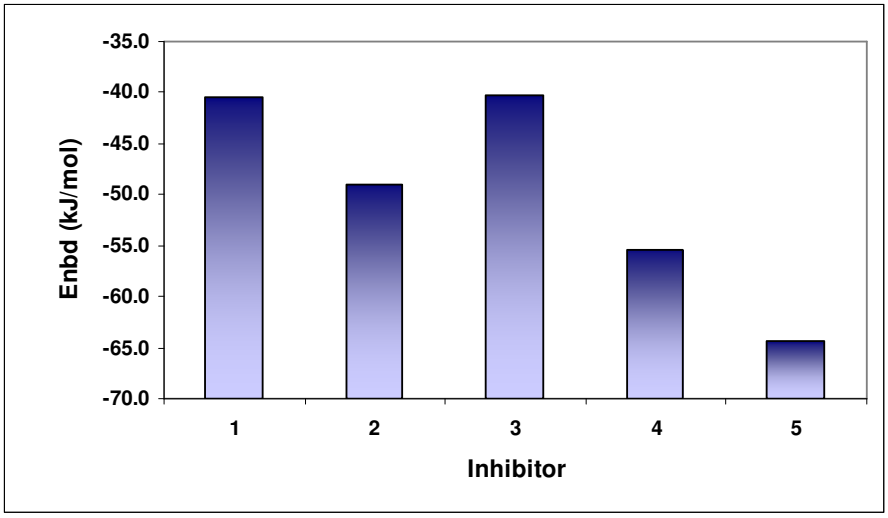

Figure 3.5: Displays difference in total non-bonded interaction energy among various inhibitors of AChE, according to their corresponding docking results.

1; Decamethonium, 2; E2020, 3; Galanthamine, 4; PPG, 5; BHG

The low complexation energy is not the only important feature of an inhibitor, but also it should be able to cover entire active-site gorge and interact with PAS amino acids in the rim of the active-site gorge in AChE. Figure 3.6 illustrates the overlaid docking solution of E2020 (see section 3.4), PPG (see chapter 4), BHG and galanthamine. Galanthamine only interacts with amino acids in the base of the gorge, while another derivative of galanthamine, PPG with a propylpiperidino substructure has a bent pose that prevents PPG of any access to the rim of the gorge and PAS, whereas BHG has a suitable ring stacking interaction with Trp279 with -

20 kJ/mol interaction energy, which works out better than of that in E2020 with interaction energy of -16.9 kJ/mol. Since amino acids in PAS (Trp279 & Tyr70) are believed to be responsible for β-amyloid plaque formation a suitable inhibitor of AChE would be thus more valuable if it can interact with PAS in the rim of the gorge. Therefore BHG seems to be valuable inhibitor of AChE.

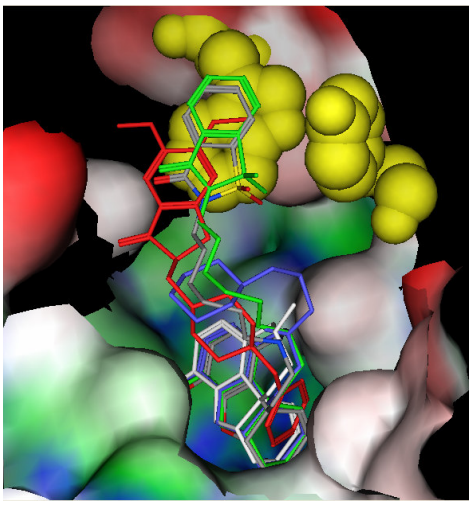

Figure 3.6: Displays galanthamine (white); E2020 (red), PPG (blue) and BHG (green). Trp279 and Tyr70 are shown in yellow color

In summary BHG is a more potent inhibitor of AChE than other AChE inhibitors such as E2020, decamethonium, galanthamine and its derivative PPG. This is according to their relative binding energies, obtained from docking experiments of each above-mentioned ligand. Docking solutions in presence the water molecules in the binding site suggest that unprotonated ligand is the favored state for binding BHG to AChE. Employing MSD for the purpose of unbound docking led to a successful prediction of the correct conformational pose by docking BHG into 1EVE. Furthermore, it demonstrated the axial conformation of the ligand generates better answer than equatorial conformation with respect to S_{Total} and RMSD values. Comparison of the final docking solution with the crystal structure gives the RMSD value of 0.76 Å. The successful result of MSD method makes it a promising approach for further application of that to design more potent inhibitors.

3.4 Docking study on E2020

The first two drugs, approved by FDA, for treatment of AD were tacrine (THA) and the more potent inhibitor of AChE, E2020, which are both reversible inhibitors of AChE.
E2020 with trivial name of donepezil hydrochloride was approved in 1996 [60], which the three-dimensional structure (3D) of its complex with *Tc*AChE deposited in Protein Data Bank has been coded with 1EVE [39]. Figure 3.7 indicates that the chemical structure of the molecule is constructed by three main components, which are dimethoxyindanone, piperidine and benzyl moieties.

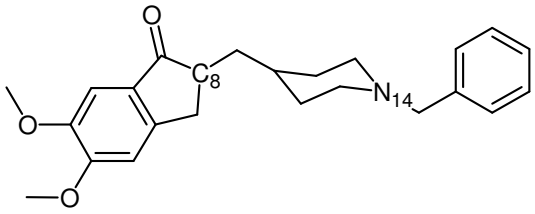

Figure 3.7: Chemical structure of E2020

Atom at position number 8 is a chiral carbon. The reported pharmacological studies on (*R*, *S*)-E2020 emphasize that both enantiomers are active and have similar pharmacological profiles [61]. The *S* configuration of this inhibitor shows five fold more inhibitors constant 17.5 nM versus 3.35 nM inhibitory constant for *R*-configuration [62]. Using docking technique and MSD method, the configurational state of the molecule at C8 as well as the possibility of protonation at N14 are taken into consideration.

3.4.1 Study on the configuration state of the molecule at C8

For the molecule, two individual series of MSD experiment were carried out, in which the ligand was considered with two possible configurations (*R* and *S*) at C8. It was docked into the binding site of the enzyme after removing any crystallographic water molecules. The numerical results of the last step of experiment are shown in Table 3.4.

Docking* Solution	RMSD (Å)	E_{ass}	LE	E_{nbd}	vdW	Eest	Ecnt	vdW+	Nhph	Nhb
7- (up)-*R*	0.89	-47.1	2.0	-49.1	-12.6	-5.7	-30.8	2.8	11	1
8-(up)-*S*	2.38	-36.8	4.5	-41.2	-10.8	-1.1	-29.3	3.0	13	0

Table 3.4: Shows the numerical result of MSD of the inhibitors in two individual experiments in which E2020 has either *R* or *S* configuration at C8.

*: 'up' stands for unprotonated

The calculation results show that the binding mode of E2020 with *R* configuration has higher S_{Total} than E2020 with *S* configuration (red numbers in Table 3.4). The RMSD of the former (0.89 Å) is also less than the later (2.38 Å), which are docking solution 7 and 8 in Table 3.4, respectively (Figure 3.8).

Figure 3.8: The overlaid X-ray structure of E2020 (green) on the docking solution of E2020 with *S* configuration (left) and the solution with *R* configuration (right)

Now, it should be studied that what would be the result, if E2020 were protonated at N14.
To answer this question some further experiments were carried out with protonated ligand at N14.

3.4.2 Study on the protonation state at E2020-Nitrogen

To answer the question of the possibility of protonation at E2020-nitrogen, two series of individual MSD runs were performed. In these experiments E2020 was protonated at N14 and the configuration at C8 was set to *R* or *S*, respectively. As it can be seen from Table 3.5 the protonated ligand with *S*-configuration should be rejected, on the basis of its corresponding RMSD value (10.48 Å) and even the protonated ligand with *R*-configuration that shows RMSD= 2.02 Å (Docking solution 9 in Table 3.5). These docking experiments are well in line

with crystallographical data that is confirmed by 0.89 Å RMSD (Docking solution 7 in Table 3.4), however, in addition, it can prove that E2020 will not be protonated in the binding state.

Docking Solution	RMSD (Å)	E_{ass}	LE	E_{nbd}	vdW	Eest	Ecnt	vdW+$^{+}$	Nhph	Nhb
9-(p)-*R*	2.02	-51.2	7.4	-58.5	-8.7	-19.6	-30.3	5.3	12	1
10-(p)-*S*	10.48	-44.2	0.7	-44.8	-2.1	-30.1	-12.6	4.9	5	2

Table 3.5: The numerical result of MSD of the inhibitor in two individual experiments in which the ligand has either *R* or *S*-configuration at C8 with protonated nitrogen;*: 'p' stands for protonated

3.4.3 Effect of the environment on the conformational pose of E2020

In this step, to consider the effect of the environment of the ligand on its position within the binding site gorge, the most important crystallographical water molecules were identified. These waters directly interact with the ligand and have a bridge-like role to mediate the interactions among the ligand atoms and its environment. The codes of the six most important waters in the corresponding crystal structure are Wat1159, Wat1160, Wat1249, Wat1254, Wat1255 and Wat1347, whose position in the binding site are shown in Figure 3.9.

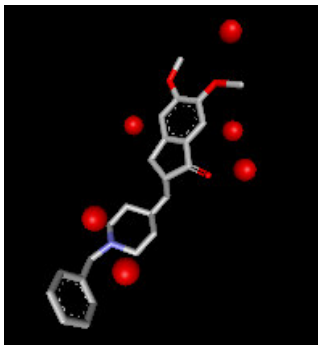

Figure 3.9: The six important water molecules around E2020 in the binding site gorge, rendered in CPK

Due to important effect of waters in binding site, the binding mode of the ligand and its structural properties were studied in the presence of the six water molecules, which interact with the ligand in the X-ray structure. For this purpose, the optimization of the hydrogens in water molecules was also considered, so that the water hydrogens were set to be flexible, by which the water hydrogens could be energetically minimized during docking process. The docking solution 11 and 12 in Table 3.6 correspond to E2020 with *R*-configuration in unprotonated and protonated states, respectively. According to the results, the S_{Total} of unprotonated ligand, with ligand energy of 0.0 kJ/mol is higher than protonated ligand (Table

3.6), which is consistent with the results of docking into empty binding, saying that E2020 can not be protonated.

Docking* solution	RMSD (Å)	E_{ass}	LE	BE	E_{nhb}	vdW	E_{est}	E_{cnt}	vdW^{+}	Nhph	Nhb
11-(up)-*R*	0.57	-58.7	0.0	3.1	-61.9	-15.2	-12.8	-34.0	2.9	12	3
12-(p)-*R*	0.56	-53.1	11.5	2.6	-67.2	-15.1	-18.2	-33.9	3.1	13	3

Table 3.6: The result of docking the ligand with R configuration in presence of the six important water molecules with flexible hydrogens

*: 'up' stands for unprotonated, p for protonated.

Figure 3.10 illustrates the amino acids that interact with E2020, in presence of the water molecules. Although the crystallographical data interestingly indicate the *R*-configuration at C8 [39] for protonated ligand, using our docking tool, this experiment shows that E2020 with *R*-configuration in its bound state with AChE should have *R*-configuration in unprotonated state, by which it energetically forms a more stable complex with AChE.

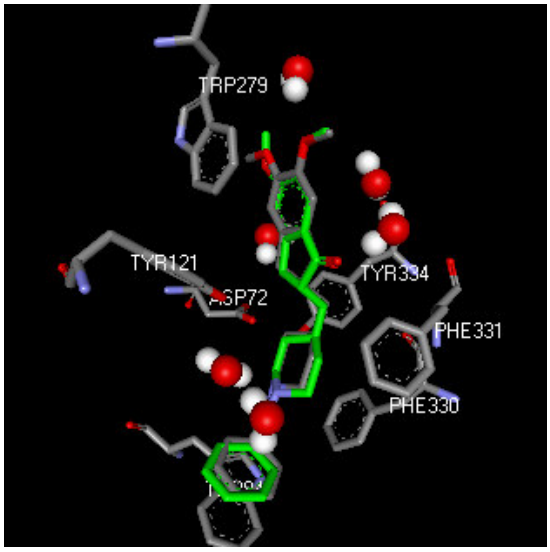

Figure 3.10: Amino acids that interact with docking solution (gray) in presence of waters with flexible hydrogen. X-ray structure of the

3.4.4 Unbound docking study on E2020

Independent of the available X-ray data, E2020 was built, minimized and then docked into the empty binding site of crystal structure of *Tc*AChE complexed with galanthamine (1DX6) [40] and complexed with decamethonium (1ACL) [63].

The first step of docking into 1DX6 generated 25 answers, among which rank number 9 had the highest S_{Total} (Docking solution 14, Table 3.7). This was selected for the next iteration. Performance of MSD led to find the final answer (Docking solution 15 in Table 3.7). Comparison of the result with the available X-ray structure gives a RMSD of 0.96 Å, whereas the first rank of the very first step has the RMSD of 2.19 Å. Furthermore the total estimated energy of the complex is improved from-38.0 kJ/mol to-41.6 kJ/mol, respectively.

Docking solution	Rank	RMSD (Å)	E_{ass}	LE	E_{nhb}	vdW	E_{est}	E_{cnt}	vdW^{+}	Nhph	Nhb
13	1 Step 1	2.19	-38.0	3.2	-41.2	-9.5	-4.4	-27.3	3.6	13	1
14	9 Step 1	0.97	-37.0	9.4	-46.4	-11.9	-3.7	-30.7	3.2	12	1
15	1 Step 3	0.96	-41.6	4.1	-45.7	-11.8	-3.6	-30.4	3.0	12	1

Table 3.7: Result of the unbound docking of E2020 into empty binding site of 1DX6

Docking E2020 into 1ACL also generated the correct solution with RMSD of 0.92 Å. (Docking solution 18, Table 3.8).

Table 3.9 compares the results of unbound docking of E2020 into binding site of 1DX6 using different methods, among which MSD predicts the best solution with regard to RMSD values.

Docking solution	Rank	RMSD (Å)	E_{ass}	LE	E_{nhb}	vdW	E_{est}	E_{cnt}	vdW^{+}	Nhph	Nhb
16	1 Step 1	0.92	-44.7	4.4	-49.1	-10.2	-11.7	-27.2	3.9	11	0
17	2 Step 1	1.04	-43.5	4.8	-48.3	-11.2	-10.1	-27.1	3.1	11	0
18	1 Step 2	0.92	-44.8	4.4	-49.2	-10.2	-11.7	-27.3	4.0	11	0

Table 3.8: Result of unbound docking of E2020 into binding site of 1ACL

Program	**Search Algorithm**	**Scoring Function**	**RMSD (Å)**	**Binding Site Flexibility**
QXP^{+} (OSD)	Monte Carlo One Step	Amber Force Field	2.19	No
FlexX	Incremental Construction	Empirical Score	14.54	No
G.O.L.D	Genetic	Empirical Score	4.41	No
QXP^{+} (MSD)	Multi-Step Docking	Amber Force Field	0.96	No

Table 3.9: Result of unbound docking of E2020 into binding site of 1DX6 using different method

3.5 Study on Decamethonium (DECA)

3.5.1 Bound docking study on Decamethonium (DECA)

Decamethonium is a bisquaternary reversible inhibitor of AChE, with a simple chemical structure of two trimethyamine, which are connected to each other via a decyl side chain [64] (Figure 3.11).

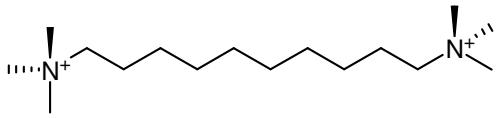

Figure 3.11: Chemical structure of decamethonium (DECA)

Because of the high flexible structure of DECA, it is a grate challenge for any docking tool. MSD method successfully performed the bound docking of this ligand. In this section the detailed structural features of the complex of DECA with AChE, through the bound docking into 1ACL, will be considered [64].

3.5.2 Docking decamethonium into the empty binding site of 1ACL

The bound docking of DECA into its complexed protein (1ACL) yielded energetic values shown in Table 3.10.

Docking solution	RMSD (Å)	E_{ass}	LE	E_{nhb}	vdW	E_{est}	E_{cnt}	vdW^{+}	Nhph	Nhb
19	0.99	-40.5	0.0	-40.5	-7.0	-13.1	-20.4	2.6	7	0

Table 3.10: The numerical data of docking DECA into empty binding site of 1ACL

Figure 3.12 illustrates how close the predicted binding mode of the DECA is to the X-ray structure of the ligand with RMSD of 0.99 Å.

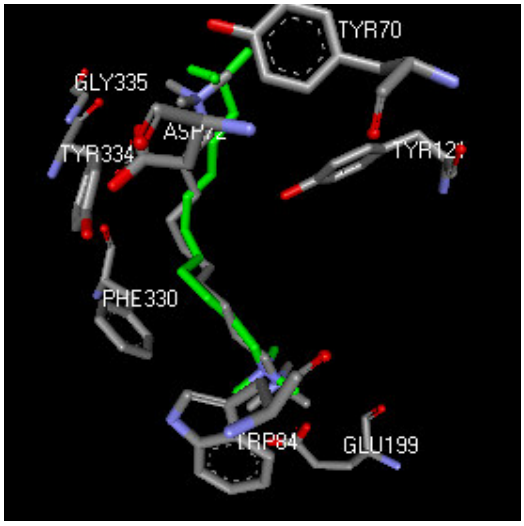

Figure 3.12: The overlaid X-ray structure of DECA (green) on the predicted pose of the ligand by docking (gray)

3.5.3 Docking decamethonium into the binding site of 1ACL including waters

In order to better understand the binding of DECA with AChE, we also looked for water molecules that mediate the interaction among ligand atoms and enzyme. Using QXP^{+} five important water molecules were defined within the binding site of 1ACL that are Wat612, Wat622, Wat634, Wat640 and Wat642 (Figure 3.13).

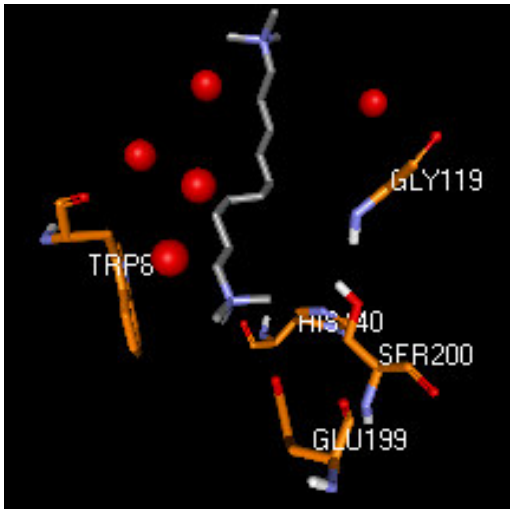

Figure 3.13: Indicates the position of the five most important waters in the binding site of 1ACL Wat612, Wat622, Wat634, Wat640 and Wat642 (red balls

By contribution of these important waters around DECA, other experiment was set up. To optimize the hydrogen position of waters, their positions were energetically minimized, by

definition flexible hydrogens on the waters. The resulting first rank answer (Docking solution 20 in Table 3.11) has an optimal binding energy, which has been improved in all the energy terms in comparison with docking result of empty binding site (Docking solution 19 in Table 3.10).

Docking solution	RMSD (Å)	E_{ass}	LE	BE	E_{nhb}	vdW	E_{est}	E_{cnt}	vdW^{+}	Nhph	Nhb
20	0.98	-46.7	0.0	1.5	-48.2	-9.0	-15.3	-23.8	2.8	6	0

Table 3.11: The numerical data of docking DECA into the active site of 1ACL, in presence of the five most important crystallographical waters with flexible hydrogen

In Table 3.12 the amino acids that directly interact with DECA are listed. Analyzing their interatomic interactions shows that one of the three methyl groups (C16) of DECA in the upper part of the gorge interacts with carbonyl oxygen of Asp72, the second methyl (C18) with carbonyl of Tyr334 and the third one (C17) with hydroxyl oxygen of Tyr70. The C7 and C9 in decyl chain have hydrophobic interactions with the aromatic ring of Phe330 the C4 interacts with carbonyl oxygen in Phe330. N1 atom of DECA in the lower part of the gorge has a cation-π interaction with Trp84 and three-methyl groups of DECA have hydrophobic interaction with carbonyl oxygen in Glu199.

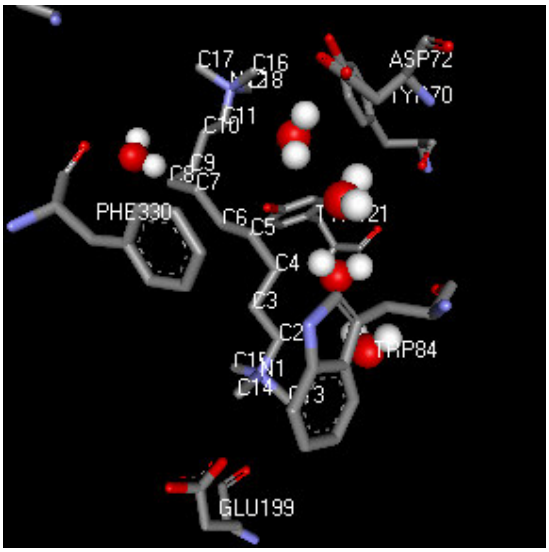

Amino acids	Interaction energy (kJ/mol)
Gly335	-4.2
Tyr70	-4.9
Asp72	-6.6
Tyr334	-7.5
Tyr121	-3.5
Phe330	-13.1
Trp84	-9.5
Glu199	-19.9

Figure 3.14: Docking solution of DECA (gray) among the most important waters and interacting amino acids

Table 3.12: List of the interaction energies of amino acids around DECA

Oxygen of Wat642 interacts with the second and the third carbon of the decyl chain, while the C10 interacts with oxygen in Wat634 in the lower part of the gorge. In addition from the magnitude of their corresponding interaction energies can be seen that the most interactive amino acids are Glu199 and Phe330 with -19.9 kJ/mol and -13.1kJ/mol energies, respectively (Table 3.12). From these data it is observed that after including waters in docking, Glu199 has lower interaction energy than Phe330, whereas the result of docking into empty binding site interact better with Phe330 than with Glu199.

To summarize the results, in this study was found that on the consequence of employing MSD for docking of DECA into the binding site of 1ACL and the most important water molecules were recognized. In addition, the correct binding mode with 0.99 Å confirmed the accuracy of docking procedure, using MSD. The interactive amino acids with docking solution of DECA presented and their corresponding interaction energies calculated in different circumstances of the gorge, in absence and in presence of waters with flexible hydrogens. Since in the corresponding literature of 1ACL [64], the structural data of AChE-DECA complex has not been described in detailed, therefore the obtained data from these docking studies provide new information on interatomic interactions between DECA and its surrounding environment in 1ACL.

The effectiveness of application of MSD method is not limited to docking of AChE's inhibitors. To prove this, in the next section the consensus docking method is applied in bound and unbound docking of the inhibitors of other proteins than AChE.

3.5.4 Unbound docking study on decamethonium (DECA)

To examine capability of the MSD for correct pose prediction of ligands with high flexibility, unbound docking of decamethonium using MSD was carried out.

This structure caused difficulties in correct pose prediction using several other docking methods. MSD was able to produce correct answer with unbound docking DECA into 1DX6 [40]. The numerical data of the experiments are given in Table 3.13. The docking solution has RMSD of 1.27Å (Docking solution 22, Table 3.13) that has 7.5 kJ/mol lower total estimated energy than first hit answer in the first step docking (Docking solution 21, Table 3.13). For this ligand it is the first time that a successful docking is reported. As the implementation of G.O.L.D and FlexX do not produce the correct answer for this ligand (Table 3.14).

Docking solution	Rank	RMSD (Å)	E_{ass}	LE	E_{nhb}	vdW	E_{est}	E_{cnt}	vdW^{+}	Nhph	Nhb
21	1 Step 1	1.27	-27.5	8.7	-36.2	-8.8	-6.4	-21.0	1.7	7	0
22	1 Step 2	1.27	-35.5	0.7	-36.2	-8.8	-6.4	-21.0	1.6	7	0

Table 3.13: Result of unbound docking of decamethonium into binding site of 1DX6

Program	Search Algorithm	Scoring Function	RMSD (Å)	Binding Site Flexibility
QXP^{+} (OSD)	Monte Carlo One Step	Amber Force Field	1.27	No
FlexX	Incremental Construction	Empirical Score	4.52	No
G.O.L.D	Genetic	Empirical Score	4.83	No
QXP^{+}* (MSD)	Multi-Step Docking	Amber Force Field	1.27	No

Table 3.14: Different programs utilized for unbound docking of DECA into 1DX6

*: As it has been shown in Table 3.13, despite of the identical RMSDs for docking solution of MSD and OSD, MSD generates an answer with much better E_{ass} and LE.

The effectiveness of application of MSD method is not limited to docking of AChE's inhibitors. To prove this, in the next section the consensus docking method is applied in bound and unbound docking of the inhibitors of other proteins than AChE.

3.6 Application of MSD for bound docking study on several inhibitors of other proteins than AChE

3.6.1 Bound docking of Win51711 and Win52084

Surprising binding modes have been observed for two antiviral compounds, Win51711 [65] (Figure 3.15) and Win52084 (Figure 3.16) [66]. These two compounds possess an almost identical structure and only differ in absence or presence of one methyl group, respectively. However, they bind with reverse orientations. This was an encouraging reason for testing MSD method to see if it is able to produce correct binding mode of both ligands particularly as they have a long flexible side chain in their structure.

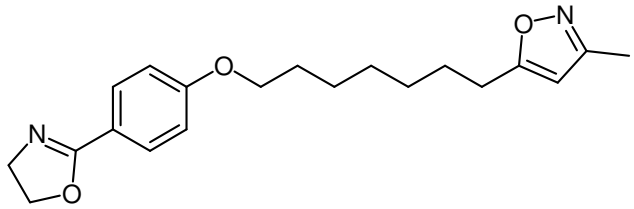

Figure 3.15: Chemical structure of Win51711

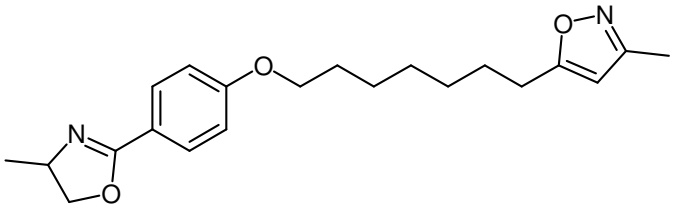

Figure 3.16: Chemical structure of Win52084

MSD result of Win51711 generates a solution with RMSD of 0.80 Å and 0.0 kJ/mol ligand energy (Docking solution 25, Table 3.15). In addition, result of docking Win52084 is a reasonable answer with RMSD of 1.06 Å with ligand energy of 0.0 kJ/mol (Docking solution 27, Table 3.15) versus 1.66 Å obtained from first step (Docking solution 26, Table 3.15).

Docking solution	Rank	RMSD (Å)	E_{ass}	LE	E_{nhb}	vdW	E_{est}	E_{cnt}	vdW^{+}	Nhph	Nhb
23	1 Step 1	1.10	-44.3	2.3	-46.6	-11.9	-0.7	-34.0	4.0	13	0
24	2 Step 1	0.80	-44.1	2.9	-46.9	-13.3	-0.1	-33.6	3.3	12	0
25	1 Step 2	0.80	-46.9	0.0	-46.9	-13.3	-0.1	-33.6	3.3	12	0
*26	1 Step 1	1.66	-47.2	1.7	-48.9	-13.5	-2.1	-33.3	3.6	12	1
27	1 Step 4	1.06	-48.9	0.0	-48.9	-13.2	-2.5	-33.2	3.7	12	1

Table 3.15: Result of docking Win51711 into 1PIV (Docking solution 23-25) and Win52084 into 1RUH (Docking solution 26-27)

*: This solution is the first hit with the highest S_{Total} answer of the first step.

Figure 3.17 indicates the isopotential electrostatic surface of Win51711 (right in Figure 3.17) and Win52084 (left in Figure 3.17). The extra methyl substitution on oxazoline affects on the electrostatic charge distribution on the molecule and it could be the reason for reverse orientation of these two ligands in the binding site of the protein.

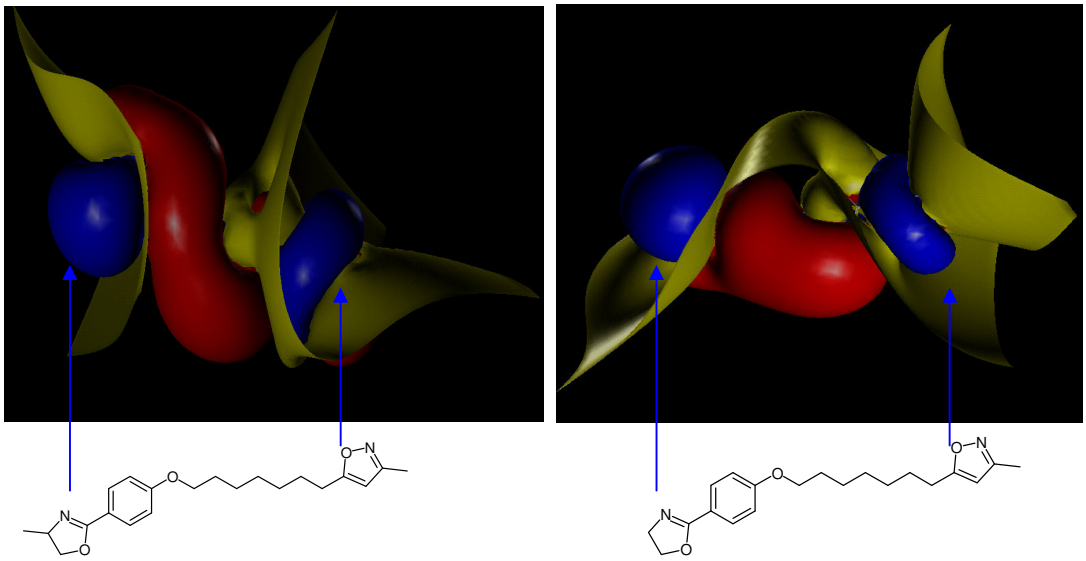

Figure 3.17: Difference in isopotential electrostatic surface of Win52084 (left) and Win51711 (right), despite of their similarity in structural skeleton. Blue/ yellow/ red indicate – n/ 0/ + n charge distribution on the ligands.

3.6.2 Unbound docking study on Deoxythymidine

Antiherpes therapies are principally targeted at viral thymidine kinases (TK) and utilize nucleoside analogues, which are inhibitors of viral DNA polymerase. The substrate of TK is deoxythymidine (Figure 3.18), whose X-ray structure (1KIM) has been deposited in protein data bank [67]. In the next step of examination of MSD, the unbound docking of deoxythymidine was performed into the uncomplexed proteins of deoxythymidine. These proteins are KI6, KI7 and 1KI8 (Table 3.16).

PDB ID	Protein	Ligand
1KIM	Thymidine Kinase From Herpes Simplex Virus Type I	Deoxythymidine
1KI6	Thymidine Kinase From Herpes Simplex Virus Type I	5-Iodouracil Anhydrohexitol Nucleoside
1KI7	Thymidine Kinase From Herpes Simplex Virus Type I	5-Iododeoxyuridine Phosphotransferase
1KI8	Thymidine Kinase From Herpes Simplex Virus Type I	5-Bromovinyldeoxyuridine
1FVT	Cyclin-Dependent Kinase 2 (Cdk2)	Oxindole

Table 3.16: Indicates kinase proteins used for docking of deoxythymidine and oxindole

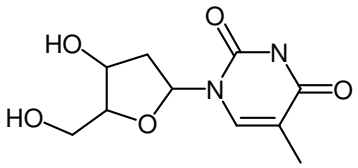

Figure 3.18: Chemical structure of deoxythymidine

In this experiment, MSD was used for unbound docking of deoxythymidine into 1KI7. This results a solution with RMSD of 1.11 Å (Docking solution 29, Table 3.17), whereas docking solution of the first step unbound docking has RMSD of 1.82 Å (Docking solution 28, Table 3.17). Furthermore, the total estimated energy of the final answer has -5.3 kJ/mol improvement in comparison with the first hit in the first step (Table 3.17).

Docking solution	Rank	Protein	RMSD (Å)	E_{ass}	LE	E_{nhb}	vdW	E_{est}	E_{cnt}	vdW^{+}	Nhph	Nhb
28	1 Step 1	1KI7	1.82	-44.8	5.1	-49.9	0.7	-29.2	-21.4	12.0	2	2
29	1 Step 4	1KI7	1.11	-50.1	11.0	-61.0	14.4	-54.5	-21.0	23.6	2	3
30	1 Step 1	1KI6	0.43	-56.2	3.9	-60.1	-3.1	-36.4	-20.6	7.8	2	3
31	1 Step 2	1KI6	0.74	-59.1	2.5	-61.6	2.5	-42.0	-22.1	13.7	1	3
32	1 Step 1	1KI8	0.59	-47.0	9.4	-56.4	-6.4	-28.4	-21.6	5.3	2	5
33	1 Step 5	1KI8	0.60	-51.3	1.7	-53.0	-5.6	-27.1	-20.3	5.2	2	4

Table 3.17: Result of unbound docking deoxythymidine

MSD result of docking into 1KI6 (Table 3.17) also generated better answer in comparison with the first step docking, such that the former has -2.9 kJ/mol lower magnitude of total estimated energy than the latter one (Docking solution 30 and 31, Table 3.17). In addition, the ligand energy of MSD answer is 1.4 kJ/mol lower than of the solution in the first step docking, while the corresponding RMSD is 0.29 Å higher than the docking solution of the first step docking run (Table 3.17). The worth of using MSD in unbound docking of deoxythymidine into 1KI8 is also observable, as the result gives -4.3 kJ/mol lower total estimated energy (Docking solution 32, Table 3.17) than the answer of the first step docking (Docking solution 33, Table 3.17). It is noteworthy that ligand energy of the former is better with 7.7 kJ/mol difference, however, the RMSD values of them are almost identical (Table 3.17).

3.6.3 Bound docking study of oxindole

Oxindole (Figure 3.19) is one of the inhibitors of cyclin-dependent kinase 2 that was taken as a ligand for bound docking into its complexed protein 1FVT [68] (Table 3.16).

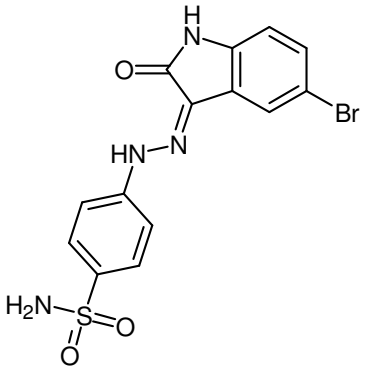

Figure 3.19: Chemical structure of oxindole

MSD results an answer with better S_{Total} (Docking solution 35, Table 3.18) in comparison with the first step docking, however the RMSDs are almost identical (Docking solution 34, Table 3.18).

Docking solution	Protein	RMSD (Å)	E_{ass}	LE	E_{nhb}	vdW	E_{est}	E_{cnt}	vdW^{+}	Nhph	Nhb
34	1FVT	0.46	-39.3	6.0	-45.3	2.8	-26.7	-21.4	13.4	6	5
35	1FVT	0.45	-42.1	4.2	-46.3	3.1	-28.1	-21.4	13.6	6	6

Table 3.18 Numerical data of oxindole bound docking into 1FVT

4 Elucidation of structural properties of (PPG)

The aim in this part of the work is application of MSD for docking study on a new derivative of galanthamine 'piperidinopropylgalanthamine' (PPG) [38] (Figure 4.1), which was firstly, correct placement of the PPG in its complex state with AChE via unbound and bound docking, secondly estimation of its inhibitory constant based on the calculated total estimated binding energy of the complex.

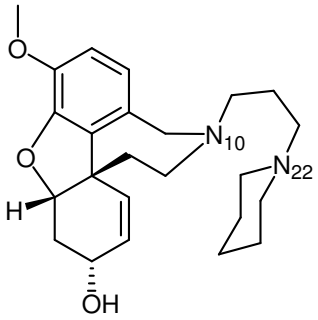

Figure 4.1: Chemical structure of piperidinopropylgalanthamine (PPG) with two possible inside inverted piperidine ring

Generally, information of the 3D structure of a ligand-protein complex provides the data on the arrangement of the atoms in space. Despite of that sometimes it is hard to distinguish different possible orientations in a substructure of a molecule. For instance, in the case of PPG, there are two possible ring inversions for piperidine ring in X-ray structure, which are inside and outside inverted (Figure 4.1). Investigation of this issue has been included as a part of our molecular docking study in this chapter. Protonation state of nitrogen atoms at piperidine (N22) as well as at galanthamine nitrogen (N10) has been also of particular importance in this work, because the corresponding data can lead us to find out whether a ligand in AChE binding site, at all can have the protonated state and if so, why and in which particular circumstances.

Since in a biological system of the protein-ligand complex, interactions take place in an aqueous environment and effect of the waters are reflected in enthalpic and entropic contributions complex energy of the system [69] [70], therefore, here, the presence of the important crystallographic water molecules have been also taken into account. The importance of the waters were recognized by QXP^{+}, according to their ability to either contact to PPG atoms or mediate interactions among ligand atoms and surrounding amino acids.

4.1 Searching for the protonation state of PPG using bound docking

In this section five crystallographic water molecules have been included into the binding site. These waters were identified by their particular role for mediating the interactions among ligand atoms and surrounding residues. The codes of these waters are Wat5, Wat9, Wat84, Wat94, and Wat275. The data given in Table 4.1 should be discussed in two groups. The first group consists of docking solutions 10-12, in which no water molecules of the binding site were taken into account. Among these three docking solutions, the protonated ligands show more favourable total estimated binding energies than the neutral molecule. Of the two possible protonation sites N10 (Docking solution 11) and N22 (Docking solution 12), protonation at N10 with a bent shape of the piperidine-propyl side chain is preferable, as it has more similarity to the known crystal structure (RMSD = 0.46 Å). A protonation at N22 can be ruled out because of the straightened N-alkyl side chain (RMSD = 1.83 Å). In addition, even though protonation at N22 yields the lower E_{ass}, the resulting structures with protonation at N10 gives the higher S_{Total} (red numbers in Table 4.1), including ligand energy of zero, suggesting a global minimum structure, which usually is assumed to be the native like structure [34]. The lower total binding energy of docking solution 12 versus solution 11 (Table 4.1) is dominated by an electrostatic interaction between the positively charged piperidine-nitrogen and (OAc^-) of aspartic acid (Asp72) mid way in the gorge. This electrostatic interaction decreases electrostatic energy (E_{est}) to -21.2 kJ/mol consequently affects total binding energy. Figure 4.2 shows the overlapping electrostatic surfaces at the protonated piperidine and the (OAc^-) residue of Asp72.

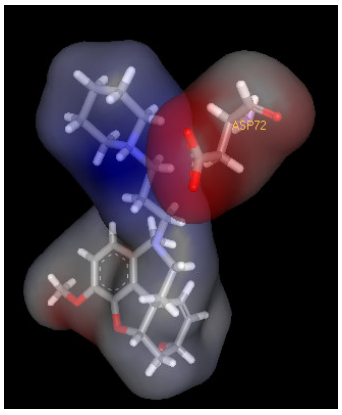

Figure 4.2: Overlapping electrostatic surfaces around protonated piperidine with positive charge (blue area) and negatively charged OAc^- of Asp72 (red area).

Docking experiment	Ligand*	RMSD (Å)	E_{ass}	LE	E_{bind}	E_{nhb}	vdW	E_{est}	E_{cnt}	vdW^{+}	Nhph	Nhb
10	Bent-In (up) [a]	0.41	-51.4	7.6	0.0	-59.0	-8.5	-18.5	-32.1	6.9	11	2
11	Bent-In N10 (p) [a]	0.46	-55.5	0.0	0.0	-55.5	-10.4	-15.5	-29.6	4.2	12	3
12	Staight N22 (p) [a]	1.83	-56.6	0.1	0.0	-56.6	-6.5	-21.2	-28.9	6.5	10	2
13	Bent-In (up) [b]	0.40	-104.0	7.0	-46.7	-64.4	-10.1	-21.9	-32.3	5.6	12	2
14	Bent-In N10 (p) [b]	0.35	-109.0	6.4	-45.7	-69.3	-7.9	-28.9	-32.6	8.1	12	2
15	Straight N22 (p) [b]	1.85	-109.0	2.0	-44.5	-66.8	-6.1	-29.1	-31.5	9.0	10	2

Table 4.1: The result of docking into the binding site of AChE-PPG, red numbers indicate the best value in different terms of docking into empty binding site, Blue numbers indicate the best value in different terms for docking into binding site with flexible water hydrogen

*: a; Docking was performed into the binding site without water, b; Docking in the presence of the five most important water molecules with flexible hydrogen atoms

The interaction of the optimal solution of protonated PPG at N10 (Docking solution 11 in Table 4.1) with its surrounding amino acids is described in detail in Table 4.2. The relevant amino acids, responsible for non-bonding interaction energy of the protonated PPG [38] consist of C-H…O, as well as C-H…N, C-H…π systems that are known as weakly hydrogen bonds [71][72], in the more hydrophobic regions of proteins [73]. Furthermore, these interactions are graphically shown in Figure 4.3. The corresponding structure shows an excellent RMSD of 0.46 Å and has the highest S_{Total}.

As it can be seen in Figure 4.3, two carbons (C25 and C26) in piperidine ring interact with carbonyl oxygen in Phe330 (C-H…O) that assists the piperidine ring flip upward to have out side inversion. The hydroxyl oxygen of Tyr334 also has a (C-H…O) interaction with C27 in piperidine ring, the same type of interaction take place among alkyl side chain of the ligand (C20 and C21) with Asp72 oxygen. A (C-H…N) plus a (C-H…π) interaction between Gly118 and cyclohexenyl ring in galanthamine moiety is also observable. A (C-H…O) type interaction can be seen between Ser122 and a carbon in cycloheptyl ring (C11) of

galanthamine (left in Figure 4.3). The nitrogen in Gly118 shows a 'lone pair-π' interaction with aromatic ring in galanthamine substructure of PPG. Two amino acids dominate interaction energies, Glu199 and Ser200, whose involved atoms with PPG have been indicated in detailed in Figure 4.3 (right). Table 4.2 lists the relevant amino acids that are responsible for binding of the N10-ptotonated PPG [38].

Amino Acids	Asp72	Trp84	Tyr121	Ser122	Gly118	Gly119	Glu199	Phe330	Phe331	Ser200	His440	Tyr334
Interaction energy (kJ/mol)	-8.0	-6.9	-6.0	-2.8	-8.4	-16.8	-26.6	-12.4	-12.6	-27.8	-2.5	-4.5

Table 4.2: Displays amino acids interacting with the neutral PPG and the corresponding interaction energies

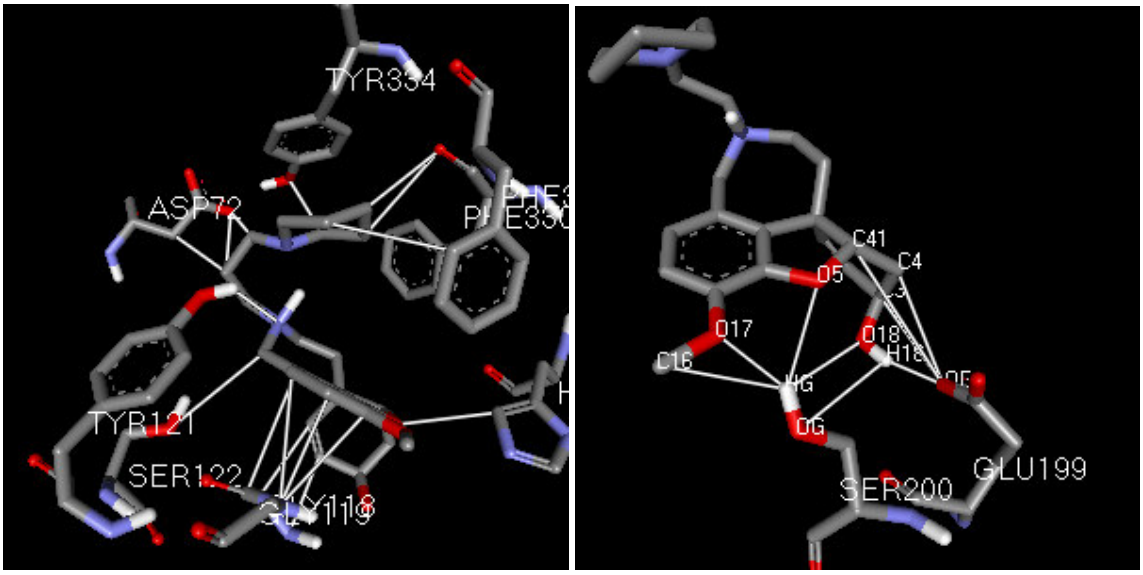

Figure 4.3: The amino acids and their specific atoms that interact with protonated PPG at N10 (left) Glu199 and Ser200 are two amino acids with the lowest interaction energies (right)

The second group of data in Table 4.1 including docking solutions 13-15, show results from docking studies, in which the five most important waters have been included as part of the binding site. Due to having the highest S_{Total}, the protonated PPG at N10 (Docking solution 14 in Table 4.1), in this group, turns out to be the most favorable docking result. As it is bound docking and then comparison of docking results with X-ray structure shows that the protonated ligand with inside inverted with the lowest RMSD and the lowest total estimated binding energy is the most reliable answer, however according to its S_{Total} value it has one score less than unprotonated ligand with inside inverted pose.

Overall, the data from Table 4.2 suggest that PPG binds to the AChE active site in a protonated state, with protonation at N10 rather than at N22 (Docking solution 13 versus 14)

with the highest S_{Total} (blue numbers in Table 4.1). Therefore PPG is one of the rare cases where the binding of a protonated ligand is made very likely. Crystallographic studies do not show hydrogens and therefore cannot differentiate between a protonated and a neutral ligand in the bound state. Modeling studies, however, on the basis of a given crystal structure can unravel such questions, when important water molecules are included in the docking experiments and when on the basis of bindings energies and of RMSD-values protonated and neutral structures can be compared. The finally proposed structure for the protonated PPG has been shown in Figure 4.4 overlaid on the crystal structure.

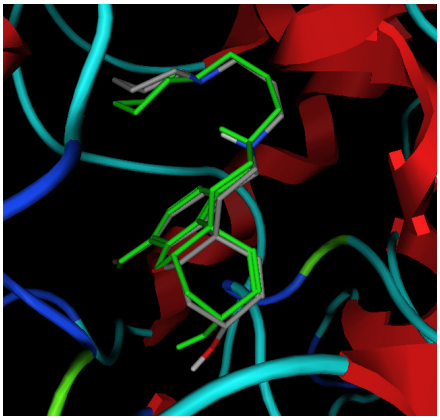

Figure 4.4: The final bound docking solution for protonated PPG (gray) overlaid on the X-ray structure (green)

The bent pose of the ligand, protonated at N10, is not only the most populated conformation as the first hit of docking, but also has the most abundant conformational pose, so that 16 solutions out of 25 resulting structures (64%) are similar to the first hit structure (Figure 4.5).

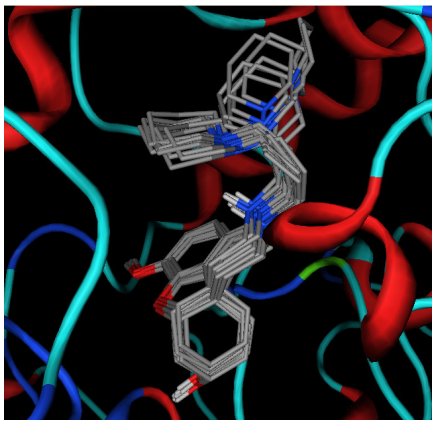

Figure 4.5: Superimposition of 25 docking solutions of protonated PPG

In view of the pK_a-values of the nitrogen-atoms in PPG, one should expect protonation at N22 rather than at N10. While galanthamine is known to have a pK_a-value of 8.2 [74], the value for piperidine is 11.05 [75]. This magnitude is decreased by changing from the secondary

amine to a tertiary as in PPG. On the one hand the basicity should increase because of the inductive effect of alkyl groups [76]. On the other hand the steric hindrance predominates as solvation of the sterically hindered ammonium-cation is becoming more difficult. As a result the pK_a-value for n-methypiperidine drops to 10.08 [75].

Therefore, in an aqueous solution protonation is more probable at the piperidine-nitrogen than at the galanthamine-nitrogen by almost a factor of 100. However, a ligand in a binding site is no longer in an aqueous environment but rather embedded in at least a partially hydrophobic surrounding. This makes a prediction of the protonation state of a ligand on the basis of pK_a-values impossible. In contrast, docking experiments take into account the entire binding site area and therefore do reflect much better the actual status of the ligand. The data from Table 4.1, particularly the result from docking solution 14 and from docking solution 11 clearly suggest that PPG is still protonated in the bound state and N10 is the most probable protonation site. It should be mentioned that the resolution of the crystal structure of PPG does not allow to unequivocally defining the orientation of the piperidine-ring with respect to galanthamine moiety. In other words, from the crystal structure data one cannot decide, if the piperidine-nitrogen is oriented towards the galanthamine moiety (inside inverted piperidine) or towards the Tyr334 residue, which is the closest amino acid to the piperidine-ring (outside inverted piperidine). If we accept that PPG is protonated in the bound state, the structure with the inside inverted piperidine creates a cage, in which the proton is trapped (right in Figure 4.6) and consequently could be even shared between the two nitrogen-atoms of the ligand (left in Figure 4.6).

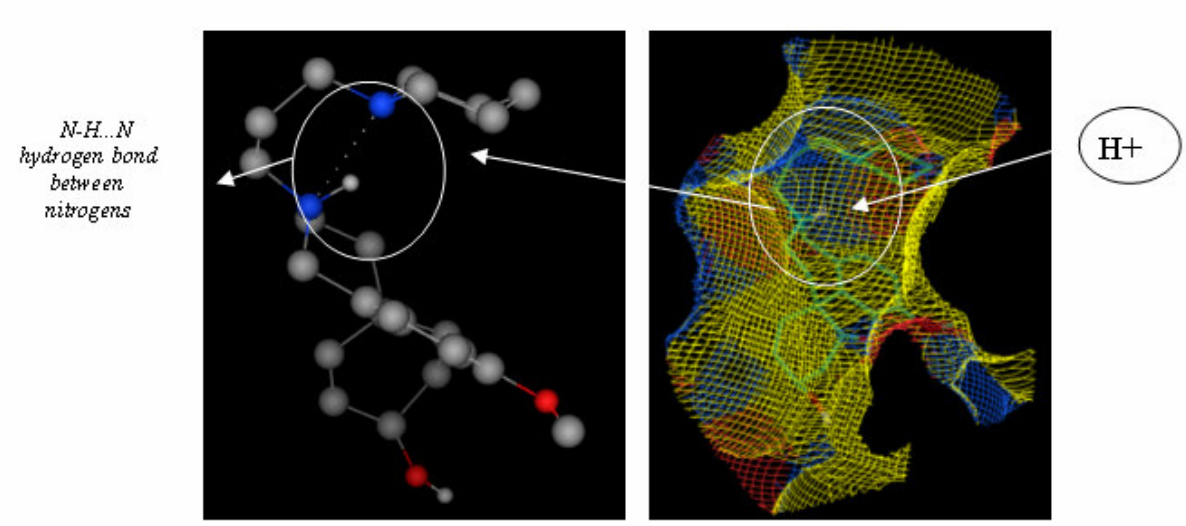

Figure 4.6: Illustrates the hydrogen bond between two nitrogens (left), H^+ is trapped into the cage-like shape of the ligand (right)

4.2 Conformation at galanthamine and piperidine substructures by unbound docking study

In this chapter MSD is used for unbound docking of PPG. It was applied to find the favorable conformation (equatorial or axial) in two nitrogens of the molecule, at piperidine and galanthamine substructures with unbound docking of the neutral ligand (deprotonated) into 1DX6 [40]. The docking results indicate the conformational conversion from 'a-e' to 'e-e' and 'a-a' to 'e-a', where 'a' stands for the axial and 'e' for the equatorial. The first letter shows the conformation in piperidine and the second letter corresponds to the galanthamine. The conformation of the flexible piperidine is converted to equatorial, by which a six-member ring is stabilized. In contrast, the conformation at galanthamine-nitrogen, maintains axial without any conversion (Table 4.3).

As it is shown, in Table 4.3, the final structures with 'e-e' conformation are obtained in entries pose 1 and 4. Particularly, entry Table 4.3 has the highest S_{Total}. Due to this advantage of the docking result with 'e-e' conformation, for further steps of docking PPG, the 'e-e' conformation was considered as the starting structure of the ligand.

entry	Starting Conf*	Ending Conf	RMSD (Å)	E_{ass}	LE	E_{nhb}	vdW	E_{est}	E_{cnt}	vdW^{+}	Nhph	Nhb
1	a-e	e-e	0.49	-52.1	6.3	-58.4	-8.3	-18.5	-31.6	7.1	11	2
2	a-a	e-a	1.07	-48.3	4.8	-53.1	-5.4	-17.9	-29.8	8.8	11	2
3	e-a	e-a	1.07	-48.7	4.4	-53.1	-5.1	-18.1	-30.0	9.2	11	2
4	e-e	e-e	0.57	-51.4	7.6	-59.0	-8.5	-18.4	-32.1	6.9	11	2

Table 4.3: Numerical data obtained from docking the ligand with different conformation at N22 and the N10 in the starting structure of unbound docking into 1DX6

*: 'Conf' stands for conformation, 'a' for axial and 'e' for equatorial

The inconvertibility of axial conformation to equatorial in galanthamine moiety raises the question, whether it might have any conformational change in nitrogen moiety of galanthamine or not. For this purpose besides galanthamine, two derivatives of it (ethyl galanthamine and demethylated galanthamine) were considered, each of which was studied with axial and equatorial conformations at galanthamine-nitrogen. The nitrogen displays the conformational conversion at galanthamine-nitrogen in the case of galanthamine and other derivatives with small substitution. The reason is that PPG has a longer oligomethylen side chain, which increases the required energy for conformational conversion.

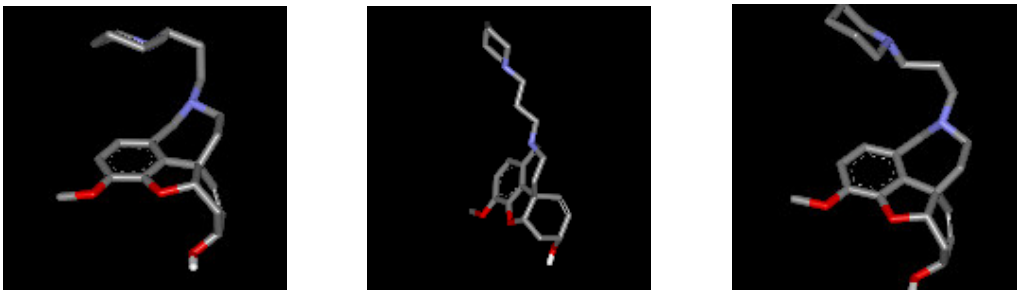

1st rank (Docking solution1) 4th rank (Docking solution2) 8th rank (Docking solution3)

Figure 4.7: Three possible poses of the ligand, among the 25 docking solutions of the neutral ligand extracted from Table 4.2. The bent pose of the PPG with inside inverted piperidine ring is ranked at the first hit

With respect to the 'e-e' conformation of the molecule, three possible shapes can be found, which are straight, bent with inside and outside inverted piperidine ring. The energetically best solution of these three conformations has been shown in Figure 4.7, while Table 4.4 lists all the corresponding docking data.

Docking solution	Neutral* Ligand	Rank	RMSD (Å)	E_{ass}	LE	E_{nhb}	vdW	E_{est}	E_{cnt}	vdW^{+}	Nhph	Nhb
1	Bent-In (up)	1	0.57	-51.4	7.6	-59.0	-8.5	-18.4	-32.1	6.9	11	2
2	Straight (up)	4	1.95	-49.1	2.8	-51.9	-8.4	-15.2	-28.3	5.2	10	2
3	Bent-Out (up)	8	1.00	-47.9	4.1	-52.0	-5.7	-17.2	-29.1	7.8	12	3

Table 4.4: Numerical data correspond to docking solutions of the neutral ligand.

*: 'up' stands for unprotonated (neutral), 'Bent-In' for neutral with inside inverted ring, 'Bent-Out' neutral with outside inverted ring.

The unbound docking of the PPG, according to the consensus scoring of MSD method, suggests that inside inverted bent pose of the PPG (Docking solution 1 in Table 4.4) is the best pose, as it has the highest S_{Total} among three other docking solutions (red numbers in Table 4.4).

4.3 Unbound docking of PPG protonated at the galanthamine-nitrogen (N10)

Next, another unbound docking experiment into 1DX6 was set up to find the energetically favored conformation for a PPG protonated at the galanthamine nitrogen (N10). Again three different structural poses of the ligand were observed among the first 25 resulting structures, i.e. a straight and two bent forms, with inside and outside inverted piperidine ring, respectively.

Docking* solution	Protonated Ligand*	Rank	RMSD (Å)	E_{ass}	LE	E_{nhb}	vdW	E_{est}	E_{cnt}	vdW^{+}	Nhph	Nhb
4	Bent-In (p)	1	0.46	-55.6	1.2	-56.8	-8.7	-16.9	-31.2	6.5	12	4
5	Straight (p)	4	1.93	-48.4	1.4	-49.8	-6.9	-14.2	-28.7	6.6	10	3
6	Bent-Out (p)	22	1.16	-42.8	7.6	-50.3	-6.7	-14.4	-29.3	7.1	8	2

Table 4.5: Numerical data correspond to docking solutions of the protonated PPG at galanthamine-nitrogen
*: 'p' stands for protonated

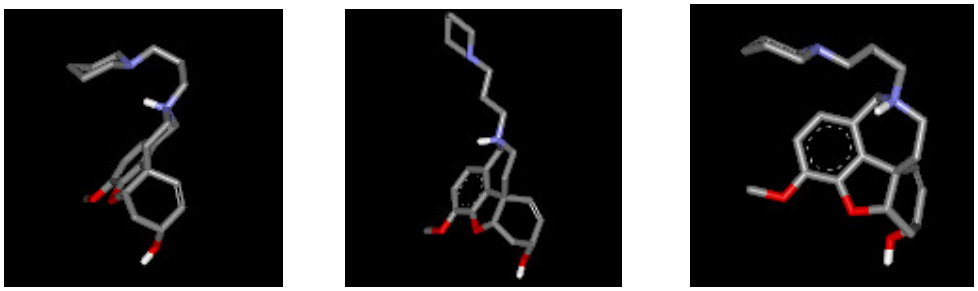

1st rank (Docking solution 4) 4th rank (Docking solution 5) 22nd rank (Docking solution 6)

Figure 4.8: The best solution of the different structural poses of PPG with protonation at the galanthamine-nitrogen, extracted from Table 4.5

The docking experiment yields a bent structure with an inside inverted piperidine ring as the first hit, which not only is the most populated conformation but shows the lowest energy in all respects as well as the highest number of hydrophobic interactions and hydrogen bonds, it thus has the highest S_{Total} among the all three structural poses of the PPG. This structure, therefore, is suggested to be the most possible conformation of PPG, protonated at nitrogen N10 (Table 4.5, Figure 4.8).

4.4 Unbound docking of PPG protonated at the piperidine-nitrogen (N22)

Unbound docking of protonated PPG at the piperidine-nitrogen (N22) into 1DX6 also yields three possible conformational poses among the first 25 hits. The energetically best of each are shown in Figure 4.9 and Table 4.6.

Docking solution	Protonated	Rank	RMSD (Å)	E_{ass}	LE	E_{nhb}	vdW	E_{est}	E_{cnt}	vdW^{+}	Nhph	Nhb
7	Straight (p)	1	1.87	-57.1	0.3	-57.4	-5.6	-22.2	-29.6	8.4	10	2
8	Bent-In (p)	3	0.52	-54.8	0.0	-54.8	-7.5	-15.2	-32.1	7.8	11	3
9	Bent-Out (p)	12	0.97	-46.7	3.0	-49.7	-4.5	-15.2	-30.0	8.7	12	2

Table 4.6: Numerical data correspond to docking solutions of PPG protonated at the piperidine-nitrogen (N22)

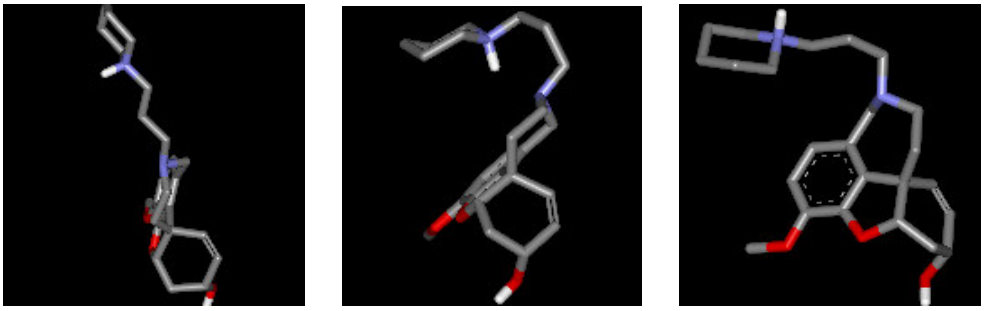

1st rank (Docking solution 7) 3rd rank (Docking solution 8) 12th rank (Docking solution 9)

Figure 4.9: The best solution of the different structural poses of PPG protonated at the piperidine-nitrogen, extracted from Table 4.6

In contrast to the related docking run with protonation at the galanthamine-nitrogen (in previous section), the energetically favored structure with protonation at the piperidine-nitrogen shows a straight side chain as the energetically structure favored and therefore deviates massively from the crystal structure. To finally select the ultimate conformation of PPG, the three first rank answers, i.e. the one from the docking run of unprotonated PPG and from docking the protonated ligand with protonation at either nitrogen, are given in Table 4.7, and compared to the crystal structure in Figure 4.10.

Docking solution	Ligand*	RMSD (Å)	E_{ass}	LE	E_{nhb}	vdW	E_{est}	E_{cnt}	vdW^{++}	Nhph	Nhb
1	Bent-In (up)	0.57	-51.4	7.6	-59.0	-8.5	-18.4	-32.1	6.9	11	2
4	Bent-In N10 (p)	0.46	-55.6	1.2	-56.8	-8.7	-16.9	-31.2	6.5	12	4
7	Straight N22 (p)	1.87	-57.1	0.3	-57.4	-5.6	-22.2	-29.6	8.4	10	2

Table 4.7: The best answer of all three previous unbound docking unprotonated and protonated at (N10, N22)

*: 'p' stands for protonated and 'up' for unprotonated

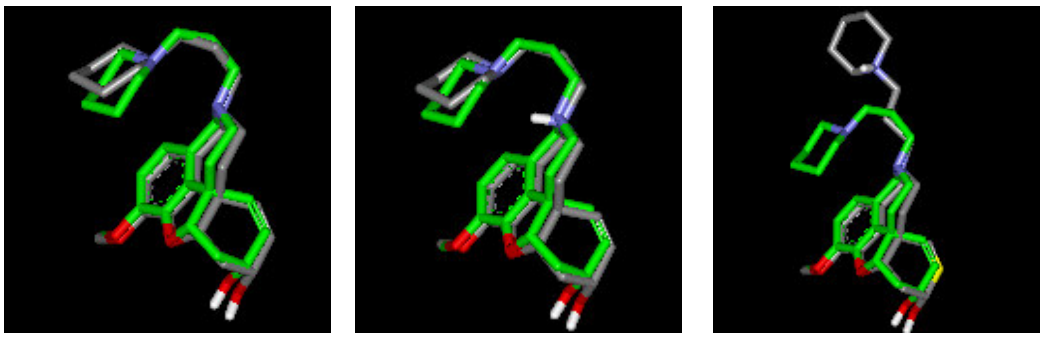

(Docking solution 1, Table 4.2) (Docking solution 4, Table 4.3) (Docking solution 7, Table 4.4)

Figure 4.10: X-ray structure of the neutral ligand (green) overlaid on the first hit answers of unbound docking of unprotonated and protonated PPG

As can be seen form Table 4.7, the protonated structures are energetically preferred, compared to the neutral PPG. However, the best total estimated binding energy is found for the straight structure (Docking solution 7 in Table 4.7), which does not agree with the crystals structure. Here, once more the PPG protonated at galanthamine-nitrogen has the highest S_{Total} among the solutions in Table 4.7 (Docking solution 4 in Table 4.7), which provides another reason for the highest possibility of the bent PPG, protonated at galanthamine-nitrogen.

Up to this step, all docking runs were performed into the binding site of the ligand-unbounded protein (1DX6), reflecting the case that a crystal structure of PPG would not be known. However as the coordinates of the AChE-PPG complex were available to us, before deposition in the PDB-database [38], the experiment was additionally run using the complexed protein (PPG protein).

Despite our finding that the PPG structure with an inside inverted piperidine-ring is the energetically favored result with the most populated conformation for the protonated and even for the unprotonated ligand, that structure is further assisted by a detailed analysis of the interaction energy of the piperidine-moiety with surrounding amino acids. Table 4.8 displays the particular interaction energies for the two piperidine conformations, and although the overall number of interacting amino acids is higher in case of the outside inverted ring, the inside inverted one shows the stronger interaction energies, which sum up in total to better interaction energy.

Amino Acids	Interaction energy (kJ/mol) for PPGP- N10 Inside inverted piperidine	Interaction energy (kJ/mol) for PPGP- N10- Out side inverted piperidine
Tyr334	-6.2	-8.6
Phe331	-16.2	-9.7
Asp72	-11.3	-5.2
Phe290	-	-3.0
Tyr121	-	-4.0
Sum	-33.5	-30.0

Table 4.8: The amino acids that interact with piperidine ring of PPG causing piperidine ring inversion.

Summarizing our results for PPG, we therefore would propose a PPG-structure with an inside inverted ring as shown in Figure 4.6. In terms of our overall aim, to find a galanthamine derivative that simultaneously can block the esterase- as well as the PAS-site, PPG would not be a suitable candidate. However the docking experiments with PPG gives valuable

information as to the need of a longer N-alkyl side chain in order to block the entire active site gorge. Such a structure would be the already described BHG.

5 Molecular docking studies on the "Back Door" hypothesis

Acetylcholine is the product of the hydrolization process, which is believed to leave the active site-gorge of AChE through the normal pathway passing the rim of the gorge. From studying on X-ray structure of AChE arise many questions about substrate solution and product release. The structure of AChE is characterized by a high negative charge (-14e for *Tc*AChE) [77], which is distributed asymmetrically over the protein. This negative electrostatic potential grows along the active-site gorge toward its base and has the largest negative value at the bottom of the gorge, so that a strong electrostatic dipole momentum is directed toward the lower part of the binding site [78]. It means this factor steers positively charged ligand down the gorge [79] that electrostaticly establishes an appropriate location for accommodating the positively charged portion of the ligand, inside the deep and narrow gorge. This could prevent the positively charged ACh acylation-product leaves the gorge easily [80]. That is, the presence of a back door is assumed for the easier clearance of the hydrolization product through the closer exit doors in the bottom of the gorge than the mouth of that. A thin wall near the base of the active site, at proximity of residues Met83 and Trp84 possibly offers an alternative pathway for clearance of the product [78].

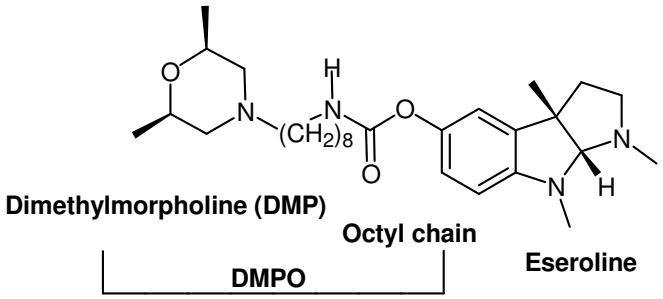

Figure 5.1: Chemical structure of MF268

MF268 (Figure 5.1) is an analogue of physostigmine with pseudo irreversible inhibitory effect on AChE, which belongs to the class of carbamate acetylcholinesterase inhibitors. It carbamoylates the catalytic serine, which afterwards is regenerated by hydrolysis. The amino acids of catalytic triad of the active site gorge (Glu327, His440, and Ser200) are involved in carbamoylation process and the ligand is cleaved in two parts during the performance of the mechanism. One part is dimethylmorpholinoocthyl (DMPO), that covalently binds to Ser200 and the other part is the leaving group eseroline (Figure 5.2).

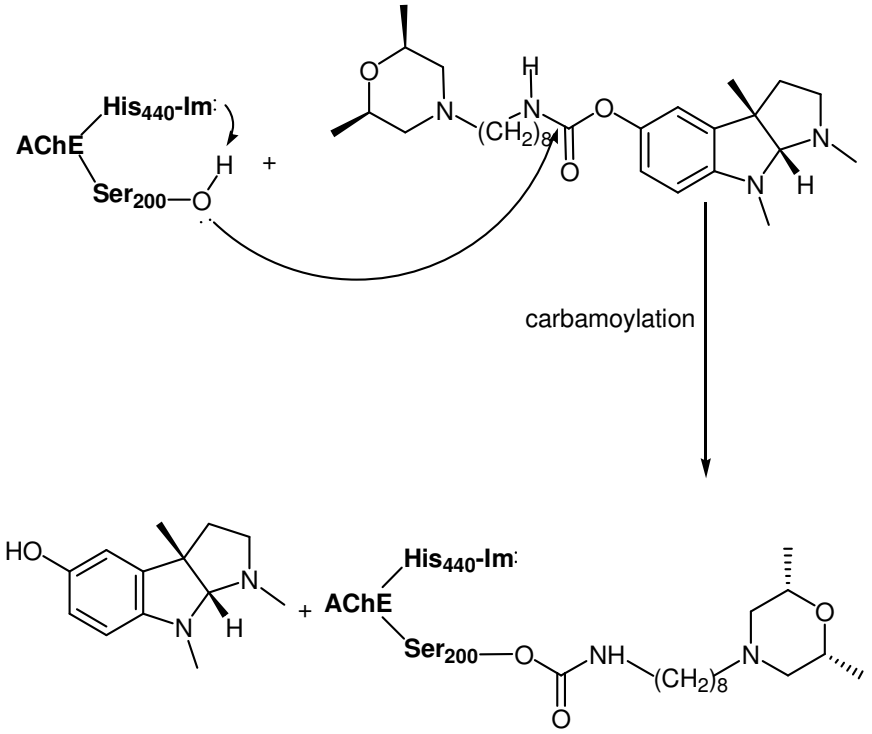

Figure 5.2: Mechanism of carbamoylation

Since the bulky eseroline is not found in the X-ray structure of the ligand-AChE complex (1OCE) [81], it thus implies the presence of a back door in the bottom of the binding site. In this approach, for clearance of the eseroline, Bartolucci et al. proposed two possible exit doors. One is a shutter-like in plane motion of Trp84, Val129 and Gly441 (red colored channel in Figure 5.3) and a flap-like conformational transition of the Ω-loop stretching from Cys67 to Cys94 (orange colored loop in Figure 5.3) [81].

Recently, Greenbalatt et al. proposed a "side door" for the clearance of the ACh acylation-product that might provide the third alternative exit for the acetyl group, rather than for choline. They suggest a facial rearrangement of the Trp279-Ser291 loop (blue colored region in Figure 5.3), which may produce a significant increase in the diameter of the gorge, facilitating a passage for the bulky, rigid inhibitors [82]. Using our MSD method, we have tried to give further answers to the on going discussions on the presence of a back or side door for product clearance from binding site of AChE.

The three-dimensional structure of *Torpedo Californica* acetylcholine esterase (*Tc*AChE) complexed with DMPO was retrieved from Protein Data Bank with accession code 1OCE [81]. MSD consensus method of QXP^+ besides G.O.L.D with Chem. and Gold Scores were employed as docking programs.

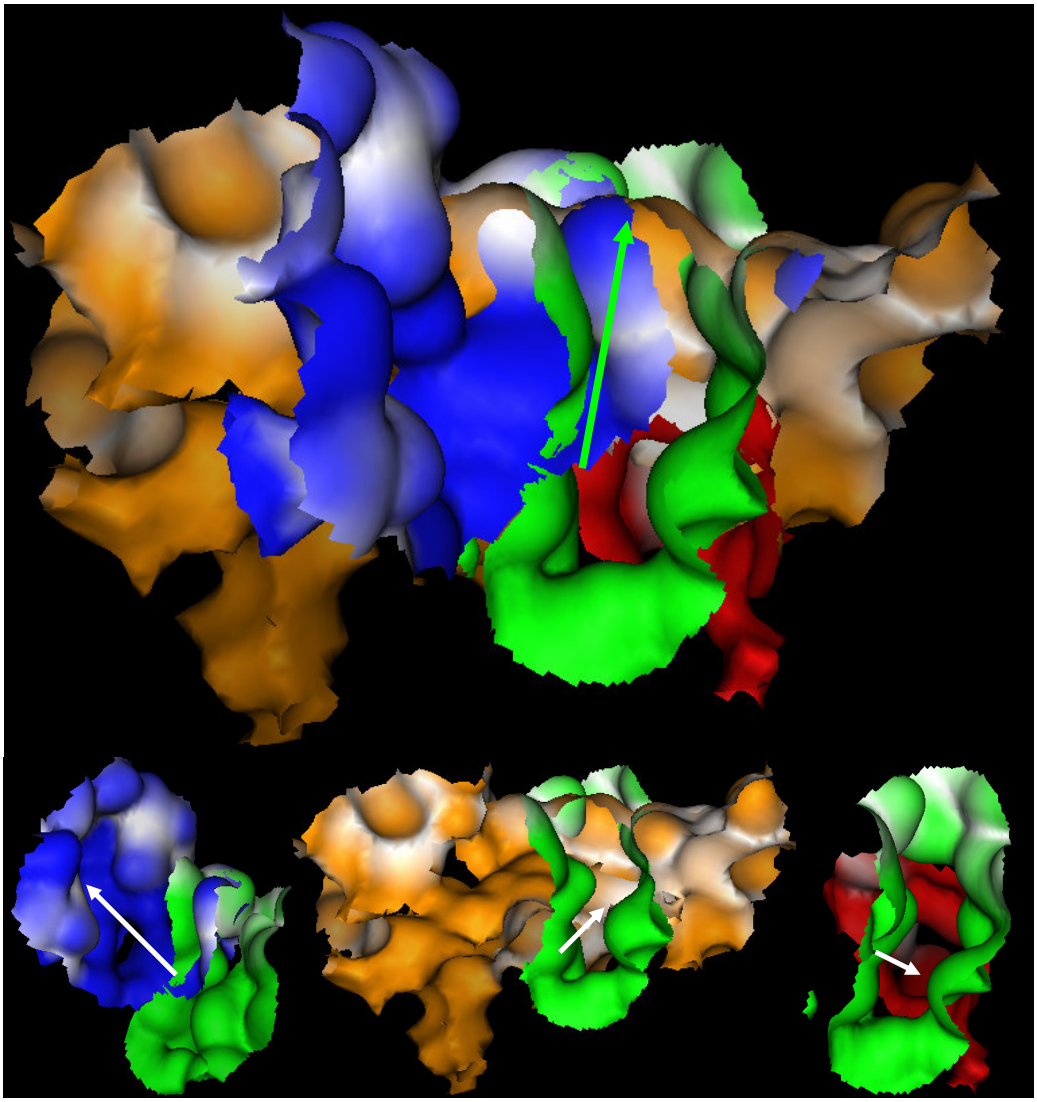

Figure 5.3 : Three alternative exit doors around binding site gorge (upper); the side door (blue, left) alternative channel (red, right); Ω-loop (orange, middle) and the green arrow shows the direction of exit through mouth of the gorge (green), white arrows displays the exit direction in each of the pathways.

5.1 Docking study on protonation of DMPO

5.1.1 MSD method

The docking experiments of DMPO in two protonated and unprotonated states were individually performed in the binding site of 1OCE, using MSD consensuses method. The obtained total estimated binding energy of the complex for protonated DMPO has -1.7 kJ/mol lower energy than of that in unprotonated DMPO, as well as a higher S_{Total} (Docking solution 2 in Table 5.1), which is not able to reproduce the ligand structure correctly, because with respect to the position of the DMPO in X-ray structure, the RMSD value of the unprotonated

ligand (1.07 Å) is lower than protonated one (1.63 Å). Figure 5.4 shows the conformational pose of DMP in both protonated and unprotonated DMP substructure of the ligand. The unprotonated one has a ring inversion of DMP, as compared to the ring conformation in X-ray structure (Figure 5.4, the upper). This ring inversion of the docking solution is caused by a hydrogen bond between DMP oxygen and Tyr70 hydroxyl group (Figure 5.4, the upper). In contrast, the docking solution of protonated DMP shows a perpendicular position of the morpholino ring with X-ray structure of the ligand (Figure 5.4, the lower). According to the resulting RMSDs (Table 5.1), DMPO is not protonated.

Docking* Solution	RMSD (Å)	E_{ass}	LE	E_{slb}**	E_{nbd}	vdW	Eest	Ecnt	vdW+$^{+}$	Nhph	Nhb
1 (up)	1.07	-28.0	1.9	5.7	-35.6	-2.3	-15.4	-17.8	5.8	7	1
2 (p)	1.63	-29.7	0.0	6.7	-36.4	-3.0	-18.8	-14.5	3.7	5	1

Table 5.1: Results of docking protonated and unprotonated DMPO into the binding site of 1OCE.

*:'up' stands for unprotonated and 'p' for protonated DMPO.

**: E_{slb} stands for the covalent bond energy of the ligand

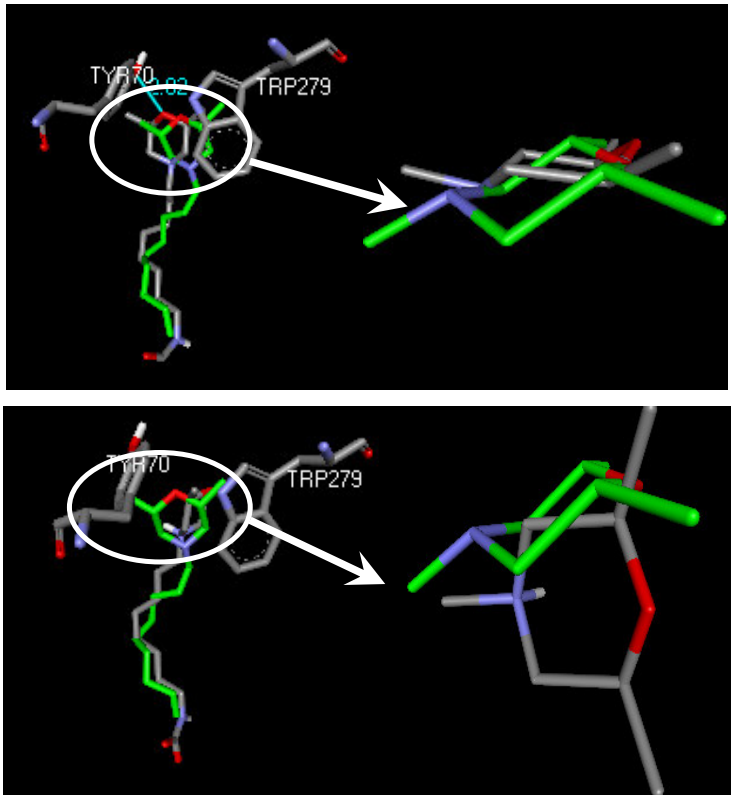

Figure 5.4: Illustrates the position of the solutions of docking DMPO (gray) with unprotonated DMP having inverted morpholino ring (the upper) and with protonated DMP having perpendicular pose of morpholino ring (the lower). X-ray structure has been colored in green.

To have a more reliable resolution for the possibility of protonation at DMP, we took advantage of another docking tool. For this purpose G.O.L.D with two scoring functions (Chem. Score and Gold Score) were utilized.

5.1.2 G.O.L.D

To examine the accuracy of MSD result, in the next step, G.O.L.D with Chem. Score was employed. Similar to the previous step, RMSD of unprotonated ligand has 1.01 Å value (Docking solution 3, Table 5.2), which is lower than of that in protonated DMPO with 2.50 Å RMSD (Docking solution 4, Table 5.2). Due to this fact that G.O.L.D scoring functions have been trained to count hydrogen-bond energy as an important component of the fitness function and each possible hydrogen-bonding pair contributes with high weight to the overall energy of binding [83] [84], therefore the fitness score for protonated ligand is 2.40 more than unprotonated ligand, because the hydrogen-bonding score of the former is higher.

The Ligplot view of the docking solutions of Chem. Score, are shown in Figure 5.5. The DMPO forms a stable adduct with AChE, so that *in vitro* enhances an irreversible-like character.

According to the docking results, in addition to the covalent bond between DMPO and Ser200, two hydrogen bonds are established between carbamet oxygen and NH of Gly118 and Gly119 at oxyanion holes. These bonds besides other hydrophobic interactions keep the ligand for a longer time in the gorge and stabilize the binding of the ligand with active site (Figure 5.5). In contrast the protonated DMPO makes a hydrogen bond at N^+ with OH group of Tyr121 and establishes three extra hydrogen bonds with catalytic triad at bottom of the gorge. This hydrogen bond is a driving force to bend the long hexyl chain downward to the base of the gorge and make a distance from rim of the gorge (Figure 5.5). It means, if the DMP were protonated, there would be more space close to rim of the gorge, for the leaving group (eseroline) to leave the binding pocket through the mouth of the gorge, whereas the unprotonated ligand better blocks the mouth of the gorge (the lower in Figure 5.5). Besides these two possibilities the backbone of DMPO blocks the space of the gorge and seems to be the main obstacle for leaving eseroline through the mouth. These factors direct the leaving group toward other possible pathways (Figure 5.3).

Docking solution	Ligand*	Total fitness score	RMSD (Å)	Hydrogen bond score
3	(up)	27.09	1.01	0.85
4	(p)	29.49	2.50	0.98

Table 5.2: Score and RMSD of docking solutions of protonated and unprotonated DMPO into the binding site of 1OCE using Chem. Score

*:'up' stands for unprotonated and 'p' for protonated DMPO.

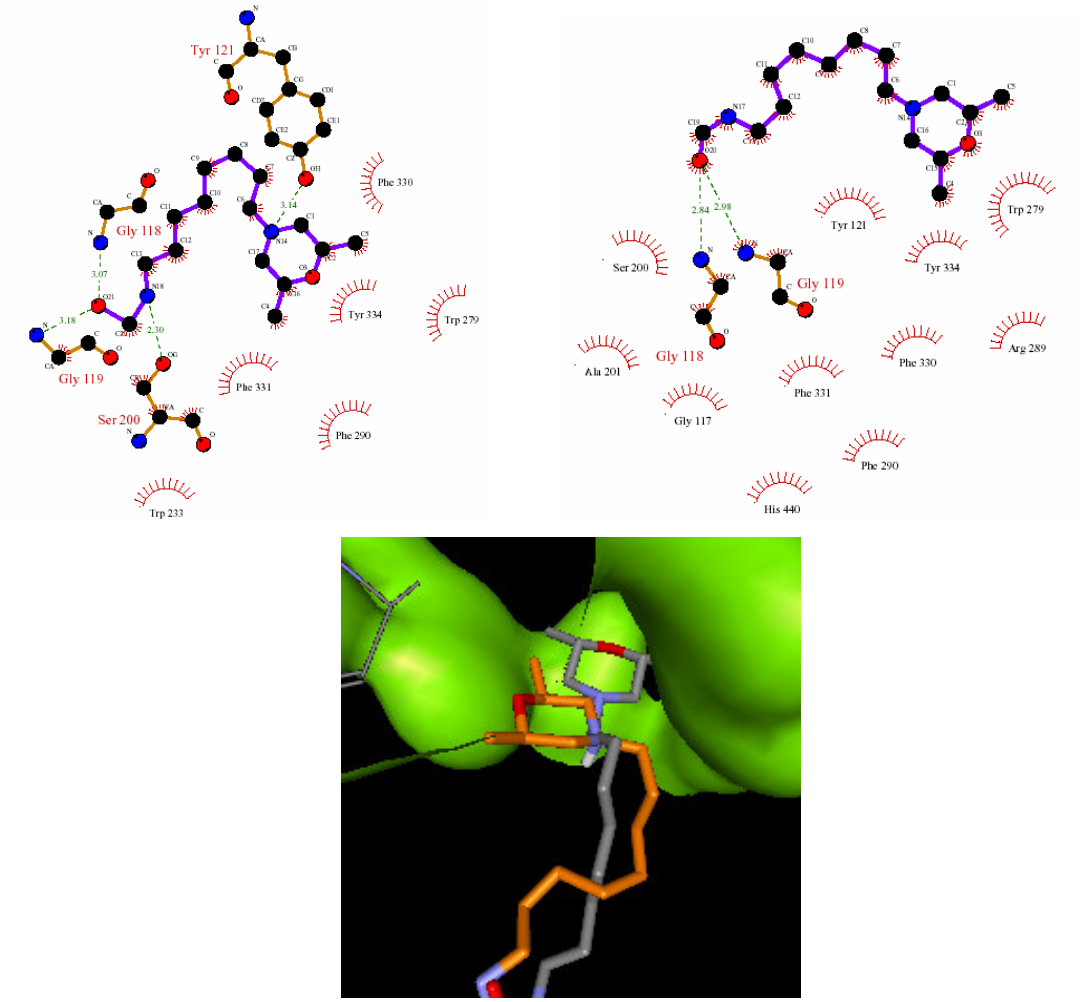

Figure 5.5: Solution of docking DMPO, unprotonated (up-left) and protonated (up-right). Overlaid docking solutions of protonated DMPO (orange) and unprotonated DMPO (gray) indicates that unprotonated DMPO better blocks the mouth of the gorge (green) than the bent pose of the protonated DMPO.

Furthermore, result of docking using Gold Score also confirms that ligand is not protonated at DMP moiety and the docking solution of the unprotonated ligand better resembles the X-ray structure, so that the corresponding solution has RMSD of 1.13 Å (Docking solution 5 in Table 5.3) versus 2.47 Å (Docking solution 6 in Table 5.3) for protonated ligand. Again, the much larger score of hydrogen bond for protonated DMPO (11.51, Table 5.3) increases the fitness score in favor of protonation, which is 43.54 versus 37.43 for the unprotonated one (Table 5.3). This is due to the extraordinary weight of hydrogen bond in G.O.L.D scoring functions.

Docking solution	Ligand*	Total fitness score	RMSD (Å)	Hydrogen bond score
5	(up)	37.43	1.13	0.75
6	(p)	43.54	2.47	11.51

Table 5.3: Score and RMSDs of docking solutions for protonated and unprotonated DMPO in the binding site of 1OCE, using Gold Score.

*: 'p' stands for protonated and 'up' for unprotonated

Up to this step, in all three experiments, the docking results of only **unprotonated** DMPO is close to the X-ray structure. Furthermore it is necessary to find the appropriate position of the leaving group after cleavage and find out if there is any alternative exit door for its clearance.

5.2 Study on the location of leaving group in the absence of DMPO

Docking experiments on eseroline were carried out, assuming three protonation states for eseroline with the neutral, protonated at N5 and protonated at N7, respectively (Figure 5.6).

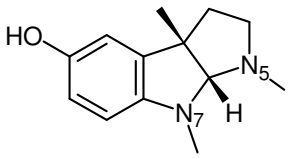

Figure 5.6: Chemical structure of eseroline

In the absence of DMPO, the eseroline in three different states was individually docked into the binding site of AChE. According to the docking solutions, probability of protonation at N5 is rejected, because docking result suggests a location for eseroline, which in the DMPO-AChE complex (1OCE) is occupied by DMPO (left in Figure 5.7 & Docking solution 9 in Table 5.4). The location of docking solutions of protonated ligand at N7 and neutral ligand are very close to each other, as it is demonstrated in Figure 5.7 (right), protonated eseroline (magenta) is perfectly superimposed on the neutral eseroline, gray (right in Figure 5.7). In contrast to N5-protonated eseroline, their nitrogens do not overlap with DMPO. The very close locations of the both states of eseroline (protonated at N7 and unprotonated) suggest that eseroline takes up this space after split off from MF268 by Ser200.

Docking solution	Ligand*	E_{ass}	LE	E_{nhb}	vdW	E_{est}	E_{cnt}	vdW^+	Nhph	Nhb
7	(up)	-32.6	0.6	-33.2	-2.0	-15.0	-16.2	5.9	6	2
8	N7 (p)	-32.5	1.4	-34.0	-3.4	-14.4	-16.1	4.4	5	2
9	N5 (p)	-34.6	0.5	-35.1	-4.1	-15.6	-15.4	3.5	5	2

Table 5.4*:* Results of docking Eseroline as regard to three different possibilities of protonation states

*: 'p' stands for protonated and 'up' for unprotonated

Table 5.4 indicates the numerical data obtained from docking eseroline in three different protonation states. The neutral eseroline has a higher S_{Total} (Docking solution 7 in Table 5.4) than protonated ligand at N7 (red numbers in Table 5.4). Unprotonated eseroline seems to be energetically slightly more favored than protonated one, although the locations of both are approximately identical.

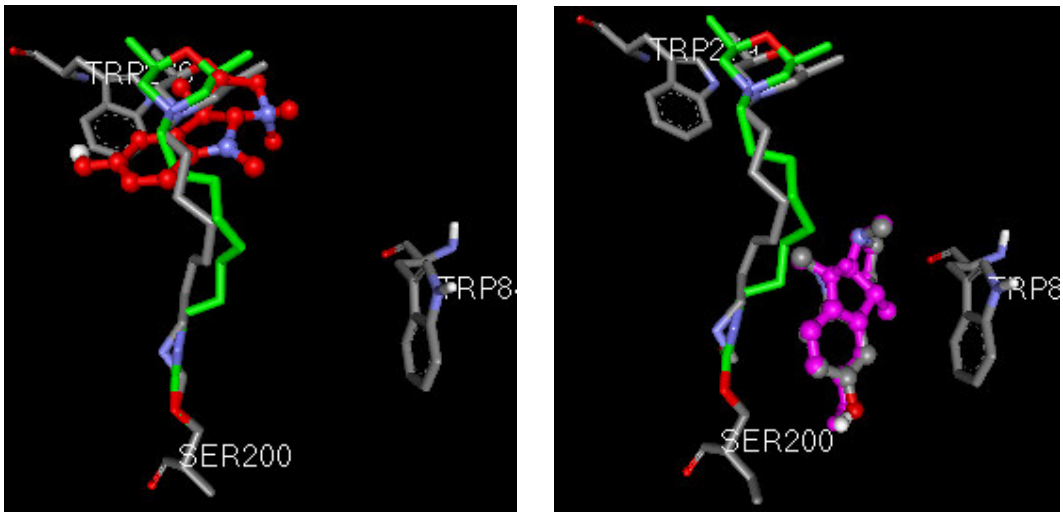

Figure 5.7: Docking solution of N5-protonated eseroline (red) bumps to covalently bonded DMPO in 1OCE (green) (left), Docking solutions of N7-protonated eseroline (magenta) is superimposed on the docking solution of the neutral eseroline colored in gray (right), both of which do not interfere with DMPO (green). The docking solution of DMPO, obtained from QXP^+, is in gray color.

5.3 Study on the location of leaving group in presence of DMPO

5.3.1 MSD method

The result of previous step demonstrates that there are only two possibilities for the leaving group, which could be either neutral or becomes protonated at N7 position, therefore in this experiment, DMPO, covalently bonded to Ser200, was included in the binding site and again

two independent MSD runs of unprotonated and protonated (N7) were performed into the binding site of 1OCE.

Docking solution	Ligand*	E_{ass}	LE	E_{nbd}	vdW	Eest	Ecnt	vdW^{+}	Nhph	Nhb
10	(up)	-29.0	0.2	-29.2	-0.5	-6.3	-22.4	10.0	6	1
11	N7 (p)	-26.7	1.9	-28.6	1.7	-8.4	-22.0	11.5	7	2

Table 5.5: Results of docking eseroline with neutral and protonated N7

*: 'p' stands for protonated and 'up' for unprotonated

Once more, the positions of the eseroline in docking results of both neutral and protonated ligand (N7) are identical. The docking solution of the neutral eseroline has larger S_{Total} than protonated eseroline (red numbers, Table 5.5). In accord with the priority of the neutral ligand in different energy terms, at the result of this experiment, the neutral state is suggested as the answer of docking with MSD.

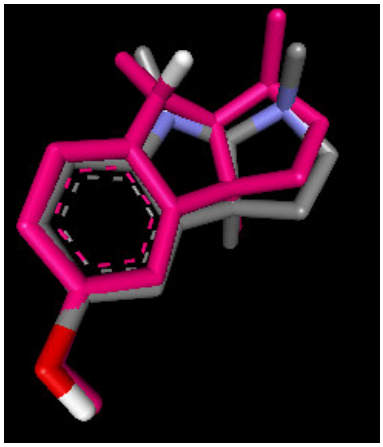

Figure 5.8: Overlaid docking solutions of protonated (magenta) and neutral (grey) using QXP^{+}

The location of the eseroline was found in the proximity of the channel that confirm alternative channel at the bottom of the gorge close to Trp84 and His440 (colored in red in Figure 5.9, left). The leaving group, eseroline, is located in the proximity of the quaternary anionic site of the binding site having a $\pi-\pi$ stacking with aromatic ring of Trp84. The hydroxyl oxygn of eseroline bonds to carbonyl oxygen in His440. The N7 nitrogen has a polar-polar interaction with hydroxyl group in Ser122. Also carbonyl group of Glu199 interacts with N5 in eseroline group. The interaction energies of the corresponding amino

acids are listed in Table 5.6. The most involved amino acid with eseroline is Trp48 with interaction energy of -16.4 kJ/mol (Table 5.6).

Amino Acids	Interaction energy (kJ/mol)
Ser122	-7.9
Gly118	-13.5
Gly117	-3.4
His440	-14.9
Glu199	-5.1
Trp84	-16.4

Table 5.6: Interaction energies of the amino acids that surround neutral eseroline

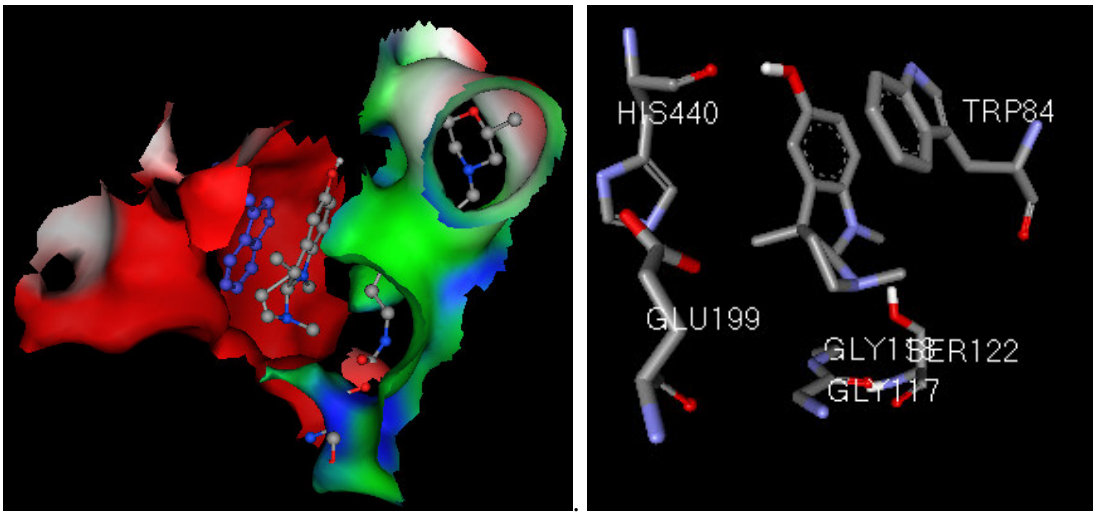

Figure 5.9: The position of docking solution of eseroline (gray) using MSD method. It is located in front of the alternative channel, colored in red. Trp84 colored in blue, located in the entrance of the gate (left), the amino acids of binding site in AChE interacting with the neutral eseroline (right)

5.3.2 G.O.L.D

By individually docking the neutral and protonated eseroline, using Gold Score, resulting solutions show a larger fitness score for the neutral 177.52 (Docking solution 12, Table 5.7) versus 124.90 for protonated eseroline (Docking solution 13, Table 5.7). These results are once more in favor of the neutral state, as the fitness score of that has 51.96 weight more than of protonated one.

Docking solution	Docking solution	Fitness score
12	(up)	177.52
13	N7 (p)	124.90

Table 5.7: Fitness score of the binding mode of the ligand in neutral and protonated states

Furthermore, Figure 5.10 demonstrates that the location of the neutral ligand (yellow) obtained from Gold Score, is much closer to the docking solution of the neutral ligand with QXP^+ (gray), whereas Gold places the protonated ligand (magenta) quite far from the resulting position of the neutral ligand. The identical positions, suggested by Gold Score and QXP^+ provide firstly, a high probability of the neutral state for eseroline. Secondly, due to the placement of docking solutions of the neutral ligand (yellow and gray) in proximity of Trp84, Tyr130 and His440 in front of the channel (Figure 5.10), it increase the probability of clearance of eseroline via this particular alternative channel.

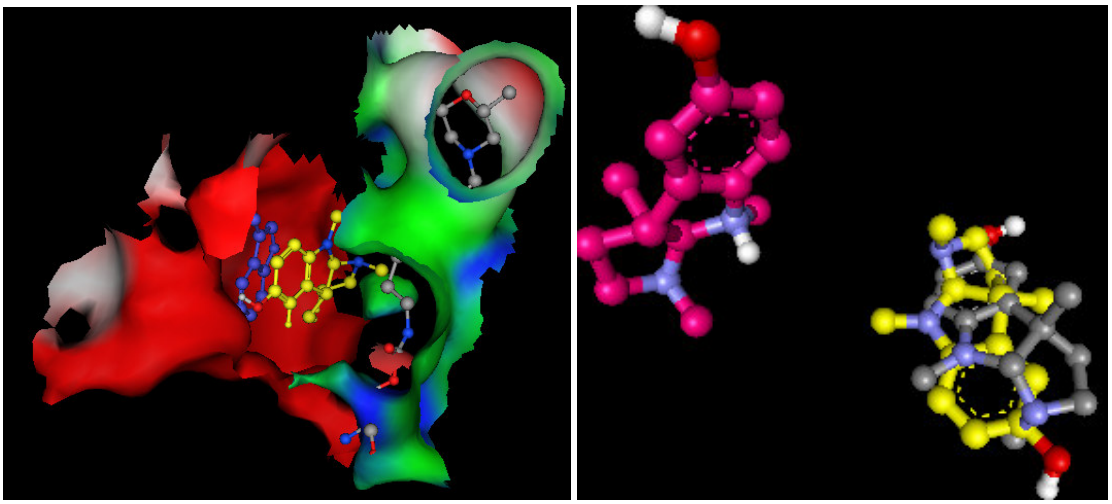

Figure 5.10: Overlaid docking results of Gold Score for the neutral eseroline (yellow) on docking solution of QXP^+ (gray). Docking solution of Gold Score for protonated eseroline (magenta) is far from the neutral ligand (right), the position of docking solution of Gold Score (yellow) is in front of the alternative exit door, red channel (left)

Docking of neutral and protonated eseroline was repeated using Chem. Score of G.O.L.D program. In this experiment again the neutral ligand has better fitness score 177.40 (Docking solution 14, Table 5.8) versus 125.44 for protonated ligand (Docking15, Table 5.8).

Docking solution	Ligand*	Fitness score
14	(up)	177.40
15	N7 (p)	125.44

Table 5.8: Fitness score of the binding mode of the ligand in neutral and protonated states
*:'up' stands for unprotonated and 'p' for protonated DMPO.

This experiment proposes that the positions of the ligand in both states, neutral (brown) and protonated (magenta) are very close to each other as it is observable in Figure 5.11 (left). In addition, the solution of the neutral ligand with both scoring functions of G.O.L.D are in identical position, brown and yellow colored ligand, (right in Figure 5.11), with very close fitness score (177.52 in Gold Score and 177.40 in Chem. Score).

In Figure 5.11 (right), it is obvious that docking solutions of the neutral ligand obtained from QXP^+ (gray), G.O.L.D with Gold Score (yellow) and Chem. Score (brown) are located very close to each other. This confirms that the most possible location of the leaving group is where the alternative channel exists, which is created by Trp84, Tyr130 and His 440, whose shutter like motion permits the eseroline to leave the active site gorge of AChE (Figure 5.11).

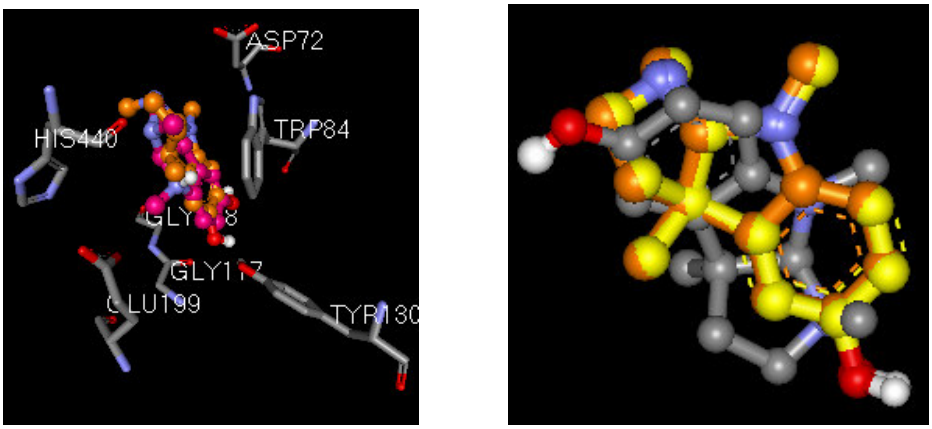

Figure 5.11: The docking solutions of the neutral (brown) and protonated ligand (magenta) obtained from Chem. Score (left), the result of Gold Score (yellow), Chem. Score (brown) and QXP+ (gray) by docking neutral eseroline (right)

5.4 Docking experiment on eseroline in presence of waters

The effect of water molecules was considered to analyze their possible influence on leading the leaving group eseroline in the direction of the alternative channel at the bottom of the gorge. Therefore in next experiment eseroline was immersed into the waters of binding site (Wat801, Wat805, Wat811, Wat812, Wat819, Wat831, Wat839, Wat840, Wat884, Wat842, Wat892, and Wat903). This subset was the starting point for next experiment when flexible waters were included in binding site. Result of this step clearly demonstrates the effect of the waters to force the ligand toward the back door channel (green ligand in Figure 5.12).

In this experiment, the docking solution of the neutral eseroline interacts with Glu445, Tyr485, Asn429, Val431, and Leu430 (green, Figure 5.12). This establishes the

circumstances, in which leaving group is led toward out of the gorge passing the back door channel made by Trp84, Tyr130, His440 (Figure 5.12).

Amino Acids	Interaction energy (kJ/mol)
Glu445	-25.6
Tyr485	-2.5
Asn429	-7.5
Val431	-4.6
Leu430	-6.5

Table 5.9: Shows the amino acids that interact with docking solution of the neutral eseroline, in a binding site with flexible waters.

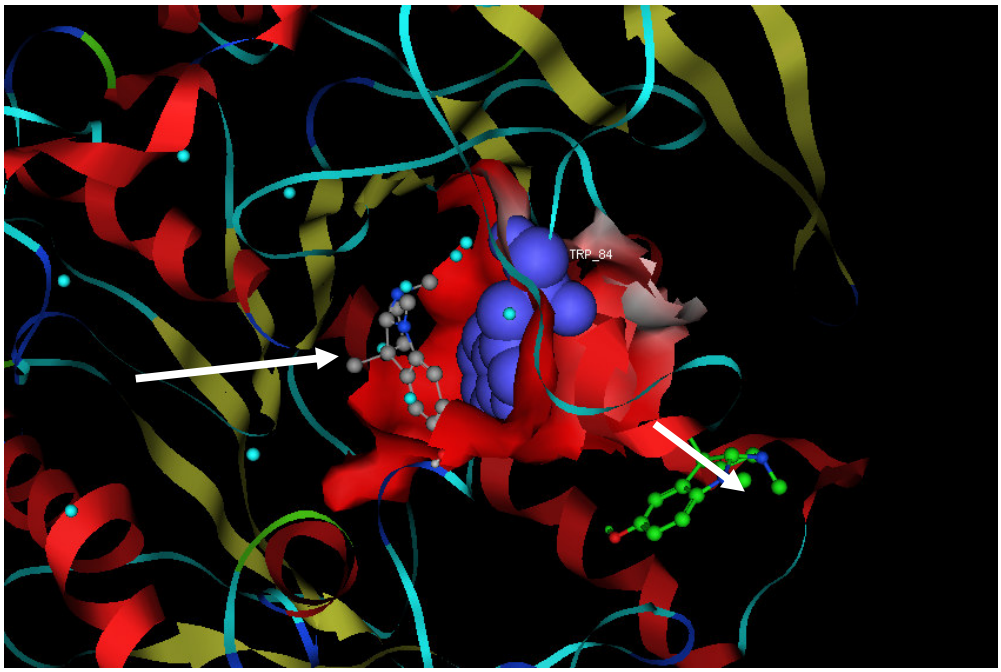

Figure 5.12: Shows the position of the neutral eseroline proposed by docking into empty binding site (gray) and with binding site having flexible waters (green), water molecules are shown in blue color. The back door channel is red that has an entrance in active-site gorge that is open by shutter like motion of Trp84 (dark blue residue).

Table 5.9 indicates that Tyr442 is the most interactive amino acid with -24.7 kJ/mol interaction energy.

The results of all the experiments provide existence of a back door in bottom of the gorge where the eseroline can leave the binding site through that specific alternative pathway.

Since, eseroline is a leaving group not seen in X-ray structure, it thus stays in active site for a very short time. Therefore it is reasonable to say that ligand must be neutral. If it were a positively charged ligand it had to stay longer, due to the electrostatic interaction with high negatively charged area at the base of the gorge. In that X-ray data should have identified its location in the gorge.

As it is shown in Figure 5.13 [79] a very strong negative magnetic field in the lower part of the gorge prevents that the positively charged ligand easily leave the gorge and it will cost considerable energy to overcome this electrostatic interactions. Also the electrostatic interactions of the amino acids in the base of the gorge would be in better electrostatic interaction with positively charged moiety of the ligand than with neutral one. In Figure 5.14, the red colored area in the base of the gorge shows the highest negatively charge in binding site of AChE.

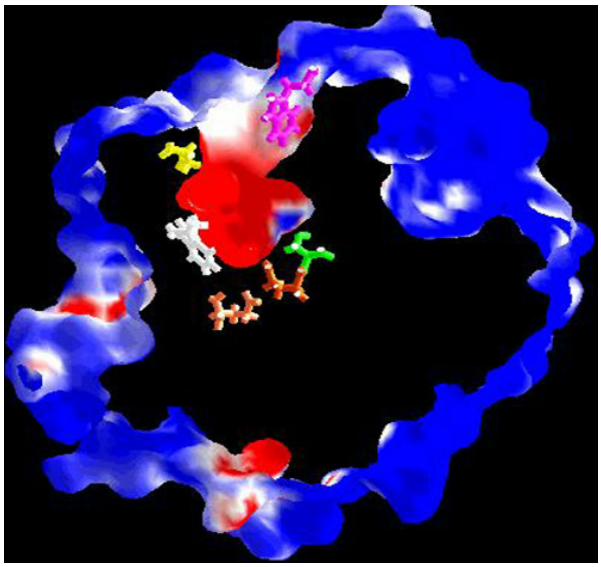

Figure 5.13: Shows the negative magnetic filed of the binding site gorge in AChE (red) and positive field (blue). Trp279 in top of the gorge (magenta), Trp84 (white), Gly118 and Gly119 in brown, Asp72 (yellow) and Ser200 is shown in green [79]

In this investigation was found that DMPO is unprotonated, as the correct structures were obtained at the result of docking unprotonated ligand using QXP^{+} and G.O.L.D. Docking results of eseroline demonstrate that it is neutral and its orientation and location after cleavage was found by simulated annealing. The result of docking into empty binding site proves that among four possible exit doors (Figure 5.3) only the alternative channel-like pathway is the exit door. Trp84, Tyr130 and His440 make this channel. In the entrance part of this channel, Trp84 is located that permits the clearance of the eseroline by a shutter like motion. Adding

flexible waters of binding site, extracted from X-ray structure, led to finding the pathway for eseroline for exiting the gorge, as the docking result shows that eseroline locates out of the gorge by the force of waters.

6 Binding mode prediction of galanthamine derivatives using MSD

In an effort to increase the affinity of galanthamine for AChE, galanthamine derivatives were designed with the aim to create bisfunctional compounds that interact with two binding sites on the AChE. The sites targeted on AChE are the anionic subsite of the active site in the bottom of the gorge, and the peripheral anionic site near top of the gorge.

One of these derivatives of galanthamine is a bisamide analogue, in which two galanthamide of the molecule are connected via an alkyl side chain. In this work, bisgalanthamides with different alkyl spacer length are studied, in which the number of methylen groups differentiate between 1 till 8 (Figure 7.1).

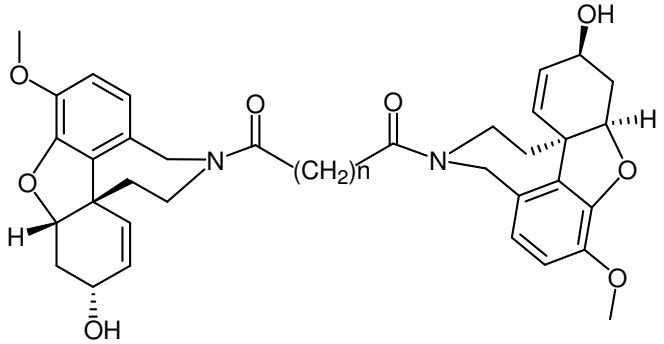

Figure 7.1: Chemical structure of bisgalanthamide, which has 1 till 8 methylen groups, in the alkyl spacer.

6.1 Binding mode prediction of bisgalanthamide analogues into AChE binding site

To find an optimal derivative of galanthamine that covers the entire space of the binding site in AChE, eight analogues of bisgalanthamide ligands with a spacer of one till eight methylen groups were considered by docking the ligands into the active site of 1QTI.

The numerical results, from eight individual MSD experiments on these bisgalanthamides, are shown in Table 7.1. As regards to the highest S_{Total} in bisgalanthamide with heptyl chain (Docking solution 2 in Table 7.1), the ligand with heptyl spacer is suggested as the optimal length for connecting amides substructures. Figure 7.2 demonstrates that in all the ligand, with 8 different spacer-lengths, the locations of the galanthamides are identical at the lower part of the gorge. The main change is distinguishable in the upper part of the ligand, which occurs due to the high flexibility of the side chain, as the longer chain has the higher degrees of freedom (Figure 7.2).

Docking solution	Nr. CH_2	E_{ass} (kJ/mol)	LE (kJ/mol)	E_{nhb} (kJ/mol)	vdW (kJ/mol)	Eest (kJ/mol)	Ecnt (kJ/mol)	vdW^+ (kJ/mol)	Nhph	Nhb
1	8	-62.5	0.0	-62.5	-13.0	-14.5	-35.0	4.2	13	1
2	7	-67.2	0.0	-67.2	-6.9	-21.3	-39.0	11.0	18	3
3	6	-68.0	0.0	-68.0	-11.2	-19.0	-37.8	6.7	13	2
4	5	-55.8	0.0	-55.8	-11.0	-11.7	-33.1	4.9	15	2
5	4	-57.0	0.0	-57.0	-12.1	-11.5	-33.5	4.7	12	2
6	3	-56.2	3.0	-59.2	-10.4	-12.4	-36.4	6.2	15	1
7	2	-52.0	0.0	-52.0	-9.7	-11.9	-30.4	5.3	12	1
8	1	-43.5	2.1	-45.6	-1.0	-10.8	-33.8	13.9	10	2

Table 7.1: Results of docking study on eight derivatives of bisgalanthamide. The ligand with heptyl side chain has the highest S_{Total} (red numbers); Nr. CH_2: Is the number of methylen in spacer

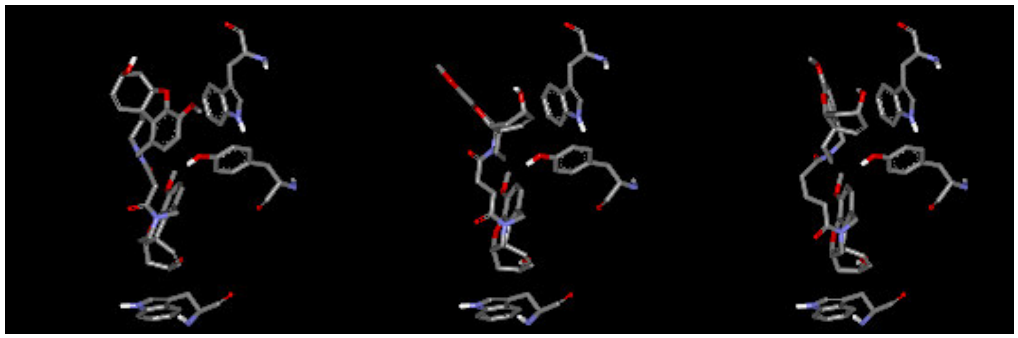

$1CH_2$ **$2CH_2$** **$3CH_2$**

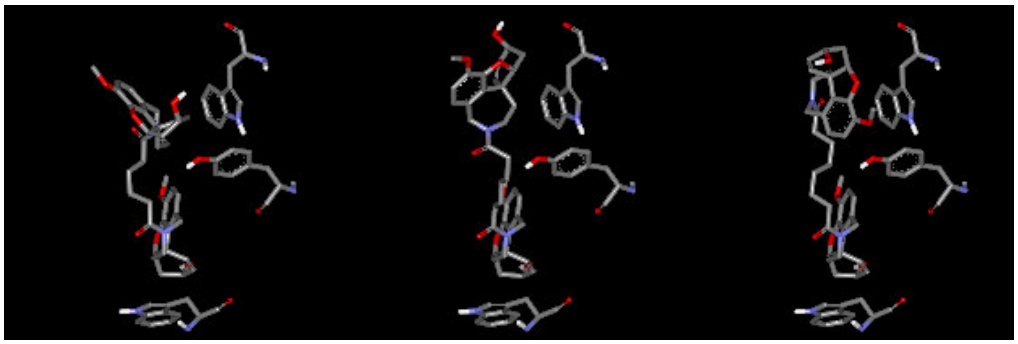

$4CH_2$ **$5CH_2$** **$6CH_2$**

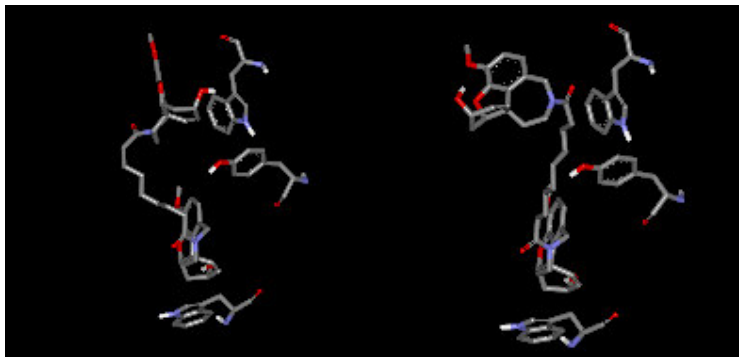

$7CH_2$ **$8CH_2$**

Figure 7.2: Indicates the position of docking solutions of eight different bisgalanthamide derivatives as regards to the position of Trp279 and Trp84 at the upper and the lower part of the gorge, respectively.

The best bisgalanthamide derivative among the eight studied amides is the one with $(CH_2)_7$ spacer. The amino acids of the gorge that interact with different part of the ligand and their corresponding calculated interaction energy are shown in Figure 7.3 and Table 7.2, respectively.

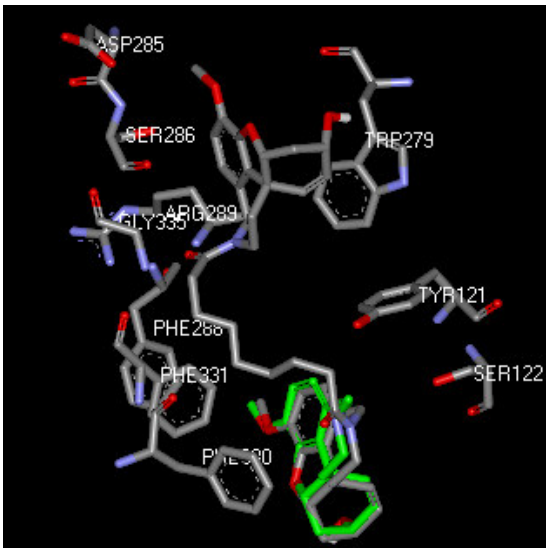

Amino acids	Interaction energy (kJ/mol)
Asp285	-6.0
Trp279	-13.8
Arg289	-5.6
Gly335	-6.4
Phe288	-13.2
Phe330	-6.7
Phe331	-18.3
Tyr121	-4.9
Ser122	-3.2
Ser286	-2.1

Figure 7.3: The overlaid X-ray structure of galanthamine (green) on the docking solution of heptlybisgalanthamide. The bisgalanthamide derivative (gray) interacts with the amino acids directly in the PAS area and with the mid part of the gorge, while galanthamine has no access to them.

Table 7.2: Lists the interaction energy of the involving amino acids in formation of the complex with heptylbisgalanthamide.

The overlaid X-ray structure of the galanthamine (green) and heptylbisgalanthamide, in Figure 7.3, shows that how well the designed ligand interacts in the rim of the gorge with Trp279 in peripheral anionic subsite, however, among the rest of bisgalanthamide derivatives there are some which also interact with Trp279, but the optimum ligand (with heptyl spacer) interacts also with component of the acyl pocket of the gorge at Phe288, Phe290 and Phe331. In the rim of the gorge it has also hydrophobic interactions with Asp285 and Ser286. The most valuable interaction energies correspond to the Phe331 (-18.3 kJ/mol) in the acyl pocket and Trp279 in PAS (-13.1 kJ/mol) (Table 7.2).

6.2 Binding mode prediction of (IHG) into AChE binding site

Another possible inhibitor of galanthamine is indanonehexylgalanthamine (IHG), in which a galanthamine moiety of the ligand is connected to the indanone via a hexyl side chain. Chemical structure of IHG indicates that indanone substructure of the ligand can make it

share in inhibitory effect of E2020 at the upper part of gorge. It can take advantage of special characteristic feature of galanthamine in the lower part of the binding site gorge in AChE. The hexyl side chain can play similar role of the high flexible side chain of BHG that was discussed in chapter 3, which can improve inhibitory effect of the galanthamine by its elongation within the entire 20.0 Å deep and narrow binding site. In order to consider the possibility of having a more potent ligand than galanthamine, E2020 and BHG, indanonehexylgalanthamine (IHG) was studied using MSD method. This would enable us to indicate the possible interaction that can be established by the new ligand as a combination of three potent inhibitors of AChE (Figure 7.4).

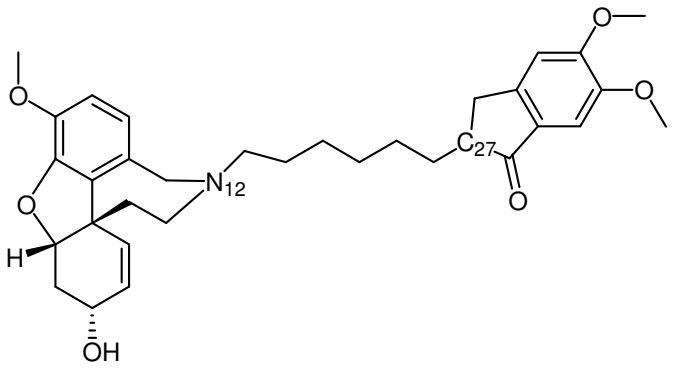

Figure 7.4: Chemical structure of indanonehexylgalanthamine (IHG)

Using docking technique, it was tried to identify the conformational state at galanthamine nitrogen (N12) and configurational state of the molecule in the chiral center (C27) at indanone moiety of the ligand.

6.3 Docking IHG in binding site of 1EVE

Due to similarity of the IHG to E2020 at indanone moiety, the ligand after minimization was docked into the binding site of AChE using 3D structure of 1EVE, which is the complexed protein with E2020. The ligand at the starting point for docking was considered in four different forms, in which C27 was either in *R* or *S*-configuration, when the conformational state at galanthamine nitrogen was either axial or equatorial. It means that four series of independent and individual multi-step docking runs were carried out, in which the ligand had 'a-*S*', 'e-*S*', 'a-*R*' and 'e-*R*' poses, where the first letter stands for axial or equatorial conformation at galanthamine nitrogen and the second letter for *S* and *R* configuration at C27 in indanone moiety of the ligand. The obtained numerical results after running MSD experiments have been shown in Table 7.3.

Docking solution	Starting configmation	E_{ass} (kJ/mol)	LE (kJ/mol)	E_{nhb} (kJ/mol)	vdW (kJ/mol)	Eest (kJ/mol)	E_{cnt} (kJ/mol)	vdW^{+} (kJ/mol)	Nhph	Nhb
1	e-*S*	-53.8	4.4	-58.2	-2.8	-15.0	-40.4	16.0	13	2
2	a-*S*	-45.5	3.6	-49.1	-6.5	-6.9	-35.8	9.8	14	1
3	e-*R*	-59.5	0.0	-59.5	-2.6	-15.9	-41.0	15.9	14	1
4	a-*R*	-47.1	8.6	-55.7	-2.4	-13.7	-39.6	15.7	14	3

Table 7.3: Shows the numerical results of docking the ligand in different conformational and configurational states in its starting point.

The highest S_{Total} belongs to the staring structure of equatorial with *R*-configuration (Docking solution 3 in Table 7.3), which is also the only one with ligand energy of 0.0 kJ/mol. Additionally the starting structures with axial conformation, after involving in multi-step minimization procedure, at the end still keeps their configuration and conformational state and no axial is changed to equatorial. This might be due to heavy and long side chain substitution on nitrogen, whose conformational change requires a large amount of conversion energy. Overlaid X-ray structures of E2020 (orange), galanthamine (green) and BHG on the docking solution of 'e-*R*'-IHG (gray) show that the potential of the ligand is improved in sense of better interacting with Trp279 at PAS. Its galanthamine nitrogen is closer to aromatic ring of Phe330 in a magnitude of 0.53 Å. It has also better aromatic-aromatic interaction with Trp84 in the lower part of the ligand than of that in galanthamine. The detailed interaction energies of the ligand with surrounding amino acids have been listed in Table 7.4. Although, IHG has the same alkyl chain as in BHG, the slightly bent form of that in IHG makes it to have better aromatic-aromatic interaction with Trp279 than in BHG (Figure 7.5).

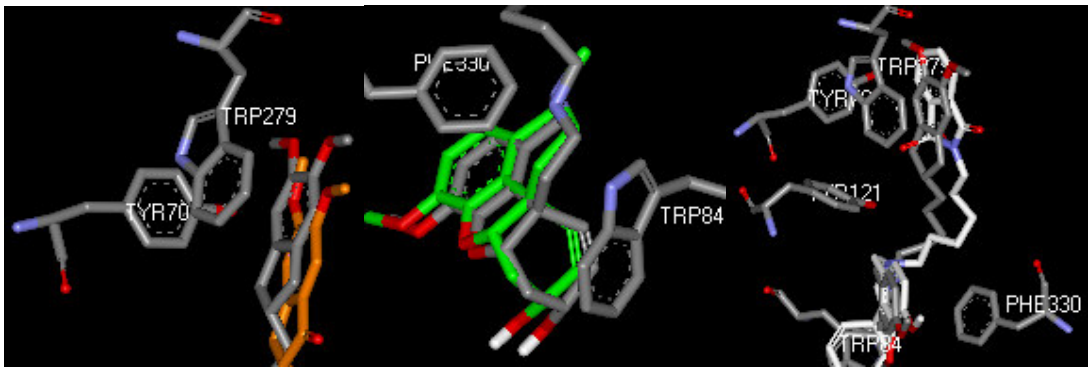

Figure 7.5: Shows the overlaid X-ray structure of galanthamine (green), E2020 (orange) and BHG (white) on the docking solution of 'e-*R*' (IHG). 'e-*R*' (IHG) has better interaction with Trp279 than E2020. Its galanthamine nitrogen is closer to Phe330 aromatic and the double bond of its hydroxyl hexenyl ring closer to Trp84 than galanthamine.

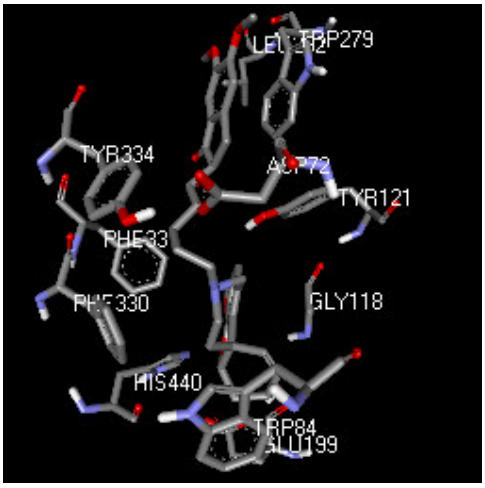

Amino acids	Interaction energies (kJ/mol)
Leu282	-3.4
Trp279	-44.0
Tyr121	-6.0
Tyr334	-8.2
Gly118	-5.7
Ser200	-21.7
Glu199	-23.0
Trp84	-22.7
Phe330	-4.4
Phe331	-8.2
Asp72	-4.8
Ser200	-21.7

Figure 7.6: The amino acids interacting with IHG (e-*R*) in the binding site of AChE (1QTI)

Table 7.4: The interaction energies of IHG with different amino acids in binding site of AChE

Comparing the interaction energy with Trp279 in E2020, BHG and in IHG, which are -16.9 kJ/mol, -20.0 kJ/mol and -44.0 kJ/mol, respectively, reveals that IHG has the best position for involving with Trp279 among three mentioned ligands of AChE.

IHG, due to its better interaction with residue in PAS and its ability to cover the binding site gorge in the upper and the lower amino acids of the gorge is suggested as a good candidate to be synthesized. For this purpose there is strongly emphasis on *R*-configuration in the chiral center at indanone substructure of the ligand.

7 References

[1] W. Moos, F. Hershenson, *Drug News &Perspectives,* **1989**, *2*, 397-409

[2] J. L. Cummings, S. Askin-Edgar, *CNS Drugs*., **2000**, *13*, 385-395

[3] D. A. Evans, H. Funkenstein, M. S. Albert, P. A. Scherr, N. R. Cook, M. J. Chown, L. E. Hebert, C. H. Hennekens, J. O. Taylor, *J. Am. Med. Aso.*, **1989**, *262*, 2551-2556

[4] G. V. Ferrari, M. A. Canales. L. M. Weiner, I. Silman, N. C. Inestrosa, *Biochemistry*., **2001**, *40*, 10447-10457

[5] C. M. Coughlan, C. K. Brean, *Pharmacol. Therapeut*., **2000**, *86*, 111-116

[6] I. Sugimoto, Y. Yamanishi, Y. Iimura, Y. Kawakami, *Cur. Med. Chem*., **2000**, *7*, 303-339

[7] E. A. Barnard, The Peripheral Nervous System, Plenum Press, New York., **1974**, pp, 201-224

[8] D. M, Quinn, *Chem. Rev*., **1987**, *87*, 955-975

[9] J. L. Sussman, M. Harel, I. Silman. *Chem. Biol. Interactions*., **1993**, *87*, 187-197

[10] J. Sussman, M. Harel, F. Frolow, C. Oefner, A. Goldman, *Science*, **1991**, *253*, 872-879

[11] P. Taylor, Z. Radic, *Annu. Rev. Pharmacol. Toxicol*., **1994**, *34*,281-320

[12] Y. P. Pang, A. Kozikowski, *J. Comput¸–Aided Mol. Des*., **1994**, *8*, 669-681

[13] G. Kryger, I. Silman, J. Sussman, *Structure Fold Des*., **1999**, *7*, 297-307

[14] M. W. Qin, H. L. Jiang, K. X. Chen, R. Y. Ji, YJ. Ye., In. *J. Quant. Chem*., **1999**, *74*, 315-330

[15] P. Camps, D. Munoz-Torro, *Mini Reviews in Medicinal Chemistry*, **2002**, *2*, 11-25

[16] J. A. Pesti, *Chem. Innovation*, **2000**, *30*, 22-28

[17] H. J. Pieniaszek,W. D. Fiske, T. D. Saxton, Y. S. Kim, D. M Garner, M. Xilinas, R. Martz, *J. Clin. Pharmacol*., **1995**, *35*, 22-30

[18] M. W. Qin, H. L. Jiang, K. X. Chen, R. Y. Ji, YJ. Ye, *In. J. Quant. Chem*., **1999**, *74*, 315-330

[19] L. S. Schneider, *Curr. Opin. Invest. Drugs*, **2000,** *2*, 427-437

[20] E. Rose, J. Aleu, J. Marsal, C. Solsona, Eur. *J. Pharmacol*., **2000**, *390*, 7-13

[21] A. Martinez, E. Fernandez, A. Castro, S. Conde, I. Rodriguez-Franco, J. E. Banos, A. Badia, Eur. *J. Med. Chem*., **2000**, *35*, 913-922

[22] I. Villalobos, J. F. Blake, C. K. Biggers, T. W. Butler, D. S. Chapin, Y. L. Chen, J. L. Ives, S. B. Jones, D. R. Liston, A. A. Nagel, D. M. Nason, J. A. Nilsen, I. A. Shalaby, W. F. White, *J. Med. Chem*., **1994**, *37*, 2721-2728

[23] J. J. Sramek, E. J. Frackiewicz. N. R. Cutler, *Exp. Opin. Invest. Drugs*, **2000**, *9*, 2393-2402

[24] P. Camps, D. Munoz-Torro, *Mini Reviews in Medicinal Chemistry*, **2002**, *2*, 11-25

[25] I. D. Kuntz, J. M. Blaney, S. J Oatley, R. Langridge, T. E. Ferrin, *J. Mol. Biol*., **1982,** *161*, 269-288

[26] R. Abagyan, M. Totrov, *Curr Opin. Chem. Biol*., **2001**, *4*, 375-382

[27] I. Halperin, B. Ma, R. Nussinov, *Proteins*, **2002**, *47*, 409-443

[28] Bissantz, G. Folkers, D. Rognan, *J. Med. Chem*., **2000**, *43*, 4759-4767

[29] M. Rary, B. Kramer, T. Lengaure, *J. Comput¸–Aided Mol. Des*., **1997,** *11*, 369-384

[30] M. Vieth, J. D. Hirst, B. N. Domin, *J.Comput. Chem*., **1998**, *19*, 1623-1631

[31] O. M. Becker, A.D. MacKerell, Jr. Benoit, M. Watanabe, *Computational Biochemistry and Biophysics*, **2001**, pp74

[32] C. McMartin, R. S. Bohacek, *J. Comp-Aid. Mol. Des*.,**1997**, *11*, 333-344

[33] S. J. Weiner, P. A. Kollman, D.A. Case, U.C. Singh, C. Ghio, G. Algona, S. Profeta, P. Weiner. *J. Am. Chem. Soc*., **1984**, *106*, 765-784

[34] J. Trosset, H. Scheraga, *Biophysics*, **1998**, *95*, 8011

[35] N. Go, H. Scheraga, *Macromolecules*, **1978**, *11*, 552-559

[36] J. Trosset, H. Scheraga, *J. Comput. Chem*., **1999**, *20*, 244-252

[37] M. Metzei, *J. Chem. Phys*., **2002**, 8, 3874-3882

[38] [Personal communication with Dr. Lamba], *International Center for Genetic Engineering and Biotechnology, Trieste-Italy*

[39] G. Kryger, I. Silman, J. Sussman, *Structure Fold Des*., **1999**, *7*, 297-307

[40] H. Greenblatt, G. Kryger, T. Lewis, I., Silman, J., Sussman, *FEBS Lett*, **1999**, *463*, 321-326

[41] M. Harel, I. Schalk, L. Ehret-Sabatier, F. Bouet, M. Goeldner, C. Hirth, P. Axelsen, I. Silman, J. Sussman*, Proc Natl Acad Sci U S A*., **1993**, *90*, 9031-9035

[42] Galli, F. Mori, L. Benini, N. Cacciarelli, Eur. *J. Pharmacol.*, **1994**, *270*, 189-93

[43] R. L. Irwin, H. Smith, *J. Biochem. Pharmacol*., **1960**, *3*, 147-149.

[44] L. Czollner, W. Frantsits, B. Küenburg, J. Fröhlich, *Tetrahedron. Lett*., **1998**, *39*, 2987-2988

[45] A. Maelicke, E. X. Aluquerque, *Drug. Design. Thecnol*., **1996**, *1*, 53-59

[46] N. C. Inestrosa, A. Alvarez, CA. Perez, RD. Moreno, M. Vicente, C. Linker, O. I. Casanueva, C. Soto, J. Garrido, *Neuron*, **1996**, *16*, 881-891

[47] A. Alvarez, C. Opazo, R. Alarcon, J. Garrido, N. C. Inestrosa, *J. Mol. Biol*., **1997**, *272*, 348-361

[48] J. A. Hardy, G. A. Higgins, *Science*, **1992**, *256*, 184-185

[49] D. J. Selkoe, *Annu. Rev. Neurosi.*, **1989**, *12*, 463-490

[50] F. J. Munoz, R. Aldunate, N. C. Inestrosa, *NeuroReport*, **1999**, *10*, 3621-3625

[51] G. Johnson, S. W. Moore, *Biochem. Biophys. Res. Commun.*, **1999**, *258*, 758-762

[52] C. F. Contreras, M. A. Canales, A. Alvarez, G. V. De Ferrari, N. C. Inestrosa, *Protein. Eng*., **1999**, *12*, 959-966.

[53] V. Giancarlo. I. Shin. I. Sillman, *Biochemistry*, **2001**, *40*, 10447-10457.

[54] E. Luttmann, E. Linnemann, G. Fels, *J. Mol. Model*., **2002**, *8*, 208-216

[55] G. Koellner, G. Kryger.C. B. Millard. I. Silman, J. L. Sussman.T. Steiner, *J.Mol.Biol*, **2000**, *296*, 713-735

[56] J. Antosiewicz, J. A. McCammon, M. K. Gilson, *Biochemistry,* **1996**, *35*, 7819-7833

[57] M. G. Nodberg, J. Marelius, S. Ohlsson, A. Persson, G. Swedberg, P. Andersson, S.E. Aqvist, A.Hallberg. *J. Med. Chem.*, **2000**, *43*, 3852-3861

[58] H. Gohlke, K. Klebe, *Angew. Chem. Int. Ed.*, **2002,** *41*, 2645-2676

[59] G. M. Bors, F. P. Huger, W. Petko, A. E. Mutlib, F. Camacho, D. K. Rush, D. E. Selk, v. Wolf, R. W. Kosley, L. Davis, H. M. Vargas, *J. Pharm. Exper. Ther.,* **1996**, *277*, 728-738

[60] K. L. Davis, P. Powchik*, J. Am. Med. Aso*., **1997**, *277*, 10-15

[61] H. Sugimoto, Y. Imura, Y. Yamanishi, K. Yamatsu, *J. Med. Chem*., **1995**, *38*, 4821-4829

[62] A. Inoue, T. Kwai, M. Wakita, Y. Imura, H. Sugimoto, Y. Kwakami, *J. Med. Chem,* **1996**, *39*, 4460-4470

[63] M. Harel, I. Schalk, L. Ehret-Sabatier, F. Bouet, M. Goeldner, C. Hirth, P. Axelsen, I. Silman, J. Sussman*, Proc Natl Acad Sci U S A*., **1993**, *90*, 9031-9035

[64] M. Harel, I. Schalk, L. Ehert-Sabatie, F. Bouet, M. Goeldner, C. Hirth, P. H. Axelsen, I. Silman , L. Sussman, *Proc. Natl. Acad. Sci.*, **1993**, *90*, 9031-9035.

[65] B. G. Benson, H. N. Bramson, S. H. Dickerson, K. M. Dold, D. J. Eberwein, M. Edelstein, S. V. Frye, R.T. Gampe, R. J. Greiffin, P. A. Harris, A. M. Hassell, W. D. Holmes, R. N. Hunter, V. B. Knick, K. Lackey, B. Lovejoy, M. Luzzio, D. Murray, P. Parker, W. J. Rocque, L. Shewsh, *Science***, 2001**, *291*, 134

[66] C. N Hiremath, R. AC. Grant, D. J. Filman, J. M. Hogle, *Acta Crystallogr D Biol Crystallogr*, **1995**, *51*, 473-489

[67] N. F. Proskurina, A. P. Yakovleva, *J. Gen. Chem., USSR*.,**1952**, *22*, 1941-1944

[68] J. N. Champness, M.S. Bennett, F. Wien, R. Visse, W. C. Summers, P. Herdewijn, E. de Clerq, T. Ostrowski, R. L. Jarvest, M. R. Sanderson, *Proteins*, **1998**, *32*, 350-361

[69] M. S. Searle, D. H. Wiliams, U. Gerhard, *J. Am. Chem. Soc*., **1992**, *114*, 1097-10704

[70] E. Grunwald, C. Steel, *J. Am. Chem. Soc.,* **1995**, *117*, 5687-5692

[71] R. Taylor, O. Kennard, *J. Am. Chem. Soc*., **1982**, *104*, 5063-5070

[72] S. Tsuzuki, K. Honda, *J. Am. Chem. Soc*., **2001**, *307*, 367-377

[73] C. A. Hunter, J. K .M. Sanders, *J. Am. Chem. Soc*., **1990**, *112*, 5525-5534

[74] G. M. Bors, F. P. Huger, W. Petko, A. E. Mutlib, F. Camacho, D. K. Rush, D. E. Selik, V. Wolf, R. W. Kosley, L. Davis, H. M. Vargas, *J. Pharmacol. Exp. Ther*, **1996**, *277*, 828-738

[75] H. K. Hall, *J. Am. Chem. Soc.,* **1964,** 3135-3138

[76] H. C. Brown, *J. Am. Chem. Soc.*, **1945**, *67*, 378-381

[77] A. Shafferman, D. Barak, *EMBO Journal*, **1994**, *13*, 3448-3455

[78] M. K. Gilso, T. P. Straatsma, J. A. McCammon, D. R. Ripoll, C. H. Faerman, P. H. Axelse, I. Silman; J. L. Sussman, *Science*, **1994**, *263*, 1276-1278.

[79] C. E. Felder, J. Sussman, I. Silman, *J. Mol. Graph. Mod.,* **1997**, *15*, 318-327

[80] J. Silman, *Science*, **1991**, 253, 872-879

[81] C. Bartolucci, E. Perola, L. Cellia, M. Brufani, D. Lamba, *Biochemistry*, **1999**, *38*, 5714-5719,

[82] H. M. Greenblatt, C. Guillo, D. Guenard, A. Arhaman, S. Botti, B. Badet, C. Thal, I. Silman, JL. Sussman, *J. Am. Chem. Soc.*, **2004**, *126*, 15405-1541

[83] G. Jones, P. Willet, R. C. Glen, *J. Mol. Biol*., **1995,** *254*, 43-53

[84] G. Jones, P. Willet, R.C. Glen, J. Robert, A. R. Leach, R. Taylor, *J. Mol. Biol*., **1997**, *267*, 727-748

8 Abbreviations

AChE	Acetylcholinesterase
BChE	Butyrylchinesterase
E2020	(R,S)-1-benzyl-4-[5,6-dimethoxy-1-indanone)-2-yl] methylpiperidine
FF	Force Field
G.O.L.D	Genetic Optimization for Ligand Docking
hBChE	human butyrylchinesterase
MF268	8-(cis-2,6-dimethylmorpholino) octylcarbamoyleseroline
MM	Molecular Mechanics
PAS	Peripheral Anionic Site
QXP	Quick eXPlore
RMSD	Root Mean Square Deviation
$\mathbf{E_{ass}}$	Total estimated binding energy
$\mathbf{E_{lig}}$	Ligand energy relative to estimated global minimum of free ligand
$\mathbf{E_{she}}$	Binding site energy relative to local minimum for empty site
$\mathbf{E_{nhb}}$	Total energy of non-bonded interactions between ligand and site
vdW	van der Waals energy of interactions between ligand and site
$\mathbf{E_{est}}$	Electrostatic energy of interactions between ligand and site
$\mathbf{E_{nhb}}$	Non-hydrogen bonding energy
GM	Global Minimum energy
LM	Local minimum energy
FDA	United States Food and Drug Administration
BBB	Blood Brain Barrier
AChEI	Acetylcholinesterase inhibitors
PDB	Protein Data Bank (www.pdb.org)
MSD	Multi-Step Docking
DECA	Decamethonium
IHG	Indanonhexylgalanthamine
BHG	Benzosulfimidohexylgalanthamine
PPG	Piperidinopropylgalanthamine